University of Alberta

Library Release Form

Name of Author: Oliver O. Youzwishen

Title of Thesis: Flexural Rehabilitation of Energy Pipelines using Fibre-Reinforced Polymer Composites

Degree: Master of Science

Year this Degree Granted: 2001

University of Alberta

Flexural Rehabilitation of Energy Pipelines using Fibre-Reinforced Polymer Composites

by

Oliver O. Youzwishen

A thesis submitted to the Faculty of Graduate Studies and Research in partial fulfillment of the requirements for the degree of Master of Science

in

Structural Engineering

Department of Civil and Environmental Engineering
University of Alberta
Edmonton, Alberta

Fall 2001

University of Alberta

Faculty of Graduate Studies and Research

The undersigned certify that they have read, and recommend to the Faculty of Graduate Studies and Research for acceptance, a thesis entitled ***Flexural Rehabilitation of Energy Pipelines using Fibre-Reinforced Polymer Composites*** submitted by **Oliver O. Youzwishen** in partial fulfillment of the requirements for the degree of Master of Science in Structural Engineering.

To Carrie

ABSTRACT

Energy pipelines constructed in discontinuous permafrost are susceptible to differential settlement, which can create strains large enough to trigger local buckling or wrinkling. Currently practiced cutout repairs for wrinkled pipe are costly and inefficient.

A finite element (FE) study was conducted to examine the behaviour of wrinkled pipe repaired with external sleeves. Increases in moment capacity and ductility were observed. Fibre reinforced polymer composites (FRP's) were identified as a suitable sleeve material because of their tailor-made material properties.

Large-scale laboratory tests were conducted to confirm behaviour observed in FE modelling. Tests showed that the moment – curvature behaviour of the pipe could be improved using a FRP sleeve system. Fracture of the fibre sleeve was observed in the tests, indicating that fibre strain must be considered during sleeve design. Refinements were then made to the original FE model, so that fibre strain could be monitored and appropriate sleeve designs used.

ACKNOWLEDGEMENTS

This study was conducted with the financial assistance of Enbridge Pipelines Inc. and the Natural Sciences and Engineering Research Council of Canada (NSERC). Enbridge Pipelines Inc. has played an instrumental role in supporting research of new repair methods for wrinkled pipelines; financially, technically and through the supply of line pipe for laboratory testing. The donation of prestressing materials used in testing by Dywidag Systems International is greatly appreciated.

The assistance of the technicians at the University of Alberta I.F. Morrison Structural Lab, Richard Helfrich and Larry Burden, was essential to the success of the experimental program. Thanks are also extended to fellow colleagues in the Structures Group, especially Dr. Heng Khoo for his assistance with ABAQUS modelling, Marc Kuzik for his help with composite materials and Mark D'Andrea for all his help during the pipe tests.

A special thanks goes to my wife Carrie. I thank her for her support during this project and during the writing of this thesis. I am especially thankful for her encouragement of my decision to undertake my Master's degree. Thank you very much.

TABLE OF CONTENTS

LIST OF TABLES

LIST OF FIGURES

LIST OF SYMBOLS

Latin Symbols

d	nominal number of pipe diameters
D	outside diameter
E	elastic modulus for an isotropic material
E_1	elastic modulus in the local fibre direction; elastic modulus for the FRP sleeve in the global longitudinal direction
E_2	elastic modulus transverse to the local fibre direction; elastic modulus for the FRP sleeve in the global hoop direction
G	shear modulus for an isotropic material
G_{12}	shear modulus in the local 1-2 plane for a FRP lamina
l_s	shear span length
$l_{\theta1\text{-}\theta2}$	initial gauge length between RVDT's
L	pipe length between load points
M_T	total mid-span moment
n	strain hardening exponent
N_{LC1}, N_{LC2}	vertical reaction loads
p	internal pressure
p_{end}	external pressure applied to end caps in finite element simulation
P_{LC5}, P_{LC6}	axial load in prestressing rods
t	finite element time increment
t	wall thickness
u_1, u_2, u_3	finite element nodal displacements
w_1	primary wrinkle
w_2	secondary wrinkle

Greek Symbols

α	coefficient of thermal expansion
$\Delta_{\%}$	elongation
Δ_{CL}	vertical displacement at mid-length of pipe
Δ_{LOAD}	relative longitudinal displacement of load points
Δ_{R1}, Δ_{R2}	longitudinal displacement of end reactions

ΔT	temperature differential = $T_{operating} - T_{installation}$
ε_1, ε_2	normal strain in the local 1 and 2 directions for a FRP lamina
ε_{nom}	engineering strain
ε_{pl}^{ln}	logarithmic plastic strain
ε_{py}	engineering strain at yield (0.005 mm/mm)
ε_{true}	true strain
ε_{ult1}	ultimate strain in the local fibre direction
ε_x, ε_y, ε_z	normal strain in global x, y and z-directions
ϕ_1, ϕ_2, ϕ_3	finite element nodal rotations
Φ_{Global}	global pipe curvature
γ_{12}	shear strain in the local 1-2 plane for a FRP lamina
γ_{yz}, γ_{zx}, γ_{xy}	shear strain in global y-z, z-x and x-y planes
$\mu\varepsilon$	microstrain ($1\mu\varepsilon = 1\text{x}10^{-6}$ mm/mm)
ν	Poisson's ratio for an isotropic material
ν_{12}, ν_{21}	major, minor Poisson's ratio for a FRP lamina
σ_1, σ_2	normal stress in the local 1 and 2 directions for a FRP lamina
σ_α	longitudinal stress due to thermal expansion
σ_h	hoop stress due to internal pressure
σ_l	longitudinal stress due to internal pressure
σ_{nom}	engineering stress
σ_ν	longitudinal stress due to Poisson's effect
σ_{true}	true stress
σ_{ult}	ultimate stress
σ_{ult1}	ultimate stress in the local fibre direction
$\sigma_{ult\ dyn.,\ stat.}$	dynamic or static ultimate stress
σ_x, σ_y, σ_z	normal stress in global x, y and z-directions
σ_y	yield stress
$\sigma_{y\ dyn.,\ stat.}$	dynamic or static yield stress
τ_{12}	shear stress in the local 1-2 plane for a FRP lamina
τ_{yz}, τ_{zx}, τ_{xy}	shear stress in global y-z, z-x and x-y planes
θ_1, θ_2	pipe rotation measured with RVDT's

1 INTRODUCTION AND LITERATURE REVIEW

Steel pipelines have become the dominant system for transporting crude oil, natural gas and other petroleum products from areas of production to market in North America. In Canada alone, there are over 100,000 kilometres of large-diameter transmission pipelines, which transport two-thirds of the nation's energy supply (Canadian Energy Pipeline Association, 2000). Pipelines have become the primary method for transporting liquid or gaseous fossil fuels because of their economy and especially their safety. For example, in 1997, there were 583 marine shipping accidents, with 24 fatalities. Railway accidents numbered 1,125, with 107 fatalities. However, pipelines recorded 27 accidents and no fatalities (Canadian Energy Pipeline Association, 2000). To achieve such high levels of safety, significant pipeline integrity programs have been implemented. These programs involve monitoring and remediation of any potential problems along the pipeline.

Since energy pipelines transport often-hazardous substances, it is paramount that containment of the product within the pipe is maintained. A loss of containment in a pipe often results in significant damage, whether it is to infrastructure or the surrounding environment. A pipeline can be breached in many different ways, including corrosion, physical impact onto the pipe or excessive strain in the pipe wall. If a pipe is subjected to severe loading conditions, such as axial loading and bending, tensile strains can develop in the pipe wall to an extent that material fracture occurs and containment is lost.

Severe loadings on a pipe often arise from the environment through which the pipe passes. As more pipelines are built in increasingly harsher environments, such as the sub-Arctic and Arctic regions of North America, severe loading conditions are likely to be encountered with greater frequency. It would be desirable to avoid severe loading altogether, but in some cases it cannot be avoided. In these instances, methods must be available to repair any damage inflicted upon the pipe. These methods must bring the pipeline back to its condition prior to damage, but they also need to be economical. Before the repair methods can be devised, however, the type of damage to the pipe must be specified. In this chapter, the problem of local buckling, or wrinkling is introduced

and current repair methods for this type of damage are discussed through a review of current literature.

1.1 Repair of Wrinkled Pipelines

When a pipeline is subjected to excessive compressive strains (from bending or axial compression) it can buckle locally in an inelastic fashion. The result is the formation of a wrinkle or wave in the pipe wall. The wrinkle creates a localization of strain in the pipe. This strain localization can serve as the initiation point of fracture of the pipe and subsequent loss of contents into the external environment. Once a wrinkle is detected, remediation is often necessary in order to insure integrity of the pipeline.

1.1.1 Statement of the Problem

Formation of a wrinkle in a pipeline does not lead to immediate fracture of the pipe (Das *et al.,* 2000). If the wrinkle is discovered before fracture occurs, measures can be taken to remedy the problem. Currently, the most accepted method of repairing a wrinkled pipe is to remove the affected section of pipe and replace it with a newer, often thicker section of pipe. While this technique is relatively simple to perform, it has significant impact on the pipeline operation. In order to cut out the wrinkled section of pipe and replace it, the pipeline must be shut down, often for periods of days. This step alone creates financial losses for the pipeline operator. After the pipeline is shut down, its contents in the vicinity of the wrinkle, between isolation valves that may be kilometres apart, must be purged. This is another costly procedure. Finally, heavy equipment must be brought in to remove the wrinkled pipe and weld in a new section of pipe. All these steps add up to significant costs to the operator.

A more attractive alternative to a cutout replacement is to repair the pipe externally. An external repair eliminates the need for a pipeline shutdown and costly purging. Unfortunately, very little work has been conducted on external repair methods to date. The work completed previous to this project examined an external repair incorporating a steel sleeve over the wrinkled pipe. The sleeve type of repair has been used extensively in the pipeline industry to repair corrosion damage to the pipe, but its application to winkle repair of the pipe has not been studied extensively. A better understanding of

sleeve repair techniques is required before they can be fully integrated into a pipeline integrity program. This study is intended to further this understanding.

1.1.2 Project Scope and Objectives

To achieve a more in-depth understanding of the behaviour of wrinkled line pipe repaired with external sleeves, a preliminary finite element (FE) analysis was conducted. The preliminary study was based on earlier finite element work completed at the University of Alberta (this work will be discussed in the literature review). The previous work examined the behaviour of wrinkled pipe with differing lengths of steel sleeves. Other parameters, such as sleeve thickness, sleeve material or number of sleeves, were not examined. The preliminary FE study conducted in this project sought to examine the effects of these parameters on the flexural behaviour of the pipe. A single load case was examined. This load case was typical of the loads the pipe would experience in the field.

An experimental program was then conducted. The experimental program simulated the conditions assumed in the FE study, both material conditions and loading conditions. The experimental program aimed to provide physical evidence of the results observed in the numerical study. In addition, experimental work would allow experience with repair techniques to be gained so that eventually the repairs could be conducted in field applications.

The objectives of this study can be summarized as:

1. expand on the previous numerical analysis of steel sleeve repairs, examining the effects of sleeve length, sleeve number, sleeve thickness and repair timing;
2. examine the effects of different sleeve materials, specifically fibre reinforced polymer composites, on the moment carrying (flexural) behaviour of the wrinkled pipe;
3. using the FE model, determine design parameters for sleeve repairs to be used in the experimental program;
4. validate the assumptions and results of the FE model by conducting large-scale laboratory tests on wrinkled pipe;

5. refine the FE model, if necessary, to better predict the behaviour of wrinkled pipe repaired with external sleeves;
6. develop procedures for installing composite sleeves on wrinkled pipes.

1.2 Literature Review

In this section, background on the problem of pipe wrinkling is presented. A brief case study of wrinkling on the Norman Wells Pipeline, which spurred this project, is given. Current repair methods for wrinkled pipe are discussed, followed by an overview of composite materials and their use in civil engineering and pipeline applications.

1.2.1 Wrinkling Phenomenon in Steel Line Pipe

1.2.1.1 Causes of Pipe Wrinkling

Inelastic local buckling (wrinkling) of a pipeline will occur when a segment of the pipe cross-section is exposed to compressive strains exceeding a certain critical value. This value has been the subject of many studies conducted to date (for example Dorey *et al.,* 2001 and Mohareb *et al.,* 1994) and has been found to vary depending on material and loading variables. The compressive strains can originate from temperature variations during the life of the pipeline or from geotechnical movements around the pipe. It is the latter cause that will be discussed in more detail.

Field observations have shown that geotechnical movements around buried pipelines are capable of imposing large displacements onto the pipe (Murray, 1997). These movements may be associated with unstable slopes, poor soil below the pipeline or regions of discontinuous permafrost. Discontinuous permafrost is of particular concern currently, given the significant pipeline projects that are planned for Arctic and sub-Arctic North America where discontinuous permafrost is prevalent. A pipeline that passes through discontinuous permafrost may be susceptible to differential settlement. Soil in thaw-unstable regions may consolidate, dragging the pipeline down with it while soil in thaw-stable regions holds the pipeline in its original position. The resulting discontinuity in support along the pipe imposes curvature, as the pipe attempts to retain its original configuration. If settlement continues, curvature will increase and eventually

the pipe will buckle locally (Murray, 1997). Upon local buckling, behaviour of the pipe changes significantly.

1.2.1.2 Behaviour of Wrinkled Pipe

To understand the behaviour of wrinkled pipe, it is helpful to plot its moment – curvature response. Figure 1.1 illustrates a generic moment – curvature response for a shell structure under internal pressure; as the curvature is increased a peak moment is reached. This is the buckling point, were localized wrinkling begins. After this point, the pipe can no longer sustain the moment at its previous level and the moment level drops with continued movement. To maintain equilibrium, the moment in the pipe at locations away from the wrinkle must also decrease. This is accomplished through elastic unloading of the pipe segment away from the wrinkle. Energy released from elastic unloading is absorbed by the wrinkle and leads to localization of deformation (Zhou and Murray, 1995). The result is a prominent deformation in the pipe at the wrinkle. The wrinkle may take one of two shapes, depending on the presence of internal pressure. If the pipe is pressurized, the wrinkle will grow outwards. This is classified as a bulge buckle. If the pipe is unpressurized (as it is during construction), a different buckling mode occurs. Outward bulging occurs initially, but eventually the bulge decreases in amplitude and the pipe begins to buckle inwards (Souza and Murray, 1994). This is known as a diamond buckle.

Regardless of the buckling mode, strains begin to localize in the vicinity of the wrinkle. As curvature is increased, these strains also increase. Laboratory tests have shown that the steel used for line pipe is very ductile and fracture of the pipe is unlikely at normal operating pressures, provided the curvature increases monotonically (Das *et al.,* 2000). However, if the pipe is loaded and unloaded such as in a freeze-thaw cycle, strain reversal can occur causing fracture in the wrinkle region due to low-cycle fatigue (Das *et al.,* 2000). In addition to the threat of fatigue fracture, pipes subjected to significant flexural strain will experience ovalization of the cross-section (Mohareb *et al.,* 1994). Severe ovalization can impact daily operation of the pipe by affecting fluid flow or by interfering with internal inspection tools that operators use to assess the condition of the

pipe. These observations of wrinkle behaviour have been made not only through laboratory testing, but also through finite element analysis. FE modelling has proven to be a valuable tool in understanding the behaviour of wrinkled pipes and is discussed briefly in the following section.

1.2.1.3 Finite Element Modelling of Pipe Wrinkling

Finite element analysis has been used extensively in the last decade to study the deformational behaviour of wrinkled pipes. Numerous studies have been conducted at the University of Alberta and have shown that the FE model can adequately predict the complex non-linear behaviour patterns of line pipe following local buckling (Murray, 1997). Modelling has been consistent with observations made both in the laboratory, on full-scale tests, and field observations of pipe wrinkling (Yoosef-Ghodsi *et al.,* 2000). Pipes ranging from 324 mm to 914 mm in outside diameter have been modelled. These pipes have been modelled plain or with circumferential girth welds (where two joints of pipe are joined in the field).

The basic FE pipe model used at the University of Alberta has been consistent throughout different projects. This model is explained in detail in Chapter 2. Improvements to the model have been made with respect to material models, boundary conditions and initial imperfections (see for example Dorey *et al.,* 2001). The most significant change to the model recently, in the context of this project, has been the addition of elements to simulate sleeve repairs (Yoosef-Ghodsi and Murray, 1999 and Yao and Murray, 2000). This change to the basic model was initiated due to wrinkling that was observed in the field on the Norman Wells Pipeline. The case study of this pipeline is discussed next.

1.2.2 Local Buckling on the Norman Wells Pipeline

The Norman Wells Pipeline is a fully buried 324 mm diameter or Nominal Pipe Size (NPS) 12 crude oil pipeline owned and operated by Enbridge Pipelines (NW) Inc., constructed between 1983 and 1985. The 826 km long pipeline transports crude oil from the Norman Wells oilfield on the Mackenzie River, Northwest Territories to a pipeline terminal in Zama Lake, Alberta. It was the first fully buried pipeline constructed in discontinuous permafrost in North America (Wilkie *et al.,* 2000). The pipeline crosses a

variety of terrains that have the potential to impose extreme strains to the pipeline. Because of this, design of the pipeline incorporated both elastic and inelastic designs. Longitudinal strain limits were imposed on the pipe design so that local buckling and severe tensile yielding would be avoided. These strain limits were 0.5% and 0.75% in tension and compression, respectively (Wilkie *et al.*, 2000).

As part of the regulatory approvals for the pipeline, Enbridge was required to monitor the pipeline for movement due to slope instability or differential thaw settlement on an annual basis. Monitoring was conducted using an internal inertial geometry tool, called "Geopig". The Geopig was capable of determining longitudinal strain in the pipe wall and very small changes in internal diameter of the pipe. By comparing strains in the pipe on a yearly basis, any significant strain growth could be identified and that location marked for visual inspection. In the early 1990's several sites where strains were increasing were placed on a "watch list" and visually monitored. During the 1997 and 1998 Geopig runs sharp increases in strain and internal diameter were detected at two sites in regions of discontinuous permafrost, Kilometre Posts (KP) 318 and 311, respectively. It was believed that wrinkles had developed at these sites.

An investigative dig was conducted at KP 318, on a slope of a creek crossing, in February 1998 (Wilkie *et al.*, 2000). A large wrinkle was discovered, confirming the hypothesis made using the 1997 Geopig data. The wrinkle was examined for any cracking and none was detected. After confirming the integrity of the pipe, it was instrumented to record slope movements and strain growth in the pipe in order to gain a better understanding of the behaviour of a wrinkle in the field. A cutout replacement of the section was scheduled for the following winter season and after a year of data collection the wrinkled section was removed.

At KP 311, 1998 Geopig data indicated that there were two potential wrinkle locations, located approximately 10 metres apart. The data indicated that the wrinkles were significantly smaller than the wrinkle discovered at KP 318 and compressive strains in the pipe were also less. Given the smaller strains in the pipe, it was deemed feasible to

explore alternate repair methods for the wrinkles. A numerical study was conducted by the University of Alberta (Yoosef-Ghodsi and Murray, 1999) to explore the effectiveness of a single steel sleeve repair on the larger of the two wrinkles. Based on the conclusions of this study, a steel sleeve repair was installed in early 1999. This sleeve is still in operation and the wrinkle location is being monitored closely using the annual Geopig data.

1.2.3 Current Repair Methods for Wrinkled Pipe

Research has been conducted recently at the University of Alberta to determine limiting strain criteria for wrinkled pipe (see Das *et al.*, 2000). The goal of this research has been to provide realistic criteria for the safety of wrinkled pipe. However, the problem of what to do with the wrinkle once it has progressed to a level deemed unsafe by the pipeline operator has not been explored in depth. To date, the repair options for wrinkle pipe have been limited. As mentioned previously, the typical method of repair is to perform a pipeline cutout and replace the affected section of pipe with a thicker-walled pipe. A thicker pipe is used so that increased resistance to future wrinkling is provided (Wilkie *et al.*, 2000). The high costs associated with this procedure have been discussed.

The lower cost alternative of an external repair for wrinkles has only begun to be explored. Finite element simulations of steel sleeve repairs have been conducted by Yoosef-Ghodsi and Murray (1999) and Yao and Murray (2000). These studies concluded that although a steel sleeve repair was able to stop the growth of the wrinkle, secondary wrinkles would develop adjacent to the sleeve. These wrinkles would then grow at a rate equal to that of the first wrinkle, if it had not been repaired. This rendered the long-term effectiveness of the repair very low (Yoosef-Ghodsi and Murray, 1999). It was hypothesized that the localized stiffness of the sleeved section of pipe compared to the unsleeved sections of pipe was promoting the formation of secondary wrinkles. By manipulating the stiffness of the sleeve, one might be able to improve the performance of the repair. This drove the decision to explore the use of alternate materials, specifically fibre reinforced polymer composite materials, in this project.

1.2.4 Fibre Reinforced Polymer (FRP) Composites

A composite material is defined as a structural material created by combining two or more components that are not soluble in each other at a macroscopic level (Kaw, 1997). The goal of the composite is to maximize the advantages of the components while minimizing their disadvantages to create a more efficient product. The use of composite materials is not a new concept. In Biblical times the Israelites combined straw and clay to form bricks that were less susceptible to cracking (Vinson and Chou, 1975). However, the use of materials such as high strength fibres and polymer matrices to form fibre reinforced polymer (FRP) composites is a development of the 20th century.

1.2.4.1 Background on FRP Composites

FRP composites are considered to be one of the modern advanced composite materials. Their use in engineering applications dates back to the early 1940s when fibreglass was first used to reinforce plastics for radar domes for aircraft antennas (Vinson and Chou, 1975). The FRP material replaced older plywood and canvas domes and proved to be excellent with respect to load-bearing capacity, thermostability and resistance to weathering. In the 1950s FRP materials began to be used extensively in the aeronautic and aerospace industries because of their combination of high strength and low density, compared to more traditional materials such as steel or aluminium. These attributes translated into tremendous cost savings and gave engineers the ability to push the design envelope for aircraft and space vehicles further than possible with conventional materials. Today, the use of FRP materials has widened to include fields such as automotives, sports, offshore oil and gas exploration and even bone replacement (Bonfield, 1988). FRP's are also being used to a greater extent in structural engineering applications. This will be discussed in Section 1.2.4.2.

The advantages of FRP materials over conventional materials arise from their composition. FRP's display very high strength because they are made of very small diameter fibres. As the fibre diameter is reduced, the probability of imperfections in the fibre is also reduced. It is these imperfections in materials that reduce their strength from their theoretical maximum value (Kaw, 1997). While the fibres have very high strength,

they are very brittle. The use of a very ductile matrix material (such as a polymer resin) adds a certain amount of ductility and toughness to the composite. The amount of matrix material, however, is minimized since the matrix adds virtually no strength or stiffness to the composite. Because the strength and stiffness of the composite are due almost entirely to the fibres, the orientation of the fibres to external loads has a significant impact on the overall behaviour of the material. By changing the fibre orientation, or using a combination of different orientations, the engineering properties of the composite can be custom designed to specific applications. This leads to very efficient use of material, where it is needed in a body, and is one of the most important features of FRP's.

FRP materials are not without their disadvantages, however. Compared to conventional metals, for instance, FRP's are costlier to fabricate. It should be noted that as FRP's are integrated more into engineering applications, this cost would be reduced. The characterization of the mechanical properties of a FRP composite is also more complex than traditional metals (Kaw, 1997). More effort must be placed into the design process when FRP's are used. While composites greatly exceed metals in strength, they do not have the same level of fracture toughness or ductility metals have. Finally, repair of FRP's is not as simple as it is for metals. Despite these disadvantages, the advantages of FRP's have created interest in different applications, such as structural engineering.

1.2.4.2 FRP Composites in Structural Engineering Applications

The use of FRP materials in structural engineering applications began to grow in the late 1980s. Use in the structural engineering field has focussed primarily on concrete structures. Large-scale deterioration of reinforced concrete structures due to corrosion of steel reinforcement has been a problem for many years, especially on bridge structures where a very corrosive environment occurs. FRP's resistance to corrosion has made this material attractive for new reinforced concrete structures, although steel is still the most commonly used reinforcing material. FRP deformed bars, grids, prestressing tendons and post-tensioning cables are all currently manufactured and in use throughout the world (Labossiere, 1993). Hybrid FRP-concrete beam columns are also being researched. In this application, a FRP tube would be used as permanent formwork, a protective jacket

for the concrete as well as providing confinement and shear and flexural reinforcement (Mirmiran *et al.,* 1999). FRP's are currently being fabricated into structural shapes using pultrusion processes. These processes allow rapid fabrication of the shapes in a variety of lengths. The result is a lightweight, high-strength, corrosion-proof member. These components have been used to construct light bridges, such as the Aberfeldy Golf Course Pedestrian Bridge in England (Labossiere, 1993).

One of the greatest areas of growth in FRP use in structural engineering has been for the rehabilitation of existing structures. FRP's ability to be easily bonded externally to existing structures has made it an attractive option for increasing the strength or ductility of these structures. Reinforced concrete bridge piers have been retrofitted to meet new seismic design requirements by wrapping them with unidirectional carbon fibre reinforced polymer (CFRP) sheets (Pantelides *et al.,* 1999). Research has also been conducted on the use of glass fibre (GFRP) sheets to improve the behaviour of masonry walls under cyclic loading that would occur during earthquakes (Kuzik *et al.,* 1999). In other instances, FRP sheets or plates have been used to strengthen existing structures to meet increased operational loads, such as heavier trucks on bridges.

It is apparent that the use of FRP's in structural engineering applications has primarily focussed on concrete and masonry structures rather than steel structures. This is not to say that there are no uses for FRP's on steel structures. In fact, FRP patches have proven to be successful in repairing cracked steel members (Kennedy and Cheng, 1998). In addition, FRP's have been used with success to strengthen natural gas cylinders for vehicles and tanks for fire fighting breathing apparatus cylinders (True, 1995). FRP's have also found uses with steel in the pipeline industry.

1.2.4.3 FRP Composite Use in the Pipeline Industry

One of the major concerns in the energy pipeline industry is pipeline integrity. Pipe corrosion has been the cause of many pipeline ruptures over the years. Thus a large effort has been put forward from the pipeline industry to control corrosion and in the instances where it occurs, to have safe and efficient ways of remediating the problem.

FRP's have been used since 1991 in the United States for the repair of corrosion defects on liquids pipelines and on gas pipelines since 1995 (True, 1995). Corrosion of the pipe wall reduces the pipes ability to withstand stresses imposed by fluid pressure. Uniaxial GFRP sleeves, marketed under the brand name of Clock Spring, have been used to strengthen these pipes. These sleeves, with their fibres orientated in the circumferential or hoop direction of the pipe, are bonded to the pipe and thus provide added resistance to hoop strains caused by fluid pressure.

Composite materials are now being researched as an alternative to steel for large on-shore pipelines. In the past fibreglass pipes have been limited to use in small diameter flow lines where a very corrosive environment exists (Ellyin *et al.,* 2000). However, new studies have shown that FRP's may be a viable solution, in some cases, for larger, more critical pipelines.

FRP materials have proven their success in many fields. Without them, some of the major advances in aeronautics and aerospace would not have been possible. Their use and value in structural engineering applications is steadily increasing. The pipeline industry has also been exposed to the advantages of FRP's, for corrosion repair and now as a potential pipeline material. It is believed FRP's will also play a role in repairing structural damage to pipelines, such as local buckling. In the following chapters, the feasibility of this concept is explored.

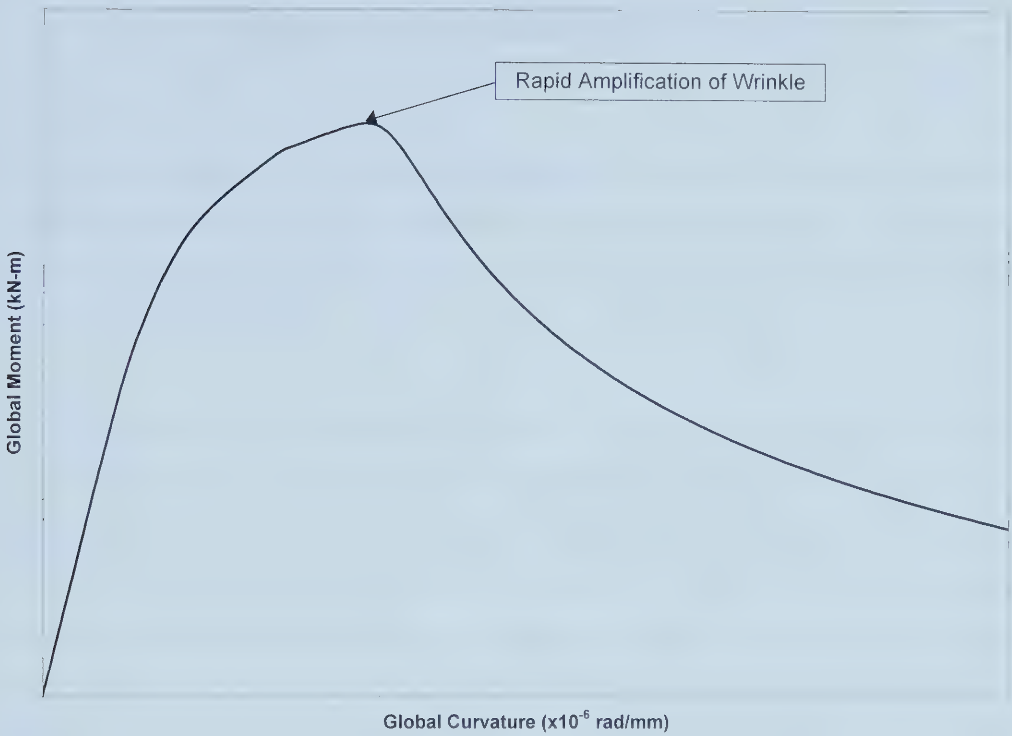

Figure 1.1 - Moment - Curvature Behaviour for a Typical Pressurized Pipe

2 PRELIMINARY FINITE ELEMENT STUDY

2.1 Goals

Finite element analysis (FEA) provides an inexpensive means of studying the behaviour of wrinkled pipes under varying load scenarios and sleeve repair methods. The results of the analysis can then be used as a basis for the design of a testing program. In turn, the results of the testing program can then be used to validate the model.

The primary goal of the preliminary FEA was to develop an understanding of the post-buckling behaviour of a pipe that has been repaired with a sleeve. Previous FEA work performed on sleeve repair of wrinkled pipe (Yoosef-Ghodsi and Murray, 1999 and Yao and Murray, 2000) was limited to repairs with single steel sleeves. This project expanded on their work by examining the effects of sleeve geometry, both in length of sleeves and number of sleeves placed on the pipe, sleeve material and timing of the repair on the behaviour of the pipe. The secondary goal of the FEA was to develop sleeve design parameters for laboratory testing. The material properties for the sleeves to be tested (thickness, elastic modulus, length) were determined using the FE model.

The commercial finite element analysis package ABAQUS/Standard Version 5.8-1 (Hibbit, Karlsson & Sorensen Inc. (HKS), 1999a) was chosen to perform the numerical analysis. This package was chosen for several reasons. Its ability to analyze large, non-linear deformations was essential for modelling of pipe wrinkling. ABAQUS provides elements suitable for modelling thin-walled pipes, which are able to undergo large displacements and large membrane strains without adversely affecting convergence of the solution. Available in the program is an elastic-plastic material model that allows the constitutive law to be input by the user in the form of a multi-linear curve with isotropic or kinematic hardening. ABAQUS also features a post-processing package that allows for efficient data reduction and graphical presentation.

FEA using ABAQUS was performed on Sun Ultrasparc 1 and 10 stations with RAM ranging from 96 megabytes to 256 megabytes. The analysis would run between 20 and 90 minutes depending on the complexity of the model and system traffic.

2.2 Finite Element Model

2.2.1 Finite Element Formulation

Finite element analysis is used today in a very wide range of problems, from structural analysis to analysis of electrical systems. The finite element formulation in ABAQUS is based upon the incremental principle of virtual work. A detailed description of the finite element formulation is beyond the scope of this report. One can refer to Bathe (1996) for a complete description.

Buckling analysis of pipe is a quasi-static, non-linear type of analysis. Thus, it requires an incremental solution technique to be used in order to obtain a solution. ABAQUS uses both a Newton-Raphson approach and a Ricks-based approach with an incremental updated Lagrangian formulation. Stress and strain are measured at time $t + \Delta t$ and referred back to the element configuration at time t. This formulation allows non-linear geometric behaviour of the model to occur concurrently with large non-linear strains in the elements.

ABAQUS incorporates an automated increment size control feature into its solution procedure. The program automatically updates the size of the time increment Δt based on the rate of convergence. If convergence occurs with a small number of iterations, ABAQUS increases the increment size to be used in the next time step. If convergence occurs with a large number of iterations, the increment size is decreased and the solution sequence is attempted at the new time step. Automatic increment control is especially useful when the critical buckling strain in the pipe is approached and convergence would not occur with a large time increment. However, the possibility exists for the solution to converge along the wrong equilibrium path if the program uses an increment that is too large. Numerical testing by DiBattista *et al.* (2000) of the automatic increment control versus manually set increments showed that the two methods gave very similar results.

Thus, the automatic increment control feature was used in the analysis conducted for this project.

2.2.2 Element Selection

Two types of elements were used in the analysis (see Figure 2.1). Elements representing the pipe wall were four-node, doubly curved shell elements with hourglass control and reduced integration (ABAQUS element S4R). Three-node, flat, small strain elements were used to model the pipe end caps (ABAQUS element STRI3).

The S4R elements are three-dimensional, general-purpose shell elements and are intended for thick and thin shell applications (HKS, 1999b). They account for finite membrane strains and allow transverse shear deformation. Each node has six degrees of freedom: three transitional (u_1, u_2, u_3) and three rotational (ϕ_1, ϕ_2, ϕ_3). The S4R elements have proved successful in modelling line pipe undergoing large deformations and large displacements in many studies (for example see Dorey *et al.*, 2001).

The STRI3 elements are thin shell, flat elements that account for only small strains. Any changes in thickness during deformation are ignored for this element. This element type proves to be useful in modelling a rigid end plate that would be fixed to the pipe ends during testing.

2.2.3 Boundary Conditions

Boundary conditions were applied to the pipe model to meet two purposes. First, boundary conditions were applied to meet the requirements of static equilibrium of the model. Second, boundary conditions were applied to accommodate a reduction in model size due to symmetry.

In order to achieve a statically stable model, the proper reaction boundary conditions had to be applied to the pipe. The reaction boundary conditions are illustrated in Figure 2.2. Both pipe ends were restrained in the vertical direction (u_2), with one end restrained in the horizontal (u_1) direction. In-plane rotation (ϕ_3) at both ends was unrestrained, so that a prescribed rotation could be applied during the loading procedure (see Section 2.2.7).

This resulted in a simple pin-roller support system. All out of plane movements (u_3, ϕ_1, ϕ_2) at the reactions were restrained. An explanation of this step is given later in this section.

The reaction boundary conditions were applied at single points at each end of the pipe. In actual pipe tests, the reactions do not occur at single points at each end. Rigid plates are attached to the pipe ends, with the reaction fittings then connected to the rigid plates. The rigid connections of the reactions to the pipe were modelled by placing constraints on the nodal degrees of freedom at each end of the pipe. The last row of nodes at each end of the model was linked to the reaction node. This was accomplished by using the BEAM multi-point constraint in ABAQUS. Any rotation or displacement prescribed at the reactions points would be transferred to the pipe ends without distortion.

A second set of boundary conditions was applied to the model in order to accommodate the use of symmetry in modelling of the pipe. Symmetry has been successfully made use of in FEA of line pipe (Murray, 1997) and likewise in this study. By passing a plane of symmetry along the length of the pipe through the radial axis (see Figure 2.3), one can model only half of the specimen and obtain the behaviour that occurs in the full specimen. This greatly simplifies the development of the model and significantly reduces the computer processing time.

In order to apply symmetry, the proper boundary conditions must be applied where the plane of symmetry intersects the pipe. Figure 2.3 shows the intersection of the symmetry plane with the top and bottom of the pipe. During bending, this corresponds to the extreme compression and tension faces of the pipe, respectively. Nodal movements (either displacements or rotations) across the line of symmetry must be restricted to enforce symmetry (Ghali and Neville, 1997). The degrees of freedom corresponding to these movements (u_3, ϕ_1, ϕ_2) were restrained for the nodes located on the symmetry plane. Because the reaction points at either end of the pipe fell on the plane of symmetry, their out-of-plane degrees of freedom were also suppressed. By applying symmetry, the possibility of any out-of-plane buckling was eliminated. This assumption has been

justified by line pipe bending studies that have been previously conducted (for example Souza and Murray, 1994 and 1996).

2.2.4 Mesh Selection

Mesh selection plays an important role in the behaviour of the finite element model. A model with a mesh that is too coarse will not accurately predict the behaviour of the pipe, since displacements must be interpolated between the nodes. The finer the mesh, the more realistic the model will be. It makes sense that the finest mesh possible be used. However, as the mesh is made finer and finer, the time to conduct the analysis grows dramatically.

For this study, the pipe body consisted of elements that were 28.6 mm in the circumferential direction and 25.4 mm in the longitudinal direction, resulting in a mesh of 18 x 96 elements. This mesh size was used for several reasons. First, the aspect ratio (the ratio of the larger element dimension to the smaller dimension) of the elements, 1.125, was considered to be a "reasonable number" based on previous experience of pipeline researchers at the University of Alberta. Second, this mesh size has shown reasonable agreement with experimental results (Yoosef-Ghodsi and Murray, 1999). No attempt to refine the mesh was made during the preliminary FE study.

2.2.5 Material Model and Residual Stresses

The material model used in the numerical study was taken from longitudinal tension coupon data for API-5L X52 grade line pipe (Mohareb *et al.*, 1993 and 1994). This was the same type of line pipe that was used in the Norman Wells Pipeline. The material exhibited typical high-strength, ductile steel stress-strain behaviour, consisting of an initial linear-elastic region followed by a strain-hardening region.

In order to input a steel material model into ABAQUS, a yield criterion and hardening rule had to be chosen. The yield criterion chosen was the von Mises yield surface. The von Mises yield surface assumes that the yield stresses associated with the three principal stress directions are equal, thus forming a cylindrical shape centred on the hydrostatic stress line. An isotropic hardening rule was chosen to describe the plastic behaviour of

the material model. This hardening rule assumes uniform expansion of the yield surface about the hydrostatic stress line as plastic strain increases. The use of an isotropic hardening rule is a simplification to the material model. In reality a kinematic hardening rule would better describe the plastic hardening of the steel. This rule adds additional complexity to the material model, compared to the isotropic rule. For cases of monotonic loading of line pipe, the isotropic hardening rule has been found to be sufficient (DiBattista *et al.,* 2000 and Dorey *et al.,* 2001).

Once the yield criterion and the hardening rule were established, the tension coupon stress-strain values were converted into values useable by ABAQUS. The expansion of the yield surface given in the isotropic hardening rule can be described with a multi-linear approximation of the true stress-strain behaviour of the tension coupons. Because the stress and strain measured from the tension coupons are referenced to the undeformed cross-section, they do not indicate the true stress and strain in the material. By applying Equations 2.1 and 2.2, measured stress, σ_{nom}, and strain, ε_{nom}, can be converted to true stress, σ_{true}, and true log plastic strain, ε_{ln}^{pl}, which can be input into ABAQUS.

$$\sigma_{true} = \sigma_{nom}\left(1 + \varepsilon_{nom}\right) \tag{2.1}$$

$$\varepsilon_{ln}^{pl} = \ln\left(1 + \varepsilon_{nom}\right) - \frac{\sigma_{true}}{E} \tag{2.2}$$

The true stress – log plastic strain relationship used in the material model is given in Figure 2.4

Residual stresses in the circumferential direction are inherent in pipes due to the rolling and welding processes. However, no residual stress patterns were added to the model, since the actual determination of a typical residual stress pattern in rolled pipe would be a very time consuming and costly procedure. In addition, ring expansion tests conducted by DiBattista *et al.* (2000) have shown that there is little difference in the material behaviour of tensile coupons and complete pipe rings tested in the expansion tests.

2.2.6 Initial Geometry and Initial Imperfections

The initial geometry of the model was derived from experimental measurements of NPS 12 line pipe by Mohareb *et al.* (1994). The pipe measured 322.954 mm in outside diameter with a 6.477 mm thick wall. A pipe length of 2,438 mm, or approximately eight times the diameter (8*d*) was chosen for the model. This length minimized the end effects in the model, while maintaining a reasonably small model size. The pipe was assumed to be perfectly straight prior to loading. This assumption is reasonable for the relatively short length of pipe that was modelled.

Even though the pipe was assumed to be perfectly straight, the diameter of the pipe was assumed to be imperfect. Numerical analysis conducted by Dorey *et al.* (2001) has shown that diameter imperfections have a significant impact on the buckling capacity of the pipe under combined bending and axial compression. Since initial imperfections in the diameter have tremendous variability in both magnitude and distribution among different pipe specimens, a simple imperfection pattern was implemented into the model. Figure 2.5 shows the "bulge" imperfection pattern that was applied at the mid-length of the pipe model. The imperfection pattern was modelled by creating a uniform bulge along the circumference of the pipe. In the longitudinal direction, the bulge followed a smooth cosine curve over a length of six elements, with a bulge height of 0.2 mm. The shape chosen for the initial imperfection closely matches the type of bulge that has been observed in experimental work. This type of initial imperfection has been shown to reasonably predict the behaviour of line pipe under bending (see Yoosef-Ghodsi and Murray, 1999).

2.2.7 Loading Conditions

Loads applied to the pipe model were intended to simulate the conditions the pipe would be exposed to in field applications. Three distinct load types were used in the model: internal pressure, axial load and imposed curvature.

2.2.7.1 Internal Pressure

An internal pressure was applied to the pipe elements to simulate the fluid pressure acting on the pipe wall during operation. A pressure of 3,300 kPa was deemed to be

representative of the pipe pressure on the Norman Wells Pipeline (Yoosef-Ghodsi *et al.*, 2000). This pressure was applied to all pipe elements and to the end cap elements. The application of the internal pressure to the end caps imposed a longitudinal tensile stress in the pipe that would be present in the lab, but not in a long pipeline in the field. Thus an axial compression load had to be added to negate this effect. This loading is discussed in the following section.

2.2.7.2 Axial Loading

Axial loading on a pipeline in the field can originate from several sources. First, in Canada, pipelines are typically constructed in the winter season, when access to remote construction sites with heavy machinery is easier. Subsequently, the pipe is installed in the ground at an ambient temperature of approximately –30°C. When the pipeline is in operation, the temperature in the pipe can typically be +15°C. This represents a temperature differential, ΔT, of +45°C. Because the temperature differential is positive, the pipe will attempt to expand during operation. However, the pipeline is restrained in the longitudinal direction. The restraint can come from soil friction around the pipe or from physical restraints such as pipe anchors, pumping / compression stations or pipe bends. The restraint creates longitudinal compressive stresses in the pipe wall due to thermal differential (σ_α), given by Equation 2.3:

$$\sigma_\alpha = -E\alpha\Delta T \tag{2.3}$$

where:

E = Young's modulus of the pipeline material (MPa)

α = coefficient of thermal expansion of pipeline material (/°C)

ΔT = operating temperature differential (°C)

Using Equation 2.3 a longitudinal stress of -109.9 MPa due to thermal expansion was determined for the model.

A second source of axial loading in the pipe comes from the internal pressure. When the pipe is constructed, it is under no internal pressure above atmospheric pressure. When the pipeline is operated under an internal pressure higher than atmospheric, the pipe expands in the circumferential (or hoop) direction. The hoop expansion creates a

longitudinal contraction in the pipe. This is known as the Poisson's effect. However, because the pipe is restrained in the longitudinal direction, the pipe is not allowed to contract. This creates longitudinal tensile stresses in the pipe wall due to Poisson's effect (σ_v). The magnitude of this stress can be determined by:

$$\sigma_\upsilon = \upsilon\sigma_h = \upsilon\left(\frac{p}{1000}\frac{(D - t)}{2t}\right) \tag{2.4}$$

where:

ν = Poisson's ratio for pipe steel

σ_h = hoop stress in pipe (MPa)

p = internal pressure in pipe (kPa)

D = outside diameter of the pipe (mm)

t = wall thickness of pipe (mm)

Using Equation 2.4 and the variables mentioned previously a longitudinal stress due to Poisson's effect of +24.2 MPa was used in the model.

A third source of axial load on a pipe can come from soil movement along the pipe. This may occur on a pipe that is installed on a sloped surface, such as a river crossing. The friction between the soil and the pipe wall will create tensile axial forces at the top of the slope, where the pipe is being pulled and compressive axial loads at the bottom of the slope, where the soil is pushing on the pipe. These forces are highly variable and difficult to quantify with any degree of accuracy. Therefore, for this study, axial loads due to soil movements were not accounted for in the model.

The final axial load that had to be accounted for in the model does not occur in field applications, but rather in laboratory studies. In experimental work with pressurized pipes, rigid plates must be welded to the pipe ends in order to contain the fluid in the pipe. The pipe now becomes a closed pressure vessel. As such, longitudinal tensile stresses are introduced into the pipe wall due to fluid pressure acting upon the end plates. This stress, σ_l, is determined by:

$$\sigma_l = \frac{p}{1000}\frac{(D - t)}{4t} \tag{2.5}$$

Because a pipe in the field is a continuous pressure vessel, this additional tensile loading is not present. Thus, in experimental and analytical work with pipe specimens, a compressive stress of the same magnitude as σ_l must be applied. For the pipe modelled in this study, a value of σ_l = -40.3 MPa was applied to the pipe wall.

The combined axial loads were applied to the model via the thick plate elements at the pipe ends. An external pressure was applied to the end plates to supply the load. The required pressure, p_{end}, in MPa was determined by:

$$p_{end} \cong (\sigma_\alpha + \sigma_\upsilon + \sigma_l)\frac{4t}{D} \tag{2.6}$$

An external pressure load of –10.1 MPa was applied to the pipe end caps to simulate all axial loading that a test pipe would be exposed to.

A pressure load was chosen as the means to apply the axial load for three reasons. First, it would cause an even distribution of the stresses to all locations of the pipe wall, avoiding any unrealistic stress concentrations. Second, it would simulate the method in which the axial load would be applied to the experimental specimens. Finally, by using a pressure load, the axial load would always remain parallel with the pipe wall as the end plates rotate with pipe. The axial load would be a follower load and thus minimize any second order moments in the pipe during bending.

2.2.7.3 Imposed Curvature

Buried pipelines may undergo displacement induced loading in addition to the loads described in the previous sections. A pipeline is subjected to curvature when differential soil settlement occurs along the pipe length. Differential soil settlement can result from frost heave, soil consolidation or slope movement. Figure 2.6 shows a typical differential settlement profile for an initially straight section of line pipe. At the transition zones between the unsettled and settled soil, the pipe is forced to curve in order to retain its original configuration away from the transitions. The induced curvature in the pipe creates flexural stresses in the pipe wall. The stresses on the compression face of the pipe add to the already present compressive stresses (due to operational loads). As soil

settlement continues, the curvature and flexural stresses increase. At a certain point, the compressive strains in the pipe wall exceed the local buckling strain of the pipe and a wrinkle forms.

In the analytical model, the curvature induced by differential soil settlement was applied by prescribing monotonically increasing rotations at the pipe ends. This was accomplished in the FE model by setting the in-plane rotation (ϕ_3) of the reaction points to a certain value. An end-moment required to cause the rotation would then be determined by ABAQUS and a moment-curvature history for the pipe was recorded.

2.2.8 Sleeve Modelling

External sleeves were applied to the wrinkled pipe in the FE analysis in order to improve the post buckling performance of the pipe. Two types of sleeves were modelled: steel sleeves and FRP composite sleeves. Both types of sleeves were modelled using S4R elements and the element sizes were identical to those of the pipe elements. The sleeves were modelled, essentially, as a second layer of elements attached to the pipe. Different attachment methods were employed for the steel and FRP sleeves because of their different construction.

Steel sleeves installed on pipelines are simply larger diameter pipes that are cut in half, placed around the pipe, rejoined by welding and then welded to the pipeline. There is a gap between the pipe and the sleeve along the sleeve length, except at the ends. This feature was incorporated into the FE model. Figure 2.7 illustrates the technique used to join the sleeve to the pipe in the model. The nodes of the sleeve at its ends were rigidly connected to the corresponding pipe nodes using the rigid BEAM constraint that was used for the reaction points. This was meant to simulate the rigid weld that would connect the sleeve and pipe. Everywhere else along the sleeve length, the sleeve nodes were independent of the pipe nodes. It should be noted that the pipe and sleeve elements were not centred about their respective nodes. Element offsets were used to insure that contact between the two surfaces would not occur at time of installation.

The procedure for applying the FRP sleeve to the pipe in the experimental program would be different than that for the steel sleeve. Therefore, a different connection method was employed in the model. The FRP sleeve would be bonded to the pipe using epoxy resin. The bond would be continuous along the entire length of the sleeve, not localized to the ends of the sleeve, which was the case for the steel sleeve. One modelling option that was considered was to simply use the same model as the steel sleeve, but to connect all the sleeve nodes to the corresponding pipe nodes with the BEAM connection. A second option was to have the pipe elements and sleeve elements share the same nodes. This would eliminate the need for a separate set of nodes for the sleeves and many BEAM connections, making the model simpler and faster to analyze. This later option was chosen for the FE analysis. The connection of the FRP sleeve elements to the pipe elements is shown in Figure 2.7. The same offset used for the steel sleeve elements was used for the FRP elements. However, the FRP sleeve elements were in direct contact with the pipe elements, since the FRP would be wrapped onto the pipe during installation.

2.2.9 Analysis Procedure

The FE analysis of a sleeve repair on a wrinkled pipe was comprised of two main phases: wrinkling of a straight pipe segment and then repair of the pipe with external sleeving. The two phases were further divided into several load steps. In the first step, the sleeve elements were removed from the analysis, so that their presence would not affect the behaviour of the plain pipe prior to actual sleeve repair. For the steel sleeve repairs, the sleeve elements were then replaced with elements with essentially no stiffness. This was necessary so that the geometry of the sleeve nodes would match that of the pipe nodes after large deformations had occurred. Replacement of the FRP sleeve elements with similar low-stiffness elements was unnecessary, since the pipe and sleeve elements shared the same nodes. After the "temporary" low-stiffness sleeve had been activated (for the steel sleeve), the pipe was pressurized to 3,300 kPa in one load increment. This constituted the first load step.

The second step involved the application of the axial load on the pipe. As described in Section 2.2.7.2, the axial load was applied via an external pressure load on the end caps of the pipe. Like the pressurization of the pipe, the axial load was applied in one load increment.

The third step was to apply prescribed rotations at the reaction points in order to trigger wrinkling of the pipe. The prescribed rotations were applied in multiple increments, according to the automatic increment control feature of ABAQUS. Initially, the end rotations were not symmetric. The rotations were applied at a ratio of 0.9:1 for the left and right ends of the model, respectively. This technique eliminated symmetric buckling, and gave a more realistic resemblance to field observations of pipe wrinkling (Yao and Murray, 2000). However, symmetric rotation would occur in experimental work and thus later models incorporated equal end rotations. Once the prescribed rotations were achieved, the next step in the analysis proceeded.

The first phase of the analysis was ended when the wrinkle had achieved a height that would be detectable in the field. The second phase consisted of the fourth load step. The fourth step began with the activation of the sleeve elements and removal of any temporary sleeve elements from the model. Next, the end rotations were increased to an arbitrary level (approximately two times the rotation at the time of sleeve repair) in order to observe the effect of the repair on the behaviour of the pipe. As was the case with the third step, the automatic incrementation control in ABAQUS was used to determine the rotation steps used. Once the prescribed rotation for the fourth step was achieved, the analysis was terminated.

During the analysis, several parameters were automatically recorded by ABAQUS for use in post processing. The end rotations and end moments were recorded at each load increment so that a moment – curvature history could be plotted. Also, the deformed shape of the pipe was stored in order to track the growth of the wrinkle as the curvature in the pipe was increased. Global moment – global curvature and wrinkle height – global

curvature formed the basis of the analysis of the FE data. This will be discussed in greater detail in the following sections.

2.3 Sleeve Repair Methods

Repair methods using various sleeves were modelled in this study. In previous analytical work (Yao and Murray, 2000) the use of a single steel sleeve to repair the wrinkled pipe was examined. The thickness of the sleeve and the timing at which the sleeve was applied were held constant. Timing of the repair refers to the level of global curvature in the pipe at the time of sleeve repair. Various sleeve lengths, ranging from $0.5d$ to $2d$ were modelled. Results showed that a gain in post buckling moment capacity would occur, but as curvature was increased, a secondary buckle would form adjacent to the sleeve repair and the moment capacity would drop. A typical moment – curvature plot from that study is shown in Figure 2.8.

This study set out to expand on the work done by Yao and Murray (2000). From their work, five parameters were identified as having the potential to impact the behaviour of the repair. Three parameters related to the geometry of the sleeve repair scheme. The number of sleeves used on the pipe, the spacing of the sleeves and sleeve length were examined in this project. The stiffness of the sleeve was believed to have a large impact on the repair. Therefore, the thickness and elastic modulus of the sleeve were studied. Finally, the timing of the sleeve repair was examined.

2.3.1 Sleeve Geometry

Three general types of sleeve repair geometries were investigated. The first geometry was that of the single sleeve. For the single sleeve repair, one sleeve would be fixed to the pipe at the location of wrinkle formation. A single sleeve repair is illustrated in Figure 2.9.

The second type of sleeve repair examined is referred to as the "even" sleeve. The even sleeve geometry is shown in Figure 2.10. The even sleeve repair consists of an even number of separate sleeves connected to the wrinkled pipe. Figure 2.10 shows a repair with two sleeves. The sleeves were placed symmetrically about the wrinkle with a gap

between them. The size of the gap was typically half of the wrinkle length. This resulted in only a portion of the wrinkle being covered by the sleeves at the time of repair. The need for a gap between the sleeves requires further explanation.

A gap between the sleeves was provided so that the wrinkle would be confined to grow between the two sleeves. It was believed that by confining the available space the wrinkle had to grow in, an increase in moment capacity would be observed. In laboratory testing conducted on compression buckling of line pipe (Das *et al.,* 2000) it was observed that an increase in post buckling load-carrying capacity could be achieved. An increase would occur if the two inside circumferential edges of the wrinkle were forced into contact (see Figure 2.11). Once the two edges were in contact, the load path was re-established and the load resistance would increase. In compression testing, this was accomplished by compressing the pipe to a point where the two edges would touch. For a pipe in flexure, this phenomenon is not likely. However, by using two sleeves with a gap, it was believed that the sleeves could force contact with the wrinkle on the outside of the pipe and produce a similar effect.

A third sleeve geometry was a combination of the single and even sleeve designs. It was designated as the “odd” sleeve design and is shown in Figure 2.12. The odd sleeve design consisted of a single sleeve, placed directly over top of the wrinkle, coupled with an additional sleeve on either side of the single sleeve. These sleeves were separated with the same type of gap used in the even sleeve.

The odd sleeve was incorporated due to potential drawbacks with the single and even sleeve designs. It was shown by Yao and Murray (2000) that for single steel sleeve repairs, secondary wrinkling would occur immediately adjacent to the sleeve and the moment capacity of the pipe would drop rapidly. This was not the case for the even sleeve repair. For the even sleeve, moment capacity would be maintained as the wrinkle was constrained by the adjacent sleeves. However, the constraint provided by the sleeves could pose a problem in field applications. Excessive contact between the sleeves and the wrinkle could serve as the initiation point for fracture in the pipe if cycles of

unloading and loading were to occur (Das *et al.*, 2000). Fracture of the pipe would be a catastrophic failure, and must to be avoided. By using the odd sleeve, it is believed that the attributes of the single sleeve and the even sleeve could be attained. The single sleeve, placed over top of the wrinkled zone, would stiffen the pipe and protect the wrinkle from fracture, but it would eventually trigger secondary wrinkle development. With proper sleeve design, the secondary wrinkle would form in the gap between the middle sleeve and the outer sleeve. Thus, the secondary wrinkle would now be constrained in its growth and the rapid drop in moment capacity could be avoided. Fracture at the secondary wrinkle was still a possibility, but the probability would be lower than that of the primary wrinkle in the even sleeve scenario, because of the delayed formation of the secondary wrinkle.

Using the even and odd sleeve configurations, the effects of sleeve spacing (the gap size) and sleeve length were examined.

2.3.2 Sleeve Stiffness

The stiffness of the sleeve was believed to have a significant impact on the behaviour of the repair. When a pipe wrinkles, a plastic hinge forms at the wrinkle location. The hinge has very little stiffness, only that from the strain hardening of the pipe steel. Therefore, any addition to the stiffness of the hinge, via an external sleeve, will have a significant impact on the behaviour of the pipe. The stiffness of the sleeve is the product of two variables, the amount of material present and the type of material used.

2.3.2.1 Thickness

The first contributor to stiffness of the sleeve is the amount of material used. If one unwraps the sleeve from the pipe, a simple rectangular plate will be formed. For a unit width or length of sleeve, the thickness of the sleeve will define its cross-sectional area and subsequently the amount of material present in the sleeve to resist loading.

Sleeve thickness was varied amongst the different steel sleeve models. For steel sleeves, the thickness values used were limited to those of commercially available line pipe (which would be used to form the sleeves). Values used were 6.35 mm, 7.93 mm, 9.53

mm and 12.70 mm. While there are thinner and thicker line pipe in production, the four sizes chosen were the most common in industry for the pipe size used for the sleeve.

For FRP sleeves, the thickness was arbitrarily chosen at 5.0 mm because the FRP sleeve would be custom made and no standard thickness existed. A thickness of 5.0 mm was chosen for simplicity and proximity to the wall thickness of the pipe specimen. The FRP sleeve thickness remained constant for all models tested.

2.3.2.2 Elastic Modulus

The material property of interest is the elastic or Young's modulus. The elastic modulus of a material is determined through the relationship between stress and strain, Hooke's Law, for the material (Kaw, 1997). Hooke's Law for a linear elastic isotropic material in three-dimensional form is given in Equation 2.7:

$$\begin{bmatrix} \varepsilon_x \\ \varepsilon_y \\ \varepsilon_z \\ \gamma_{yz} \\ \gamma_{zx} \\ \gamma_{xy} \end{bmatrix} = \begin{bmatrix} \frac{1}{E} & -\frac{\upsilon}{E} & -\frac{\upsilon}{E} & 0 & 0 & 0 \\ -\frac{\upsilon}{E} & \frac{1}{E} & -\frac{\upsilon}{E} & 0 & 0 & 0 \\ -\frac{\upsilon}{E} & -\frac{\upsilon}{E} & \frac{1}{E} & 0 & 0 & 0 \\ 0 & 0 & 0 & \frac{1}{G} & 0 & 0 \\ 0 & 0 & 0 & 0 & \frac{1}{G} & 0 \\ 0 & 0 & 0 & 0 & 0 & \frac{1}{G} \end{bmatrix} \begin{bmatrix} \sigma_x \\ \sigma_y \\ \sigma_z \\ \tau_{yz} \\ \tau_{zx} \\ \tau_{xy} \end{bmatrix} \qquad (2.7)$$

where:

ε= normal strain in the x, y or z-directions

γ= shear strain in the y-z, z-x or x-y planes

σ = normal stress in the x, y or z-directions

τ = shear stress in the y-z, z-x or x-y planes

E = elastic or Young's modulus

ν = Poisson's ratio

G = shear modulus = $\dfrac{E}{2(1+\upsilon)}$

The steel sleeves were modelled as isotropic with an elastic modulus of 203,500 MPa and a Poisson's ratio of 0.3. These values are typical for all modern steels. The steel in the sleeves was assumed to have the same stress-strain characteristics as the steel for the pipe, since both would be line pipe steel.

The FRP sleeves required a more complicated material model, compared to the steel sleeves. For steel, the material is assumed to be isotropic. That is, the material properties are identical in all directions. Isotropy allows Hooke's Law to be defined in all directions (as shown in Equation 2.7) with only two independent elastic constants, E and ν. Isotropy greatly simplifies the parameters required to describe material behaviour. Because the FRP sleeve is made up of two materials (fibre and matrix) that have different elastic moduli in different directions, an isotropic model cannot be used to describe the material. For an anisotropic material (material with different properties in different directions), 21 independent elastic constants are required to relate strains and stresses. However, several assumptions can be made about FRP that reduce the number of elastic constants that need to be defined (Kaw, 1997).

The first assumption that can be made is that FRP is orthotropic. An orthotropic material has three mutually perpendicular planes of material symmetry. For a FRP composed of continuous fibres arranged in a rectangular array (as is the case for most unidirectional fibre composites), this assumption is valid. By applying this assumption, the required elastic constants can be reduced from 21 to 9. If the FRP is thin and there are no significant loads applied out-of-plane, the composite can be considered to be in a state of plane stress. That is, all out-of-plane stresses (σ_3, τ_{23}, τ_{31}) are equal to zero. This reduces the number of elastic constants required from 9 to 4 and simplifies Hooke's Law to the form given in Equation 2.8:

$$\begin{bmatrix} \varepsilon_1 \\ \varepsilon_2 \\ \gamma_{12} \end{bmatrix} = \begin{bmatrix} \frac{1}{E_1} & -\frac{\upsilon_{12}}{E_1} & 0 \\ -\frac{\upsilon_{12}}{E_1} & \frac{1}{E_2} & 0 \\ 0 & 0 & \frac{1}{G_{12}} \end{bmatrix} \begin{bmatrix} \sigma_1 \\ \sigma_2 \\ \tau_{12} \end{bmatrix} \tag{2.8}$$

To meet the requirements of Equation 2.8, four material properties (E_1, E_2, v_{12}, G_{12}) were required to describe the FRP material for the sleeve. For simplicity in defining FRP material properties, the primary axes of the FRP composite (1 and 2) coincided with the longitudinal (1) and hoop (2) directions of the pipe. Several combinations of E_1 and E_2 were used in the models to simulate the different FRP composites currently produced. The major Poisson's ratio (v_{12}) and the in-plane shear modulus (G_{12}) were held constant for all the models. The shear modulus was held constant because very little shear deformation was expected for the sleeve application and shear was not anticipated to have an impact on the sleeve behaviour. Table 2.1 summarizes the material variables used for FRP sleeves in this study.

2.3.3 Timing of Sleeve Repair

The final parameter studied in the preliminary FE analysis was the timing of the sleeve repair. In the previous analytical work conducted by Yao and Murray (2000), the sleeve repair was made almost immediately after local buckling had occurred in the pipe. While this is likely the best time to make a repair, it was deemed unreasonable that a repair could physically occur at such an early stage. In order to place a repair sleeve on a pipe, the wrinkle must first have a magnitude sufficient for detection. The method for detection used on the Norman Wells Pipeline wrinkles was the internal geometry inspection tool, the Geopig. While the Geopig is able to detect very small changes in internal diameter of the pipeline, which would occur at the onset of wrinkling, the frequency of inspection is usually limited to once per year. It has been observed (Wilkie *et al.*, 2000) that during the period between inspections, wrinkle height can increase substantially. Therefore more realistic repair timing had to be incorporated into the FE model. Because the wrinkle could be found at any time, an arbitrary application point,

beyond initial wrinkling, was chosen for the majority of the models analyzed. The repair sleeve was applied at a curvature of approximately 60x10^{-6} radians/mm, equivalent to 40% of the total curvature imposed onto the pipe. The wrinkle magnitude at time of repair of was approximately 15 mm. This was deemed a reasonable magnitude based on wrinkles discovered in the field.

A limited number of models using FRP sleeves were generated with repair timings other than 60x10^{-6} radians/mm. It was believed that the effect of repair timing would be independent of sleeve material or geometry, so only one type of sleeve detail was used to study this effect.

2.3.4 Model Designation

Two forms of model designation were adopted for the preliminary FE study. Steel sleeve repairs were described using the general designation **W**s**X**d**Y**g**Z**, where:

W = type of sleeve geometry: 1 for single sleeve, 2 for even sleeve, 3 for odd sleeve;

X = length of sleeve(s) in nominal diameters of the pipe: 1 for a 1*d* or 305 mm long sleeve, 2 for a 2*d* or 610 mm long sleeve, 05 for a 0.5*d* or 152 mm long sleeve;

Y = length of the gap between sleeves for the even and odd geometries, in inches;

Z = wall thickness code for the sleeve: a = 6.35 mm thick, b = 7.93 mm, c = 9.53 mm, d = 12.70 mm.

FRP sleeves used a designation with the general format of **V**s-**WW**-**XX**-**YY**-**Z**, where:

V = type of sleeve geometry; 1 for single sleeve, 2 for even sleeve, 3 for odd sleeve;

WW = elastic modulus of the sleeve in the longitudinal pipe direction (E_1) in MPa *10^3;

XX = elastic modulus of the sleeve in the hoop pipe direction (E_2) in MPa *10^3;

YY = length of sleeve(s) in inches;

Z = length of the gap(s) between the sleeves in inches.

2.4 Preliminary Finite Element Analysis Results

Using the parameters discussed in Section 2.3, the preliminary finite element parametric study was conducted. The results of this study are presented in the following sub-sections. The results for the steel and FRP sleeve repairs have been separated because of the different ways the sleeves were modelled for each material (as shown in Figure 2.7). It will be shown, however, that there are many similarities in the behaviours of the repairs between the steel and FRP sleeves. These similarities are due to the response of the pipe to wrinkle development, rather than the details of the sleeve used. Regardless, for consistency, the two sleeve materials have been separated in the discussion.

2.4.1 Steel Sleeve Repairs

2.4.1.1 Single Sleeve Geometry

Yao and Murray (2000) examined the single sleeve repair. A NPS 14 pipe section with a wall thickness of 6.477 mm was used to form the sleeve. The use of a NPS 14 sleeve resulted in a clearance of 9.5 mm between the outside of the undeformed NPS 12 pipe wall and the inside wall surface of the NPS 14 sleeve.

Of the parameters discussed in Section 2.3, the study by Yao and Murray examined only the effect of the sleeve length on the repair. The moment-curvature plot of a 1*d* sleeve repair is shown in Figure 2.8. Similar behaviour was observed for different sleeve lengths; with the maximum moment after sleeve repair increasing as the sleeve length was increased. All single sleeve repairs resulted in the formation of a secondary wrinkle immediately adjacent to the sleeve repair. The drop in moment capacity seen in Figure 2.8 after sleeve repair can be attributed to secondary wrinkle development.

The 1*d* sleeve repair analyzed by Yao was repeated in this study. The application point was delayed to 60×10^{-6} radians/mm. Figure 2.13 shows the moment – curvature plot for this case. A jump in moment capacity to the pre-buckling level occurs following the application of the sleeve, but capacity drops, as the secondary wrinkle forms adjacent to the sleeve.

2.4.1.2 *Even Sleeve Geometry*

The main characteristic of the even sleeve that distinguishes it from the single sleeve geometry is the spacing of the two sleeves, referred to as the gap size. In order to design an effective even sleeve, the appropriate gap size must be used if the stiffening effect described in Section 2.3.1 is to be achieved. Figure 2.14 shows the moment – curvature response for two even sleeve repairs, one with a 2-inch (50 mm) gap and the other with a 4-inch (100 mm) gap. If the gap size is too small, the two sleeves essentially act as one sleeve and no improvement in performance is achieved. When the gap size is increased, the stiffening that was predicted is observed, although at very high curvature level. If the gap was slightly smaller, the stiffening effect would have occurred sooner, giving improved results. Based on these observations, one can extrapolate that if the gap is set too large, no stiffening effect will occur. It should be noted that the optimum gap size is dependant on the geometry of the wrinkle. For the NPS 12 pipe modelled in this study, the initial wrinkle was approximately 150 mm long. By covering approximately one half of the wrinkle with the sleeve, the stiffening effect would be optimized. For a different size pipe, the gap size used in this study may not be effective. This gap size would have to be determined on a case-by-case basis.

The second parameter explored was the sleeve thickness. In Figure 2.15 the results of four repair schemes are shown. Each scheme consisted of 1*d* sleeves with a 4-inch (100 mm) gap. The sleeve thickness was varied from 6.35 to 12.70 mm. Very little change in behaviour is seen amongst the different sleeve repairs. It is likely that the gap size chosen was too large. If the gap size was reduced one might predict that as the sleeve thickness increased, performance might increase due to the added stiffness.

The effect of sleeve length is shown in Figure 2.16. One can see that as the length of the sleeve is increased, the peak moment after sleeve application is increased. This is consistent with what was observed in the single sleeve analysis. As one increases the sleeve length, more of the pipe is stiffened and thus the moment capacity is increased. However, the impact of sleeve length is minor compared to the impact of the gap size for the even sleeve configuration.

2.4.1.3 *Odd Sleeve Geometry*

Gap size, sleeve thickness and sleeve length were examined for the odd sleeve configuration. Figure 2.17 gives the moment – curvature response for two odd sleeve designs with different gap sizes. Based on the results of the even sleeve analysis, gap sizes of 4 inches (100 mm) and 5 inches (125 mm) were modelled. The shorter gap does give improved results, but not as drastic as was observed for the even sleeve. When the deformed shape of the model was examined, it was determined that the gap in the odd sleeve was not performing the same function as the gap in the even sleeve. Rather than creating a space that the wrinkle could grow in so that stiffening could take place (as was the intent with the even sleeve gap) the odd sleeve gap affected the amount of restraint the secondary wrinkle would experience. It did this by impacting the location of the outside sleeve. The shorter the gap, the closer the outer sleeve would be to the main sleeve. When the secondary wrinkle formed, it would form in a certain location adjacent to the main sleeve, regardless of the location of the outer sleeve. As the gap size was reduced, the portion of the secondary wrinkle located in the stiffer outside sleeve was increased. This caused the moment capacity of the pipe to be increased slightly.

If the effect of sleeve thickness on the behaviour of the pipe is examined, the opposite trend that was observed for the even sleeve repair is seen. Figure 2.18 shows that the repair with a 12.7 mm thick sleeve behaves much like the single sleeve repair, while the 9.53 mm repair is much more stable. This difference can be explained by looking at the growth of the primary wrinkle, designated w_1, and the secondary wrinkle, w_2, versus curvature in Figure 2.19. For the thicker sleeve, w_1 is stopped very quickly after the application of the sleeve. The accumulated strain in the system is quickly shed through the rapid growth of w_2. For the thinner sleeve, w_1 continues to grow, but at a lower rate than the un-repaired pipe. Significantly less strain is built up in the system and thus w_2 grows much more slowly. This observation is very significant for the design of an optimum sleeve repair. These figures show that the growth rate of w_1 has a significant effect on the ability to maintain moment capacity in the pipe. Therefore, by efficiently controlling w_1, a sound repair scheme can be provided.

The impact of sleeve length in the moment curvature behaviour of the odd sleeve repair is shown in Figure 2.20. As was observed with the single and even sleeve configurations, an increased sleeve length for the odd repair resulted in an increase of the post-buckling moment capacity prior to the formation of w_2.

2.4.2 FRP Sleeve Repairs

2.4.2.1 Single Sleeve Geometry

A limited number of single FRP sleeves were modelled. The impact of E_1 and E_2 on the behaviour of single FRP sleeves was the only parameter studied. All of the single FRP sleeve models analyzed displayed the same failure pattern seen in steel single sleeves, the formation of w_2 immediately adjacent to the sleeve. By studying Figure 2.21, it becomes evident that the moduli of the sleeve have a definite impact on sleeve behaviour. For a long sleeve, lower values of E_1 and E_2 lead to better performance of the sleeve. This occurs because w_1 is allowed to grow somewhat longer due to lower stiffness of the sleeve. It is observed that E_1 has a significant impact on the behaviour of a long sleeve. Comparing the curves for 15-15 and 150-15, a distinct difference is present. This makes sense because for a long sleeve that is bonded along its entire length to the pipe, E_1 will have a large impact on the overall stiffness of the sleeve.

2.4.2.2 Even Sleeve Geometry

The same parameters studied for the steel even sleeves were studied for the FRP even sleeve: gap size, sleeve stiffness (E_1 and E_2 for the FRP sleeve) and sleeve length. Figure 2.22 gives the moment – curvature plots for varying gap size sleeves. As was the case with the even steel sleeve repair, a gap that is too short will make the two separate sleeves act like a single sleeve. One difference in the FRP sleeve behaviour, compared to similar steel even sleeves, is the lack of the stiffening effect. A likely explanation for this involves the placement of the FRP sleeve on the wrinkle relative to the wrinkle height. For the steel sleeve repair, a space existed between the outer surface of the pipe and the inner surface of the sleeve. This was illustrated in Figure 2.7. Subsequently, when the wrinkle would come into contact with the sleeve, contact would occur higher up on the wrinkle, leading to the stiffening effect at an earlier curvature. Because the FRP sleeve

was directly attached to the pipe without a space, contact occurred lower on the wrinkle. The load path was not re-established at the same levels of curvature as the steel sleeve. It is believed that if the total amount of curvature applied to the FRP sleeve was increased, the stiffening effect would have been observed.

It was anticipated that the moduli of the sleeve would have a large impact on the behaviour of the repair. This was confirmed in the analysis. Figure 2.23 shows the moment – curvature behaviour for the same FRP sleeve geometry with various levels of E_1 and E_2. For the even sleeve detail, E_1 has a major impact on the repair. At high levels of E_1, the multiple sleeves act like one sleeve, similar to what was seen for gap sizes that were too small. E_1 had the impact observed because of how the gap region was modelled.

In the field application of an FRP sleeve repair, it was assumed that a thin layer of FRP would be applied to the whole repair region in order to form a sound base for bonding of the major sleeve sections. This would result in thin "weak" sections of the sleeve, the gaps, and thicker "strong" sleeve sections. For high levels of E_1, the gap sections acted as a bridges for the sleeve stiffness in the longitudinal direction of the pipe, creating in essence one long sleeve. As E_1 is reduced, this effect is minimized and the strong sleeves act separately. Having a thin layer of FRP in the gaps does have a benefit. The extra material aids the strong sleeve sections in slowing down the wrinkle growth and thus improving moment capacity. The gap material also has the potential to assist in w_1 slowdown if the strong sleeves are accidentally placed too far apart. If this occurred without material in the gaps, the repair would likely not give any benefit.

Figure 2.23 indicates that E_2 has a very significant impact on the performance of the sleeve. At very low levels of E_2, the moment capacity of the system is not increased significantly and the ductility gained is not very large. Ductility in the context of this study is defined as the curvature for a given level of moment. As E_2 is increased, the moment capacity and ductility increase. These patterns are explained when the growth of w_1 is studied in Figure 2.24. As E_2 is increased, the growth rate of w_1 decreases. A

similar pattern was observed with the steel odd sleeves as the sleeve thickness was increased. This makes sense since the stiffness of the sleeve in the hoop direction is a function of the modulus (E_2) and thickness of the sleeve. In the case of the FRP sleeve, the hoop modulus was varied while the thickness was maintained. It is apparent that FRP composites are well suited for an even sleeve type of repair, since both the hoop modulus and sleeve thickness can be easily changed to give an optimum repair detail.

From the even sleeve analysis, it is shown that the sleeve length has a minor effect on the performance of the sleeve. In Figure 2.25 the behaviour of repairs with sleeves 6 inches (150 mm), 4 inches (100 mm) and 3 inches (75 mm) long is displayed. While there is some variability in the models, the change is not significant. This pattern is expected since, as was shown previously, E_2 plays a dominant role in the performance of the sleeve, when E1 is low. As long as sufficient coverage is placed close to the wrinkle in the longitudinal direction, the hoop modulus of the sleeve will be utilized. A longer sleeve would only have an effect if the longitudinal stiffness of the sleeve were increased.

2.4.2.3 Odd Sleeve Geometry

The effects of modulus, gap thickness, gap size, sleeve length and timing of the sleeve repair were examined for the FRP odd sleeve geometry. Figure 2.26 shows the moment – curvature behaviour for a series of odd sleeve repairs. As E_2 is increased and E_1 is kept at a low value, the post-buckling moment capacity is increased. This is consistent with the observations of the FRP even sleeve repair. At high levels of E_1, the behaviour of the sleeve displayed small variations with changes in E_2, with slightly higher ductility resulting from lower values of E_2. It was observed that even though the gap size used in the models was the same as that used in the steel sleeve repair, w_2 did not form in the gaps, but at the outside of the sleeve area. The thickness of the gap was believed to have an impact on the location of w_2 formation and thus was investigated.

To study the effect of the gap thickness on the sleeve repair, a high modulus sleeve (E_1 and E_2 of $150*10^3$ MPa) was used. Figure 2.27 shows that as the gap thickness is reduced, the peak post-buckling moment is also reduced. Development of w_2 occurs

outside the sleeve zone for the 0.25 mm and 0.10 mm thick gaps. For gaps of 0.01 mm and smaller, w_2 formation occurs inside the sleeve zone and the behaviour remains relatively constant. This figure indicates that even a very small amount of FRP in the gap region prevents the initiation of secondary wrinkling between the sleeves. Therefore, for the odd sleeve configuration, material in the gap should not be provided if controlled w_2 formation is desired.

The effect of the gap size was then examined. Figure 2.28 shows that, like the steel odd sleeve, the FRP odd sleeve with a shorter gap increases the moment capacity more than the larger gap. It should also be noted that when the gap size was reduced to 3 inches (75 mm), w_2 formed outside the sleeve zone. This did not occur in the steel sleeves modelled. This behaviour is due to the different bonding methods employed for the steel and FRP sleeves. The steel sleeve was not continuously bonded to the pipe along its length. This allowed the wrinkle to form underneath the outer sleeve when the gap size was decreased. In the case of the FRP sleeve, the continuous bond between the FRP and the pipe restricted such growth and forced the wrinkle outside the sleeved area.

The effect of sleeve length on the behaviour of the FRP odd sleeve repair is shown in Figure 2.29. As the sleeve length is increased, the moment recovery increases. This is consistent with an increase in global stiffness of the pipe. The ductility changes in the pipe, however, are not consistent with previous findings in this study. That is, using a longer sleeve does not decrease ductility. When the wrinkle development of these models is examined in Figure 2.30, the ductility of the pipe is shown to increase when secondary wrinkling is allowed to occur in the gap. When w_1 is not stopped, but slowed with a shorter sleeve, the drop in ductility seen in Figure 2.29 occurs. This observation represents another key difference between the odd and even sleeve repairs and must be considered during sleeve design.

The final parameter studied in the odd sleeve geometry analysis was the timing of the sleeve repair. Based on the results from Yao and Murray (2000), it was anticipated that repairs completed at an earlier stage of wrinkle growth would show improved results.

The moment – curvature plot shown in Figure 2.31 confirms this assumption. If the wrinkle is caught at an earlier stage of growth, the repair can increase the moment capacity of the pipe a greater extent.

Based on the results of the preliminary numerical study presented in this chapter, an experimental program consisting of half-scale and full-scale laboratory specimens was carried out. This experimental program is described in Chapter 3.

Table 2.1 - Material Properties for FRP Sleeve Models

Longitudinal Modulus, E_1 (MPa)	Hoop Modulus, E_2 (MPa)	Shear Modulus, G_{12} (MPa)	Major Poisson's Ratio, ν_{12}
15,000	15,000		
75,000	75,000	7,500	0.27
150,000	150,000		

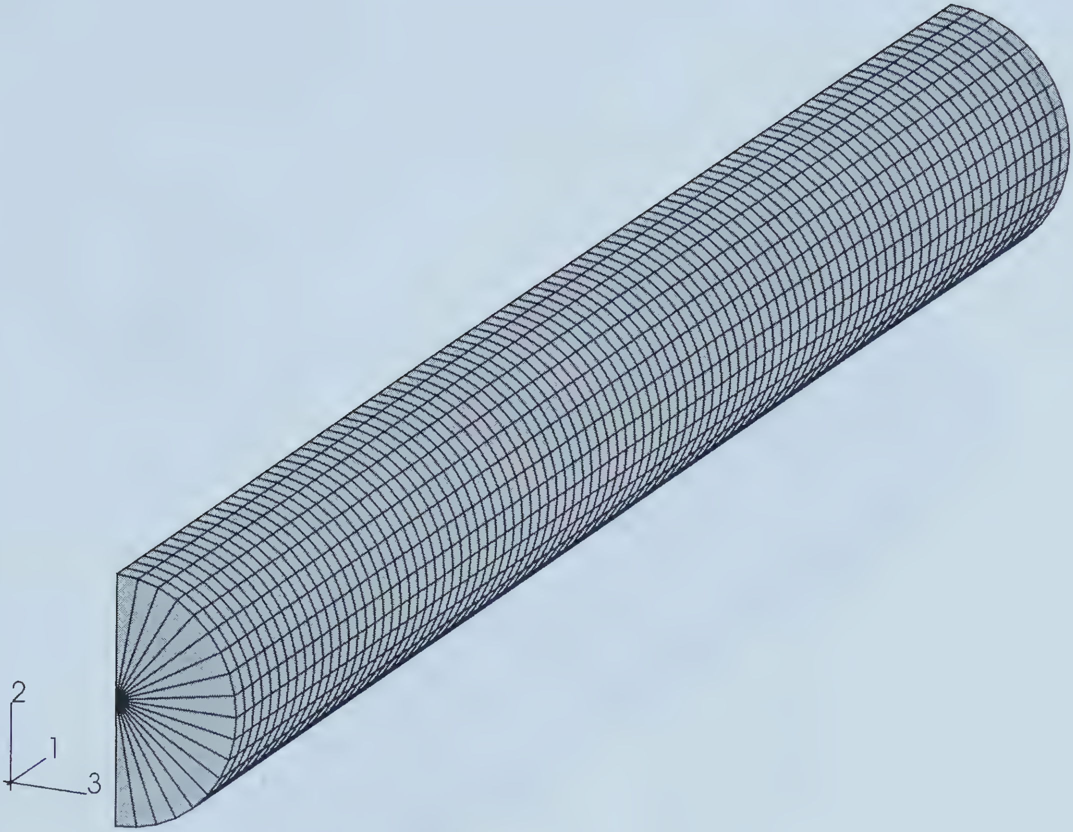

Figure 2.1 - Finite Element Discretization of Line Pipe Specimen

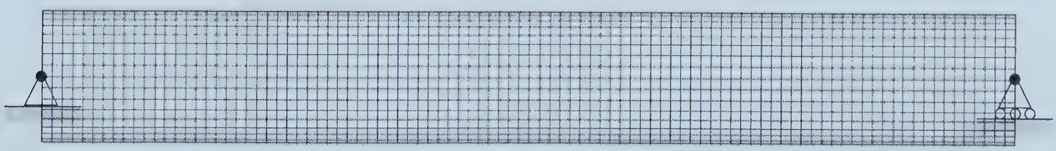

Figure 2.2 - Reaction Boundary Conditions

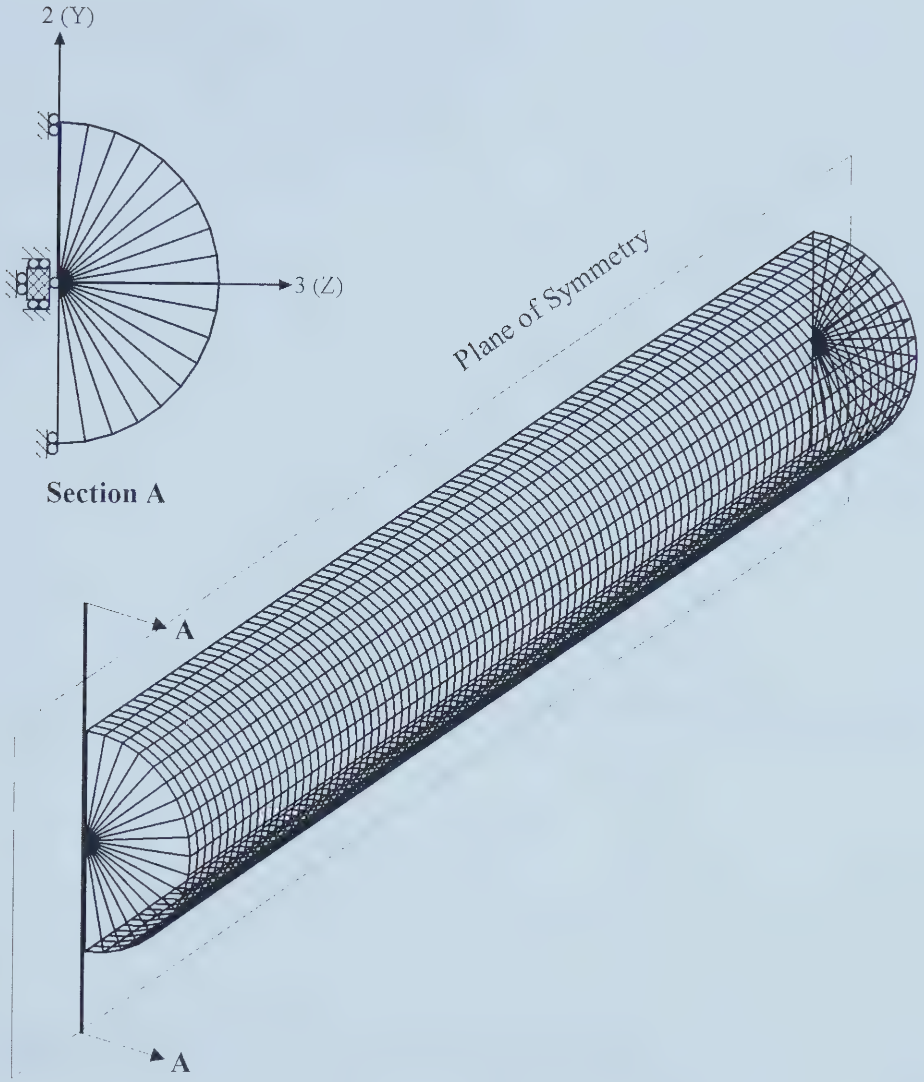

Figure 2.3 - Symmetry of Model and Corresponding Boundary Conditions

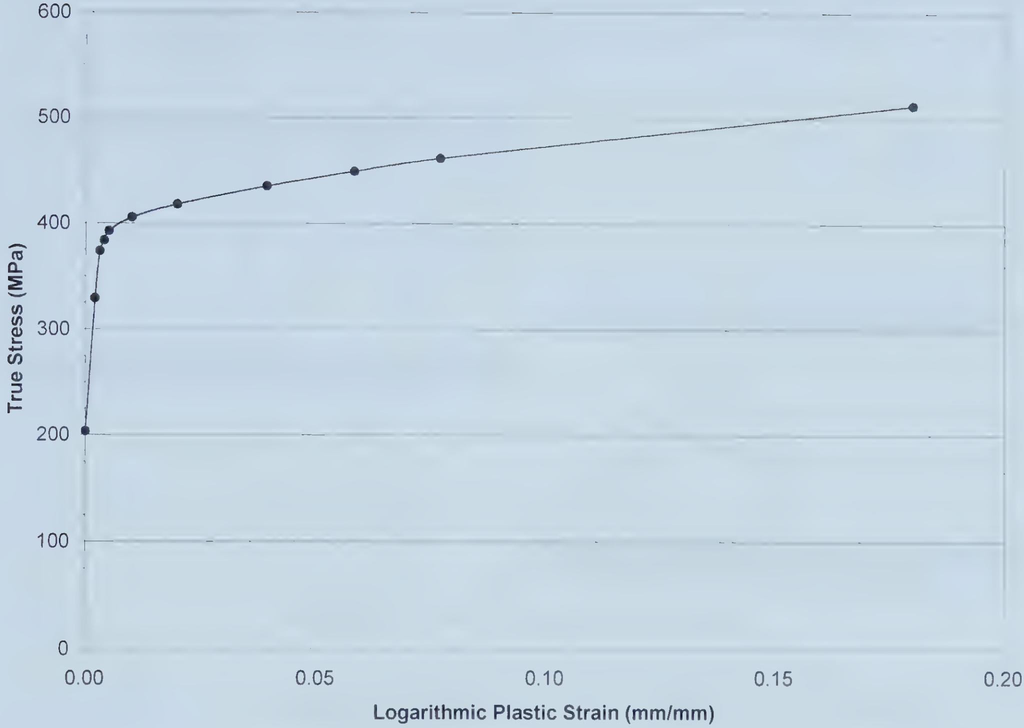

Figure 2.4 - True Stress vs. Logarithmic Plastic Strain for X52 Pipe Material

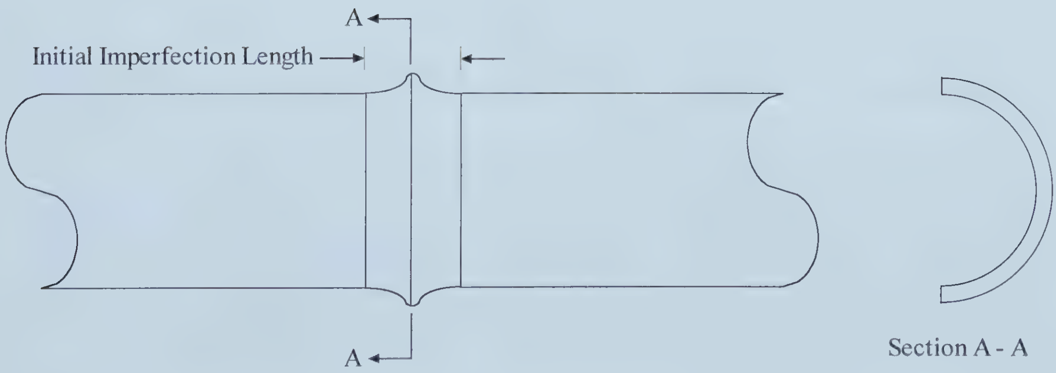

Figure 2.5 - "Bulge" Initial Imperfection Pattern used for FE Model

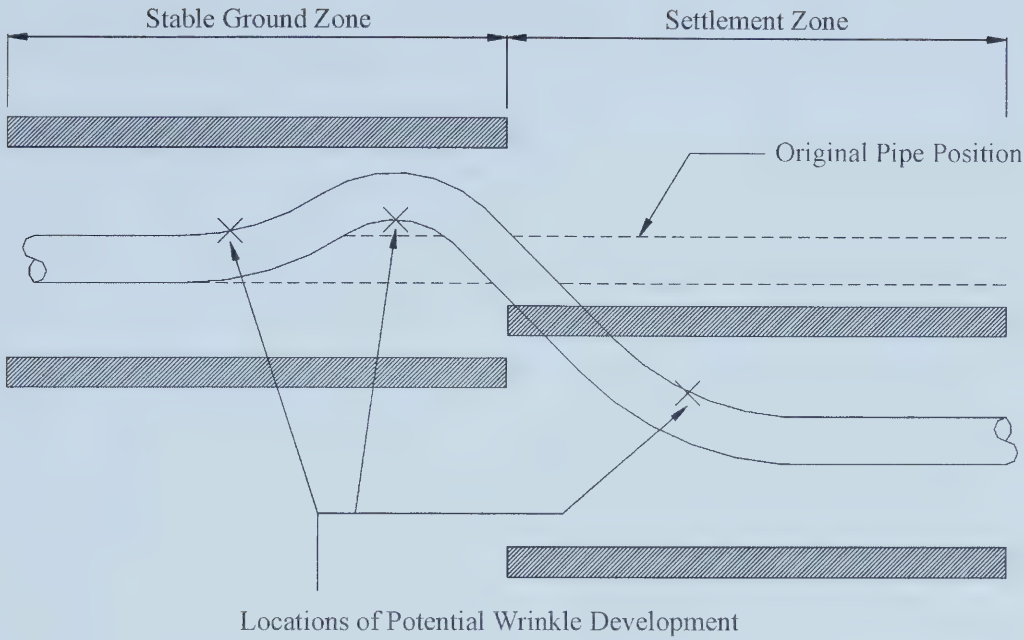

Figure 2.6 - Schematic of Pipeline Response to Differential Settlement

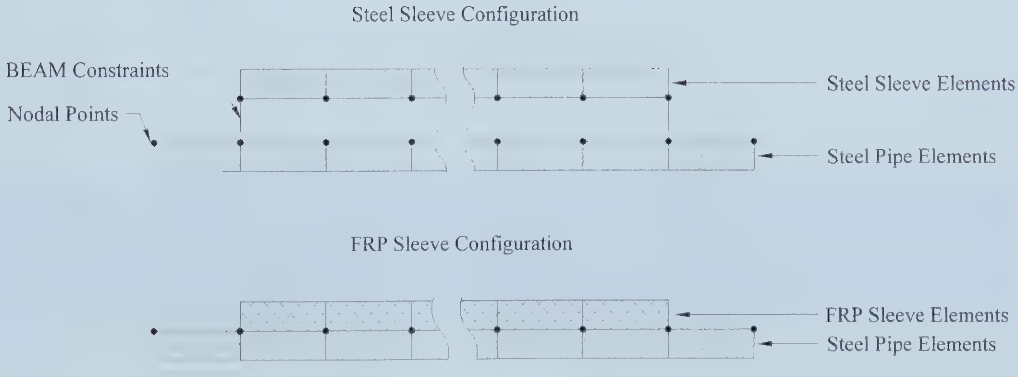

Figure 2.7 - Bonding Methods for Steel and FRP Sleeves in the FE Model

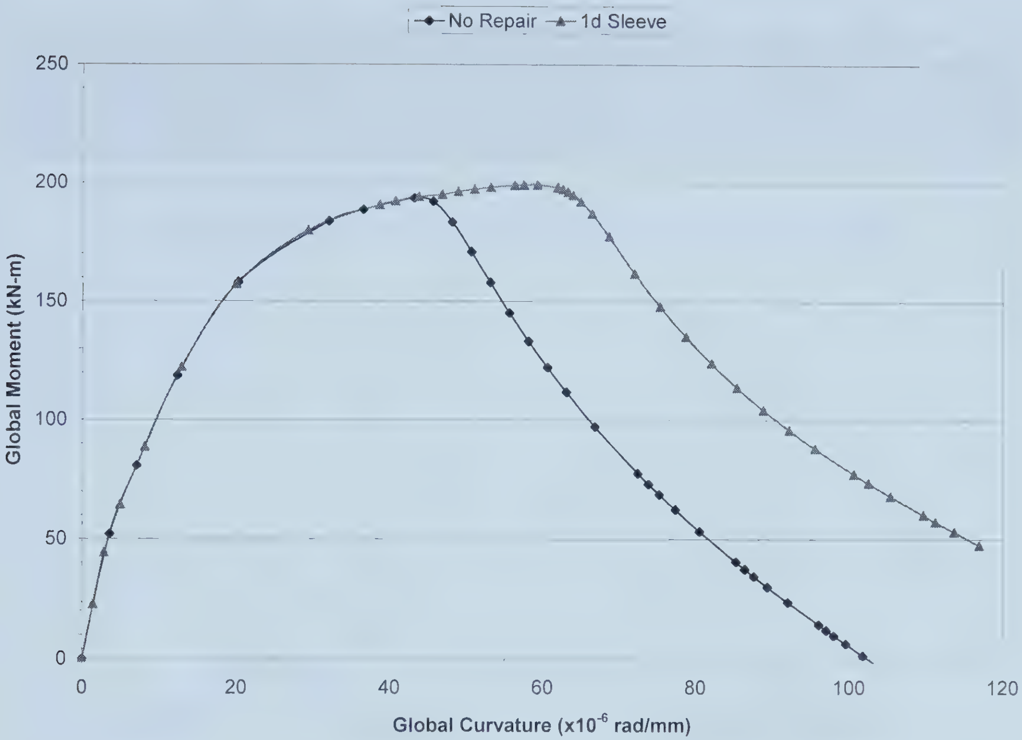

Figure 2.8 - Global Moment vs. Global Curvature for Single Steel Sleeve Repair (Yao and Murray, 2000)

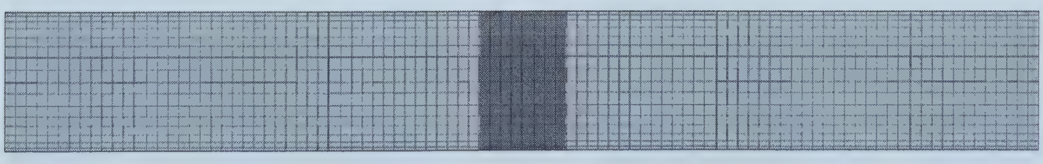

Figure 2.9 - FE Mesh for a Typical Single Sleeve Geometry

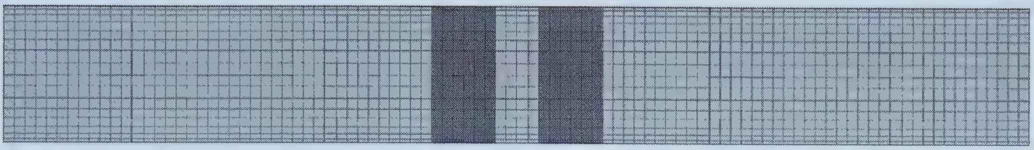

Figure 2.10 - FE Mesh for a Typical "Even" Sleeve Geometry

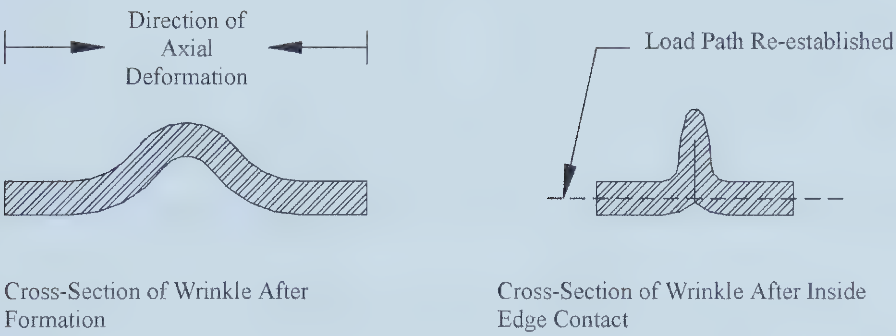

Figure 2.11 - Contact of Wrinkle Edges in Compression Loading

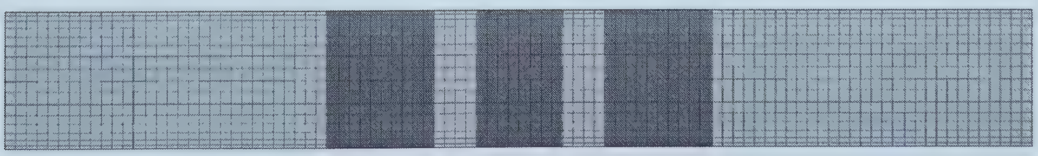

Figure 2.12 - FE Mesh for a Typical "Odd" Sleeve Geometry

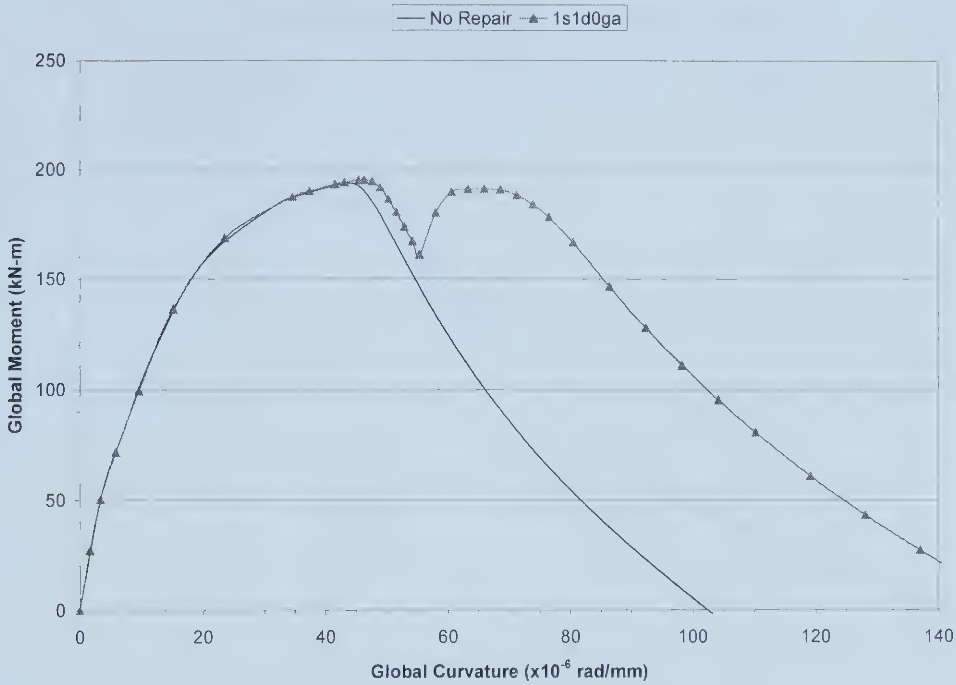

Figure 2.13 - Global Moment vs. Global Curvature for Single Steel Sleeve Repair

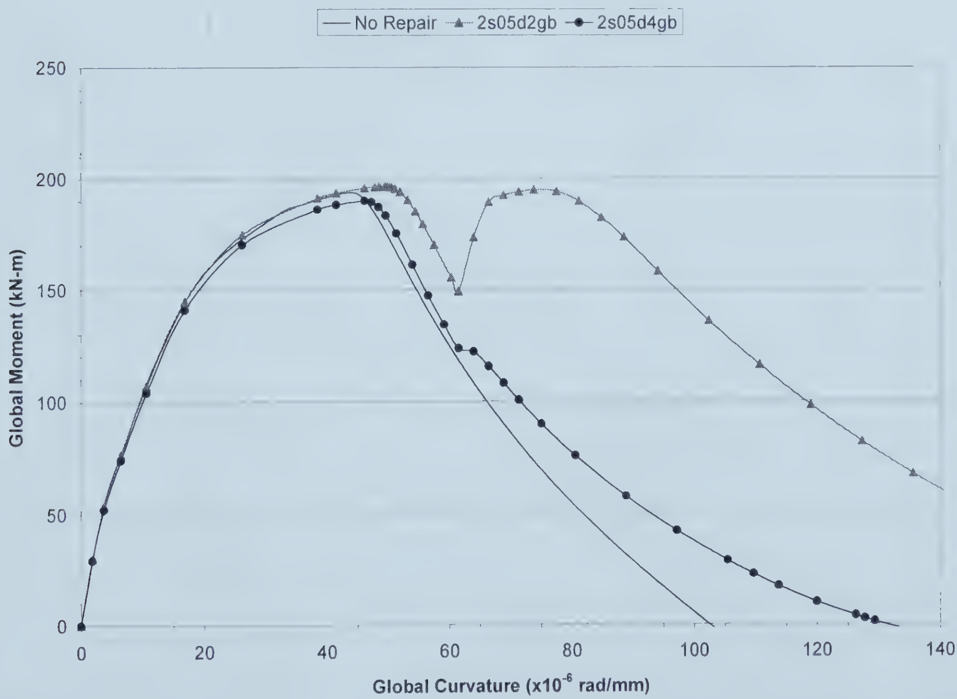

Figure 2.14 - Global Moment vs. Global Curvature for Even Steel Sleeve Repairs (Varying Gap Length)

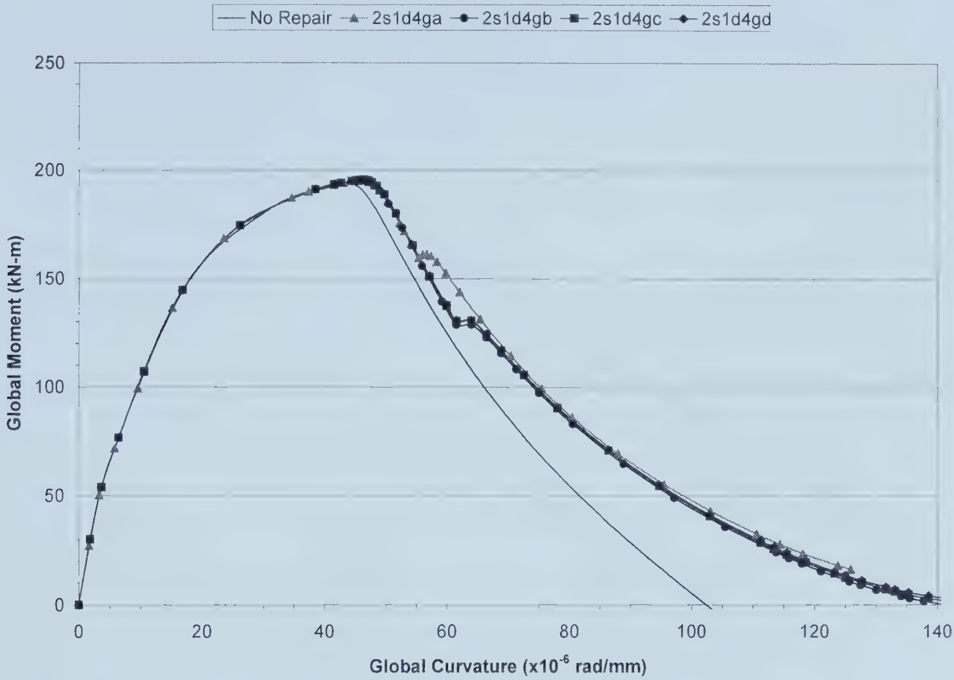

Figure 2.15 - Global Moment vs. Global Curvature for Even Steel Sleeve Repairs (Varying Sleeve Thickness)

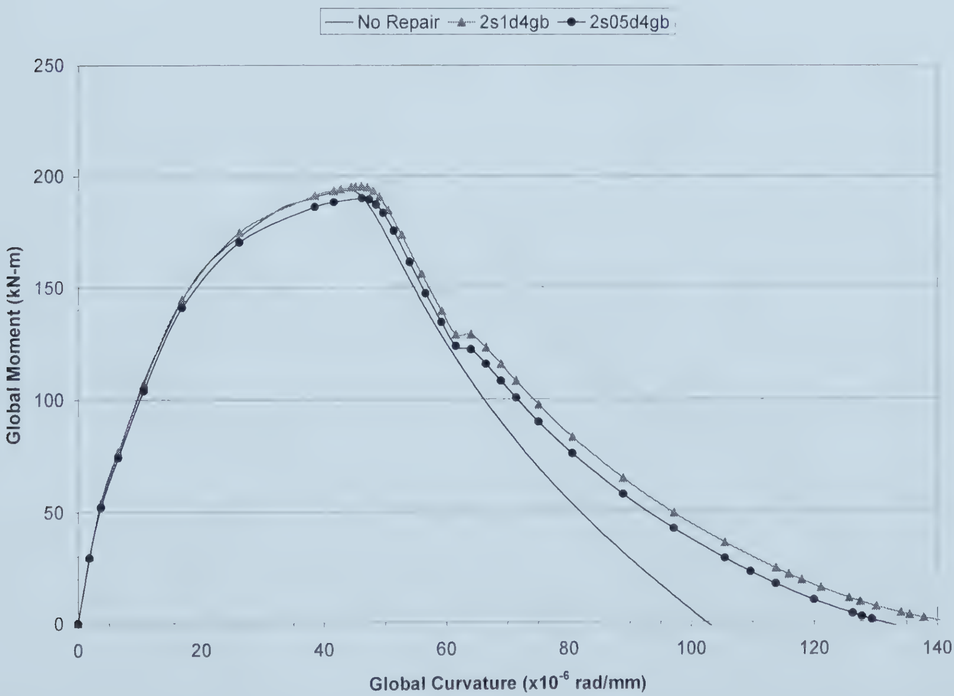

Figure 2.16 - Global Moment vs. Global Curvature for Even Steel Sleeve Repairs (Varying Sleeve Length)

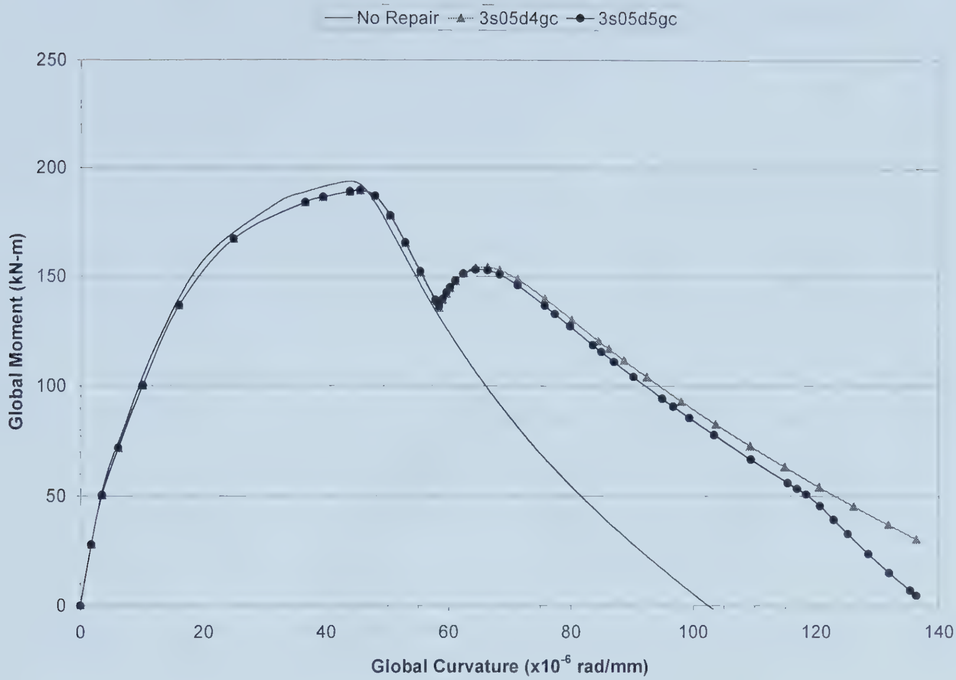

Figure 2.17 - Global Moment vs. Global Curvature for Odd Steel Sleeve Repairs (Varying Gap Length)

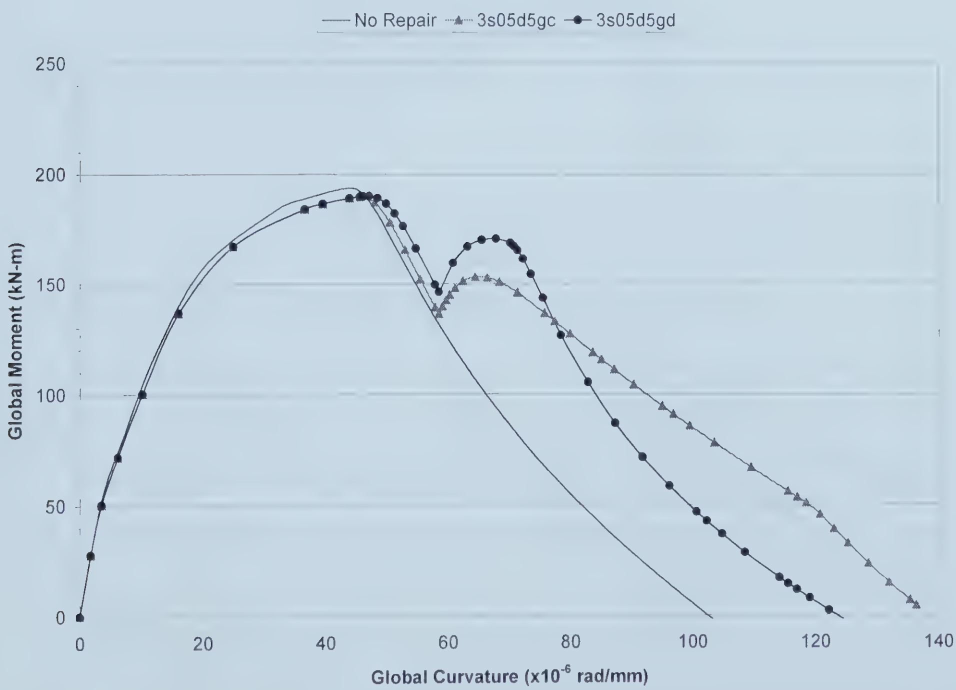

Figure 2.18 - Global Moment vs. Global Curvature for Odd Steel Sleeve Repairs (Varying Sleeve Thickness)

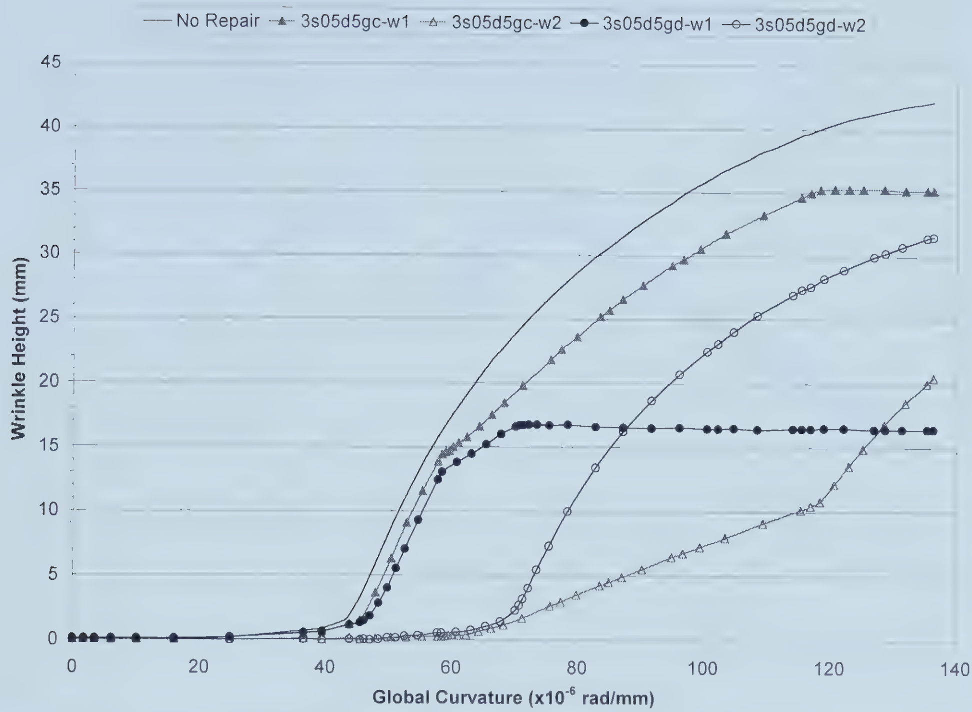

Figure 2.19 - Wrinkle Height vs. Global Curvature for Odd Steel Sleeve Repairs (Varying Sleeve Thickness)

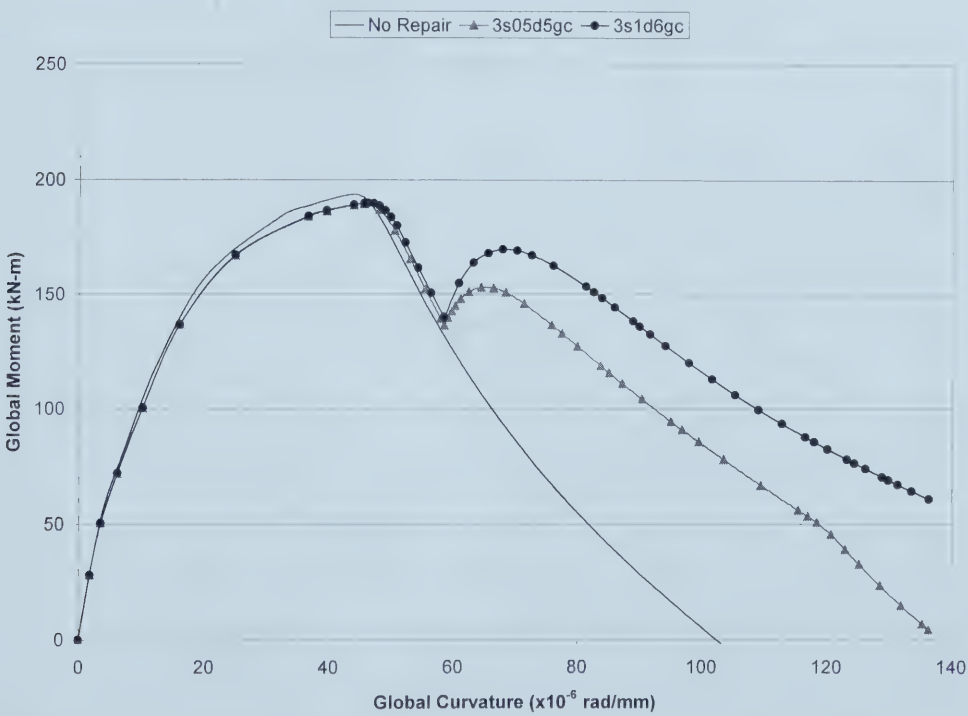

Figure 2.20 - Global Moment vs. Global Curvature for Odd Steel Sleeve Repairs (Varying Sleeve Length)

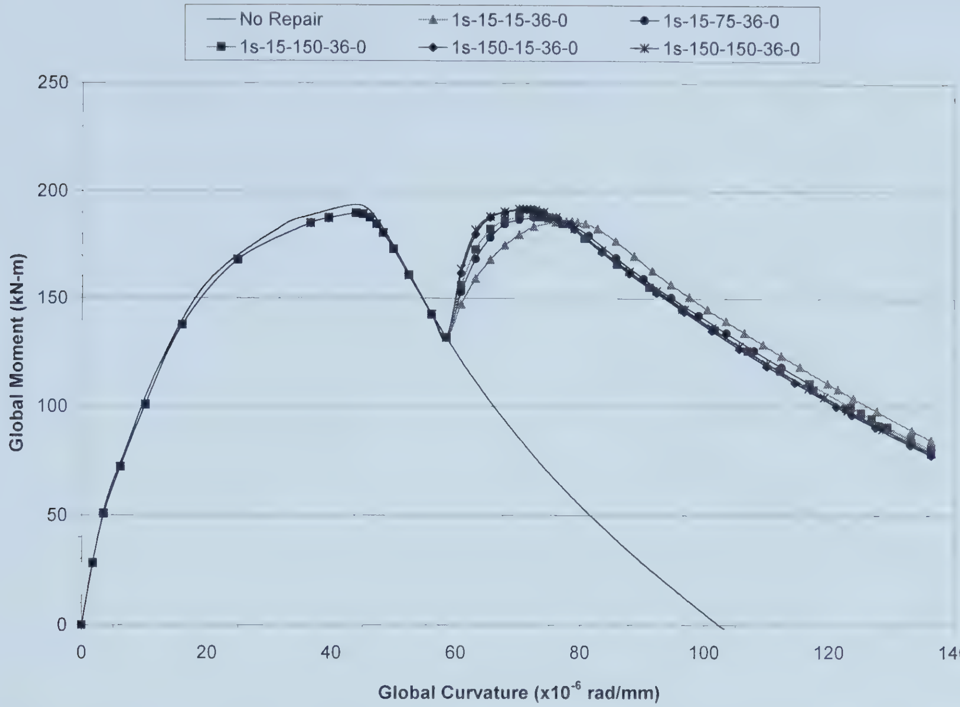

Figure 2.21 - Global Moment vs. Global Curvature for Single FRP Sleeve Repairs (Varying Elastic Moduli)

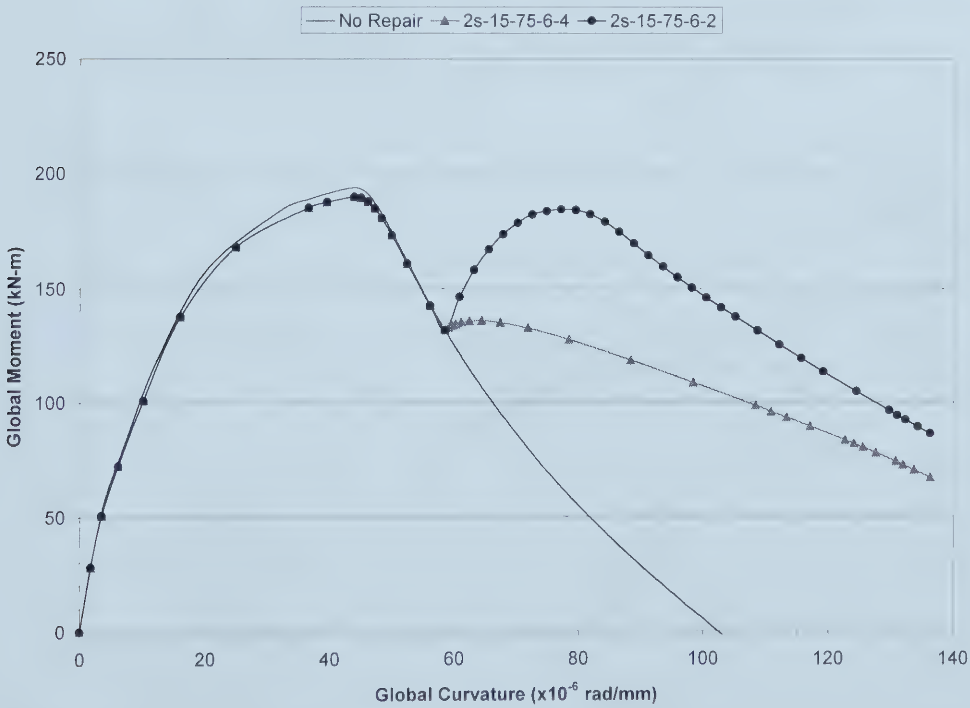

Figure 2.22 - Global Moment vs. Global Curvature for Even FRP Sleeve Repairs (Varying Gap Length)

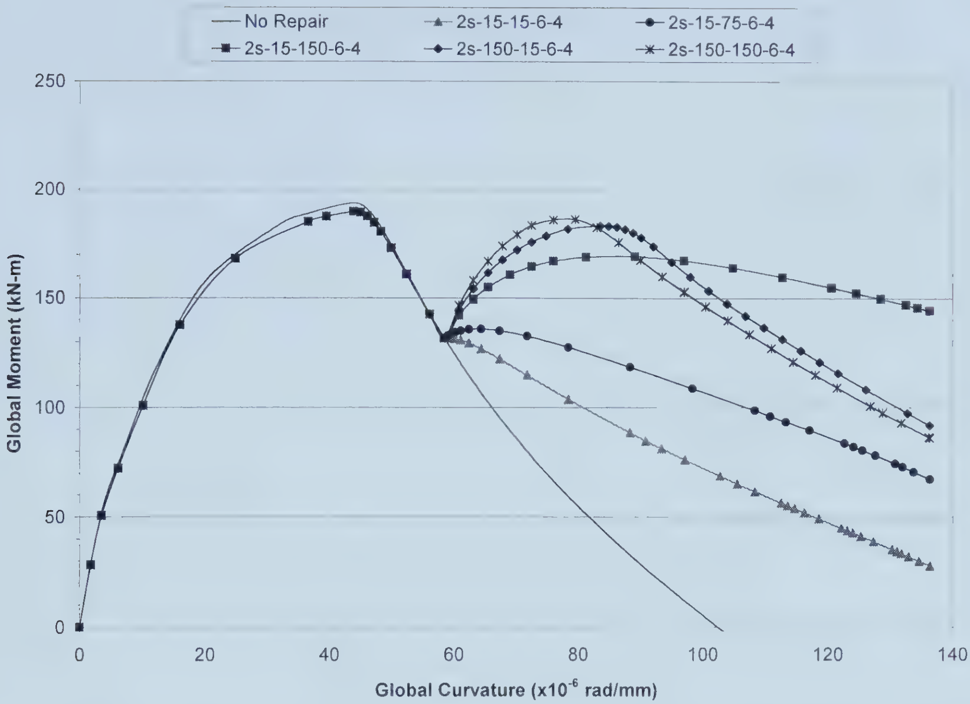

Figure 2.23 - Global Moment vs. Global Curvature for Even FRP Sleeve Repairs (Varying Elastic Moduli)

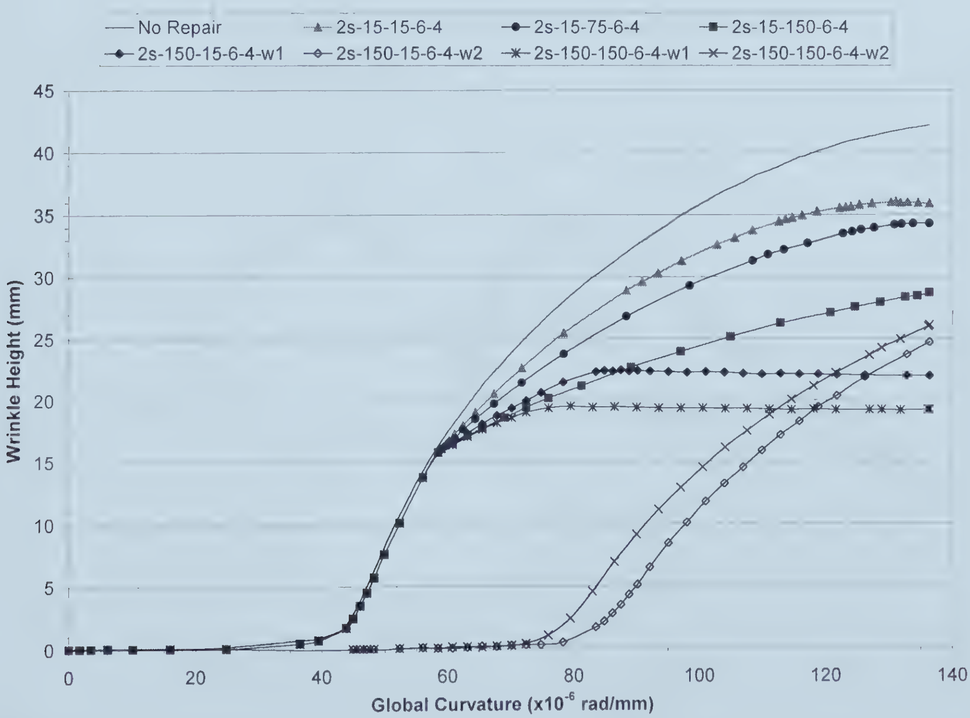

Figure 2.24 - Wrinkle Height vs. Global Curvature for Even FRP Sleeve Repairs (Varying Elastic Moduli)

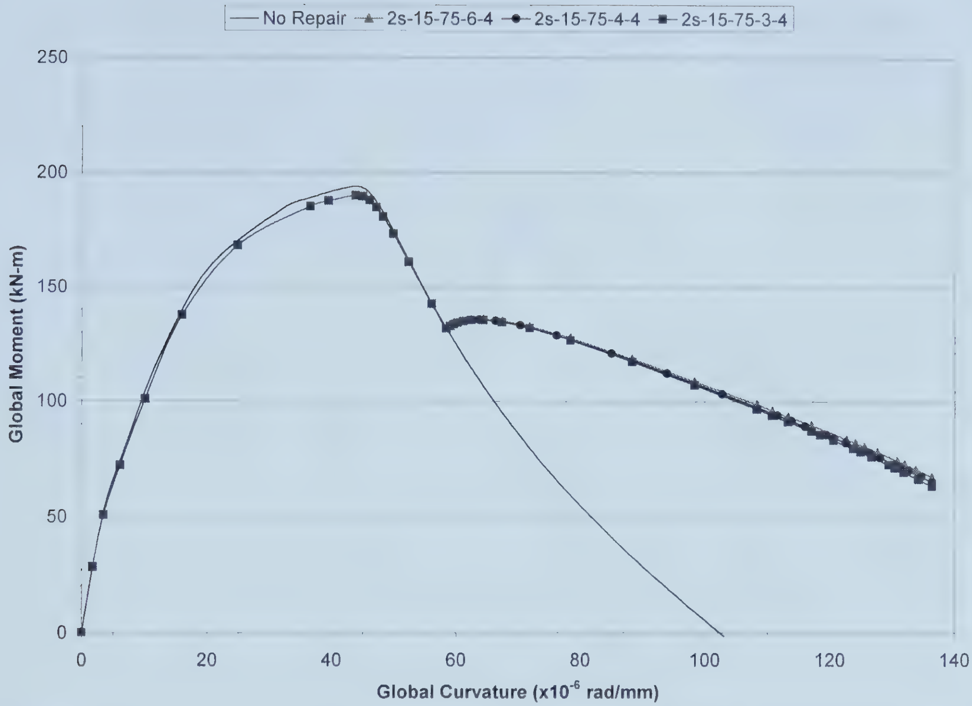

Figure 2.25 - Global Moment vs. Global Curvature for Even FRP Sleeve Repairs (Varying Sleeve Length)

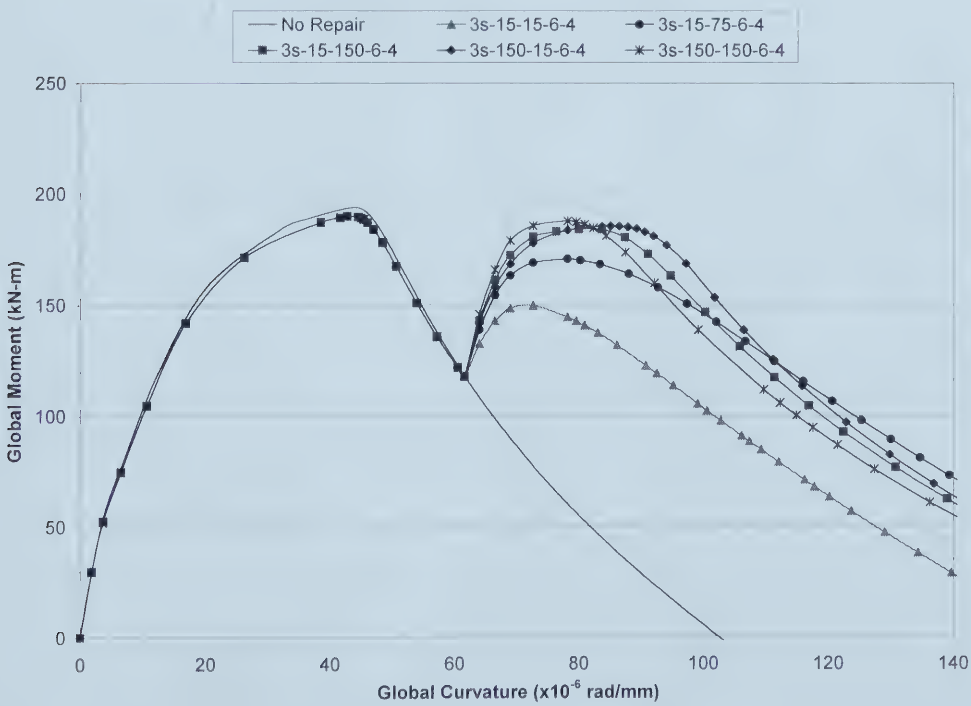

Figure 2.26 - Global Moment vs. Global Curvature for Odd FRP Sleeve Repairs (Varying Elastic Moduli)

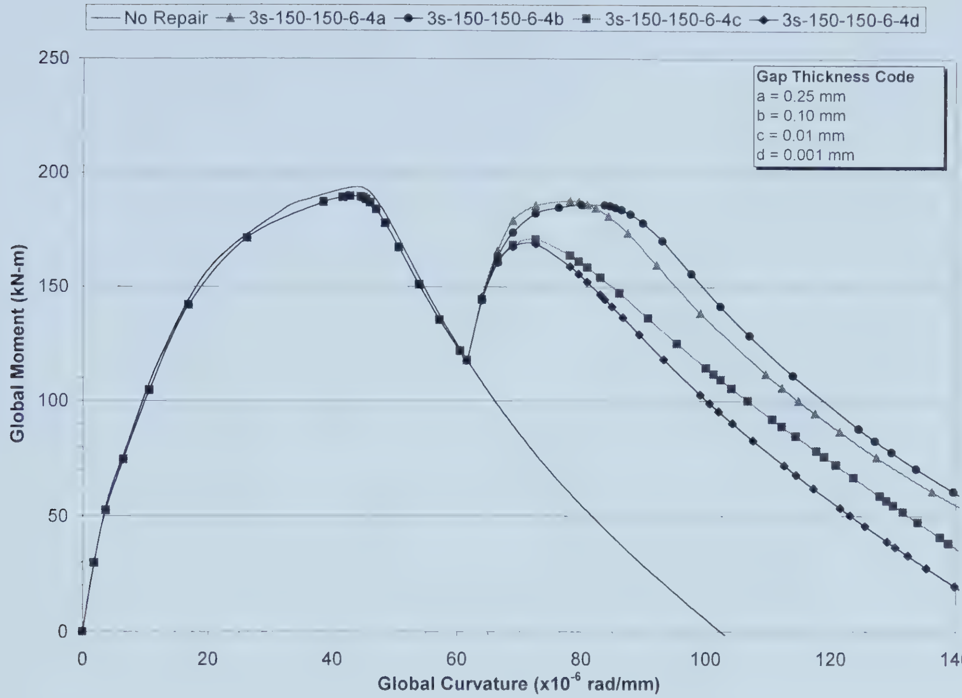

Figure 2.27 - Global Moment vs. Global Curvature for Odd FRP Sleeve Repairs (Varying Gap Thickness)

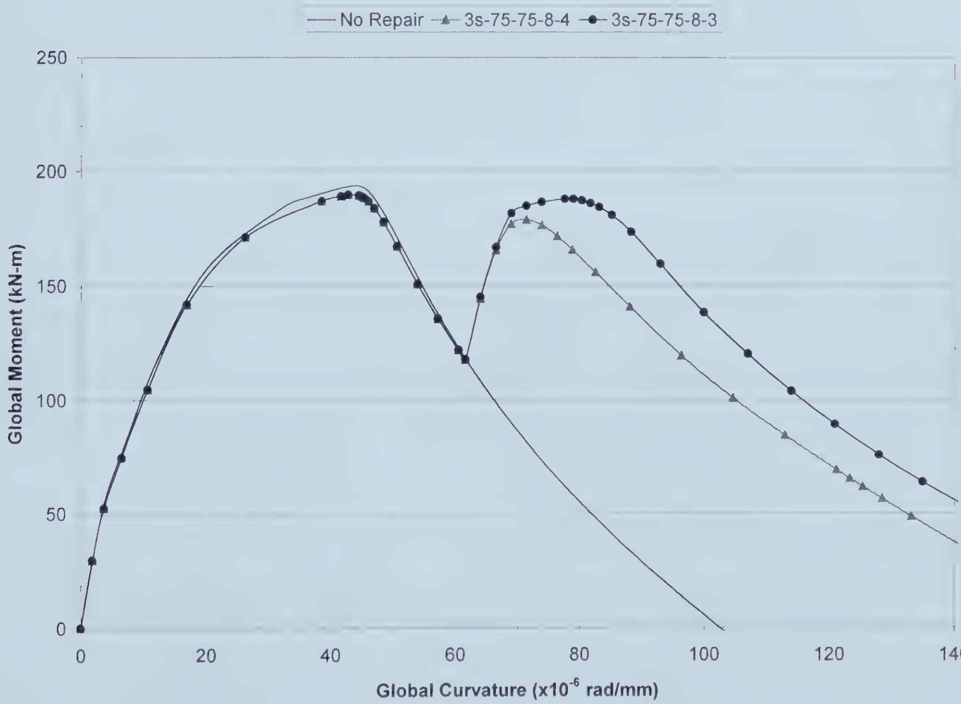

Figure 2.28 - Global Moment vs. Global Curvature for Odd FRP Sleeve Repairs (Varying Gap Length)

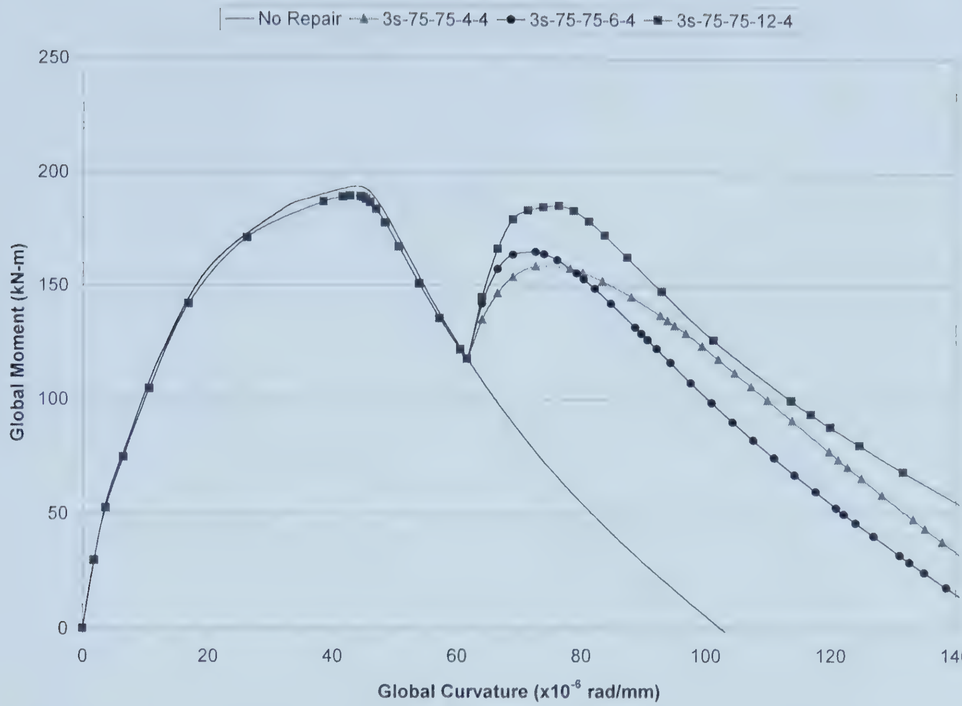

Figure 2.29 - Global Moment vs. Global Curvature for Odd FRP Sleeve Repairs (Varying Sleeve Length)

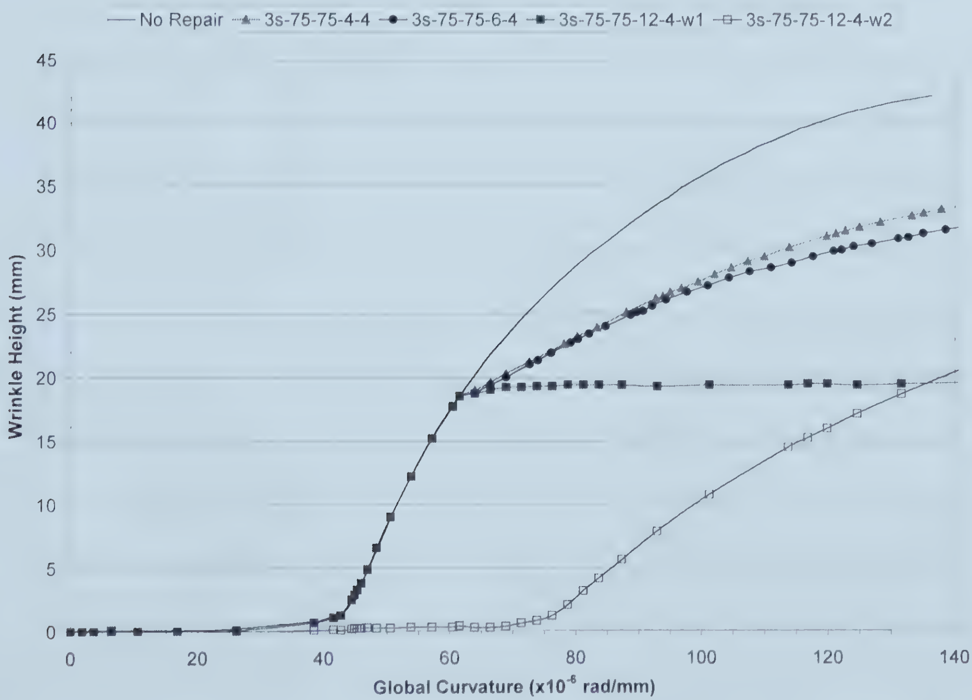

Figure 2.30 - Wrinkle Height vs. Global Curvature for Odd FRP Sleeve Repairs (Varying Sleeve Length)

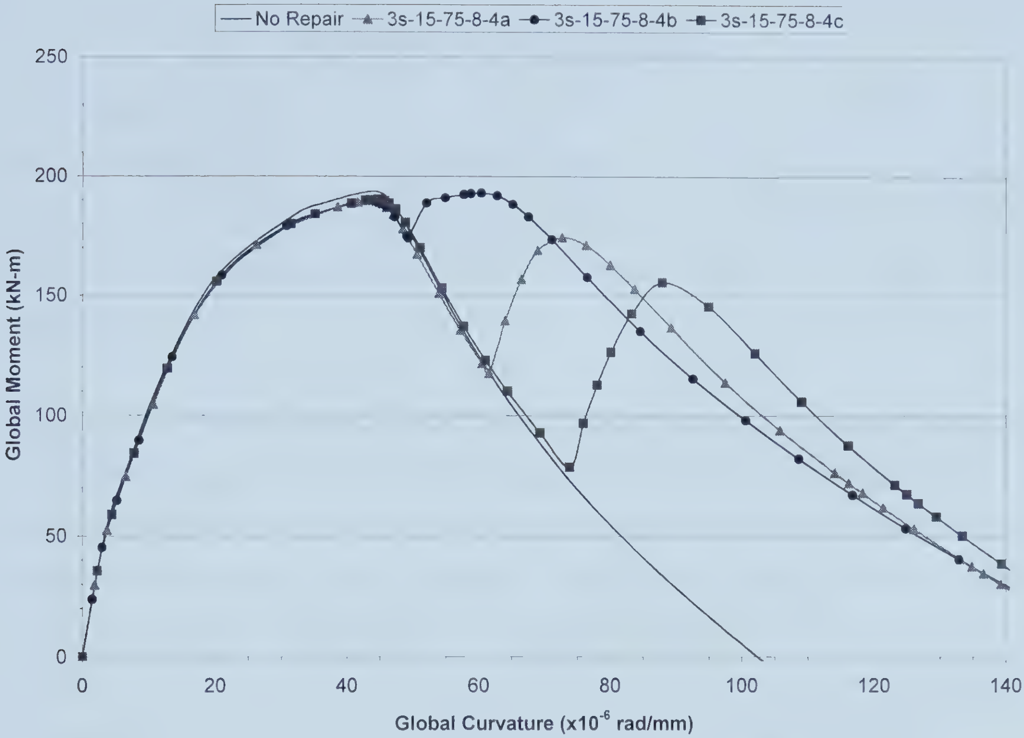

Figure 2.31 - Global Moment vs. Global Curvature for Odd FRP Sleeve Repairs (Varying Repair Timing)

3 EXPERIMENTAL PROGRAM

3.1 Objectives

The experimental portion of this project was conducted to study the behaviour of sleeve repair of wrinkled pipelines in a laboratory environment. The experimental program was divided into three phases: half-scale testing, full-scale testing and ancillary material testing.

A series of four half-scale tests on NPS 6 (168 mm in outside diameter) pipe were conducted at the beginning of the testing program. There were three main objectives of the NPS 6 pipe tests. The first objective was to gain experience with a new test setup that was designed for the experimental program. A second objective was to gain experience with the techniques that would be required to properly install a FRP sleeve system onto a steel pipe. The final objective of the half-scale testing was to compare the behaviour of the repaired pipe in the laboratory to that observed in the finite element modelling.

Following the tests on NPS 6 pipe, a series of two full-scale tests on NPS 12 pipe were conducted. The primary objective of the full-scale tests was to observe the behaviour of a full-size pipe repaired with FRP. The secondary objective of the NPS 12 tests was to validate the results of the finite element model described in Chapter 2 so that the model could be used in future work to optimize repairs for specific pipe wrinkles.

Finally, a series of ancillary material tests were conducted throughout the experimental portion of the project. The goal of these tests was to obtain the necessary material properties of the steel pipe and FRP used. The actual material properties would be then input into the finite element model for comparison of FE and test results.

3.2 Experimental Parameters

One of the goals of the experimental program was to obtain laboratory results that could be compared to the analytical results discussed in Chapter 2. In order to make a valid comparison, the geometric and loading parameters employed in the numerical analysis

were duplicated in the experimental study. In the finite element study, NPS 12 pipe with a diameter-to-thickness (D/t) ratio of 51 was modelled. The same type of pipe was used in the full-scale testing phase of the experimental program. In the half-scale tests, NPS 6 pipe with a D/t ratio of 52 was used. Previous research conducted by Dorey *et al.* (2001) determined that local buckling of pipe depended highly on the D/t ratio of the pipe, but was essentially independent of the diameter of the pipe. Therefore, it was anticipated that by using a similar D/t for the NPS 6 and NPS 12 specimens, the results of the half-scale tests and the full-scale tests would be comparable.

The three loading parameters identified in the finite element model (internal pressure, axial load and monotonically increasing curvature) were duplicated in the laboratory testing. Figure 3.1 shows a general schematic of the system used in the experimental program to duplicate the loads applied in the model. An internal pressure of 3,300 kPa was applied to both the NPS 6 and NPS 12 pipe using water pressurized with an external pump.

In the finite element model the axial load was applied via an external pressure load on the end plates. In the laboratory, external hydraulic jacks would be used to apply a load to the end plates. In order to apply the same longitudinal stress to the pipe for the NPS 6 and NPS 12 specimens, different axial load levels were required. For the NPS 6 pipe, the total axial load applied was 186 kN. The axial load applied to the NPS 12 specimens was 710 kN.

Monotonically increasing curvature was applied to the FE model by prescribing a rotation at the pipe ends. In the test program, curvature was applied by imposing vertical displacement on the pipe at two points along its length. The two points were equally spaced from the end reactions, creating a region of constant curvature between them. The region of constant curvature would behave in a similar manner as the entire length of pipe used in the FE model.

3.3 Half-Scale Laboratory Tests

3.3.1 Test Matrix

A total of four NPS 6 pipe tests were conducted in the experimental program. One control test and three FRP sleeve repair tests were performed. As discussed in Section 3.2, the loading conditions were held constant throughout the tests. The variables amongst the repair tests were: sleeve material, sleeve geometry (configuration, length, thickness) and timing of the repair. Table 3.1 outlines the test matrix for the NPS 6 test series.

The specimens are identified using the general designation of **v-WX-yy-Z**, where:

- **V** = nominal pipe size,
- **W** = sleeve material (C for carbon, G for glass),
- **X** = sleeve configuration (O for odd, E for even),
- **yy** = number of layers of FRP in the "strong" sleeve sections,
- **Z** = timing of the repair (E for early, M for moderate, L for late).

Two types of FRP material were used, carbon and glass fibre. Both were constructed of uniaxial fibre sheets. The same type of epoxy was used for both the carbon and glass fibre sleeves.

3.3.2 Test Specimen Preparation

The test specimens used for the half-scale phase of the experimental program were plain NPS 6 pipe sections (no girth welding) with an outside diameter of 167.95 mm and a wall thickness of 3.22 mm. This gave a D/t ratio for the half-scale pipe of 52.2. The steel used for the pipe was graded as API-5L X52, with a specified minimum yield strength (SMYS) of 359 MPa.

Although the exact manufacturing origin of the pipe is unknown, visual inspection indicated that the pipe was manufactured using the high-frequency resistance seam welding (RSEW-HF) process, commonly referred to as electric resistance welding (ERW). The highlights of the ERW process are shown in Figure 3.2. The pipe sections begin as flat steel sheets that are coiled for storage. The coils are cut for length and then

fed through a series of rollers that gradually cold work the flat sheet into a tubular section. A final pass through the fin section finishes the rounding process and contours the longitudinal edges of the sheet for welding. The pipe is passed through a high frequency welder that heats the edges of the strip to approximately 1,400 °C. Pressure rolls are used to squeeze the two edges together to form a fusion weld. The weld is then treated to remove welding stresses and produce a uniform normalized grain structure along the longitudinal seam. Following welding, the pipe is passed through a series of rollers to properly size the diameter of the pipe and to remove any bows along its length. Following hydrostatic testing, the pipe ends are finished to the desired bevel.

The pipe was manufactured to a standard joint length of 18,324 mm. In order to facilitate the test apparatus, the pipe joint was cut into six equal segments of 3,054 mm. Each specimen was sandblasted to white metal to provide the proper surface preparation for the eventual application of an FRP sleeve (Kennedy and Cheng, 1998). The ends of the specimens were bevelled at an angle of 60° to the longitudinal axis in order to accommodate welding of the end plates. Cutting, sandblasting and bevelling of the specimens was conducted by a third party prior to delivery to the I.F. Morrison Structural Engineering Laboratory at the University of Alberta.

Upon delivery to the Structural Engineering Laboratory, the specimens were marked with the locations where instrumentation, reactions and load points would be placed. Following mark-up, the end plates that would transfer the axial load to the pipe and contain the water for pressurization were welded to the pipe ends. The plates were welded to the pipe while the pipe was in a vertical position. This setup, shown in Figure 3.3, allowed the pipe to be properly aligned and centred on the plate and plumbed so that the plate would be welded perpendicular to the pipe. After the end plates had been welded, the specimen was filled with water. Filling took place in the vertical position so that the pipe would be free of air voids. The pipe was filled through holes drilled into the plates prior to welding. One hole was drilled and threaded in each of the plates. An inlet valve and hose were attached to the hole at the bottom of the pipe, while the top hole served as a vent. When the pipe was completely filled, the valve at the bottom of the pipe

was closed and the hose disconnected. The vent hole was then sealed with a threaded plug. Finally, strain gauges were installed and the pipe moved into the test fame.

3.3.3 Test Setup

3.3.3.1 Pipe Bending

In Section 3.1, it was mentioned that one of the objectives of the NPS 6 pipe test series was to gain experience with a new test setup. In previous pipe buckling tests conducted at the University of Alberta, pipes were tested in a vertical position using a MTS 6000 universal testing machine. The MTS 6000 was used to apply axial load to the pipe and curvature was applied via eccentric jacks and rigid moment arms. This test configuration is shown in Figure 3.4. Due to high demand for the MTS 6000 system by other research projects, it was decided that an independent test frame would be used in this project to load the pipe.

A common method to test the flexural capacity of structural sections is to conduct a four-point bending test. A general schematic of this type of test was shown in Figure 3.1. The four-point bending test involves the application of two equal point loads at equal distances from two point reactions. Figure 3.5 shows that this type of loading geometry creates a region of zero shear and constant moment between the load points. By creating a region of constant moment, a region of constant curvature is also created, allowing the moment – curvature behaviour of the section to be studied over a sufficient length. For the NPS 6 test series, the point loads were located 600 mm from the centreline of the reactions, resulting in a constant moment region of 1,554 mm. The resulting length-to-diameter ratio (L/D) for the constant curvature section was 9.25. A L/D ratio of this magnitude was considered more than sufficient to eliminate any effects of the boundary conditions or loading points on the development of the wrinkle.

Use of the four-point configuration eliminated the need for eccentric jacking and rigid moment arms that were used in previous projects to create curvature along the pipe. In this project, the point loads were applied using hydraulic jacks acting perpendicular to the pipe. The orientation of the hydraulic jacks is shown in Figure 3.6. In order to minimize

local effects of loading, it was decided that the load would be transferred from the jacks to the pipe via wide nylon loading straps. The ends of each strap were looped so that a short transfer beam could be run through them. A stocky HSS section was used for the transfer beam. Holes were drilled at the centreline of the beam and a high-strength alloyed steel threaded rod was bolted on. The threaded rods were passed through the hydraulic jacks (jacks with a centre hole were used) and fixed in place using thick plates and structural nuts. The use of the nylon straps required the loading system to act in tension. To accomplish this, the jacks were placed against the load frame beams. Two heavy channel sections were chosen for the load frame beams. They were placed back-to-back, with a gap of 50 mm between them to accommodate the loading rods and instrumentation. By placing the jacks on the bottom of the channel sections and the reaction points on the top, the loading straps were put into tension when the rams of the jacks were extended.

3.3.3.2 Axial Load Application

Modifications to the general four-point bending test were required since the pipe was to be subjected to both bending and axial load. In previous pipe bending tests, the axial load was applied via the MTS 6000 testing machine. The testing head would bear against one end of the pipe while the other end would bear against a strong floor that the MTS was fixed to. A similar configuration could have been used in this project with independent jacks placed at the ends of the pipe. However, this would have required a complicated and large reaction frame. A simpler method of applying the axial load was devised.

In Figure 3.6 the self-contained axial load system that was used is shown. Axial load was applied to both ends of the pipe via external prestressing rods. Two rods were used so that the total axial load would be symmetric about the vertical plane of the pipe, eliminating out-of-plane action. The rods passed through holes drilled in the end plates at the mid-height of the pipe. The holes were located a minimum distance from the pipe wall, so that excessive weak axis bending would not occur in the plates. At one end of the pipe, the rods were anchored to the plate using a combination of prestressing nuts and anchor plates. At the other end, the rods passed through centre-hole jacks and were fixed

into place using another set of nuts and anchor plates. The jacks were set to bear against the end plate. As the jacks were extended, the prestressing rods were placed into tension. To maintain equilibrium in the system, the pipe was forced to push against the anchors of the rods. This placed the pipe into compression and provided the necessary axial load without a complicated load frame. It should be noted that the end plates were allowed to rotate with the pipe ends as curvature was applied. The accommodations for this are discussed in the following sub-section.

3.3.3.3 Boundary Conditions

In the finite element model discussed in Chapter 2, pin – roller boundary conditions were applied to the pipe ends so that the ends would be free to rotate and the pipe would be free to move longitudinally. In the laboratory tests, several methods were employed to achieve the same boundary conditions. Because the experimental setup was a four-point bending configuration, the pin – roller boundary conditions had to be applied at the reactions and the load points. Figure 3.7 shows the reaction configuration used. The end reactions consisted of a knife-edge assembly mounted on top of steel rollers. The rollers were then mounted on a smooth, steel bearing plate. The knife-edge simulated the pin connection, allowing in-plane rotation. To insure that the pipe had sufficient contact to the reaction plates, concrete saddles were cast and placed between the pipe and the knife-edge assembly. The knife-edge and roller assembly allowed the pipe ends to rotate and move longitudinally.

The pin – roller boundary condition also had to be enforced at the load points. In most four-point bending tests, this is accomplished using the same assembly used for the reaction points. However, the use of flexible nylon straps to apply the load made this unnecessary. The flexibility of the straps, coupled with their friction connection to the transfer beams, allowed the pipe to rotate and translate at the load points without constraint.

One final boundary condition had to be accounted for in the test setup. As mentioned in the previous sub-section, the axial load was applied to the pipe via external prestressing

rods. The rods were anchored to the end plates via anchor plates and prestressing nuts. One can appreciate that as curvature is applied to the pipe, the pipe ends will want to rotate as well. The prestressing rods, on the other had, will want to remain straight, since they are under tension. If the rods were directly fixed to the end plates, serious deformation would occur in the plates and rods as they oppose each other's motion. To prevent this, rockers were placed between the end plates and the rod anchorage. The rocker assembly for the jack side and the anchor side are shown in Figure 3.8. Using the rockers, the rods remained straight as the end plates rotated with the pipe.

3.3.4 Instrumentation

A combination of electronic and manual instrumentation was used in the laboratory tests to record the behaviour of the pipe. A general schematic of the instrumentation used is shown in Figure 3.9. Manual instrumentation was limited to a series of Demec points installed at the top of the pipe (extreme compression face) in the constant moment region (shown in Figure 3.9 as D1 through D6). A 200 mm long Demec gauge was used to record maximum compression strain along the pipe in this region. When the compressive strain had exceeded the gauge range, a digital calliper was used to measure the distance between Demec points and strain was calculated using the distance between the points measured at the start of the test. In previous vertical pipe bending tests, a matching set of Demec points was installed on the tension face of the pipe so that curvature could be calculated. However, in the case of the four-point bending setup, it was deemed too hazardous to take manual readings underneath the pipe during loading.

The remainder of the instrumentation shown in Figure 3.9 were electronic measuring devices. All devices were connected to a central data acquisition system (Fluke) that was in turn connected to a desktop computer. The desktop computer used the commercial software package LabView to record the data from the Fluke and display it in graphical form. The data could later be transferred into a spreadsheet program for data reduction.

The electronic measuring devices used can be divided into two categories, strain devices and transducer devices. The strain measuring devices used in the test were 5 mm foil

strain gauges, which measured local strain in the pipe. A total of 12 strain gauges were used in each of the first two NPS 6 tests. This number was reduced to 7 gauges for the remaining two NPS 6 tests. The locations of the gauges are shown in Figure 3.9 as S1 through S12. Gauges S1 and S2 were placed at the mid-height of the pipe along the mid-length of the shear span. S1 was orientated in the hoop direction to measure strain due to pressurization and S2 was orientated longitudinally to measure the strain due to axial load at the start of the test. A matching pair of gauges, S11 and S12, was placed symmetric about the mid-length of the pipe for redundancy. Four pairs of gauges (S3 and S4, S5 and S6, etc.) were placed in the constant moment region, symmetric about the mid-length. They were located at the compression (S3, etc.) and tension (S4, etc.) faces of the pipe. These gauges were used as a backup method to calculate curvature in the elastic range. In the last two NPS 6 tests, the redundant gauges (S5 and S6, S7 and S8, S11 and S12) were not installed. However, a new gauge was placed in the hoop direction on the FRP sleeve at the crest of the wrinkle. The relevance of this gauge will be discussed in Chapter 4.

Several different types of transducer measuring devices were used in the experiments: load cells, rotation meters, cable transducers, linear variable displacement transformers (LVDT's) and pressure transducers. A total of six load cells were used to measure applied loads during the test. They are shown in Figure 3.9 as LC1 through LC6. A load cell was placed under each reaction (LC1 and LC2) to measure the applied point load. As a check, load cells were placed against the jacks that were used to apply the point loads (LC3 and LC4). If the readings from the load cell pairs on each end of the pipe (LC1 and LC3, LC2 and LC4) began to differ it would be an indication that unequal loading was occurring and remedial action could be taken. Finally, two load cells were used on the prestressing rods (LC5 and LC6) to measure the axial load applied to the pipe.

Rotation meters were used to measure the in-plane rotation of the pipe. Based on the rotation and the gauge length between meters, the global curvature of the pipe could be calculated. The rotation meters (R1 and R2) were placed at the ends of the constant

moment region at the mid-height of the pipe. In the FE model, the rotation of the pipe ends was measured at the points rotation was prescribed. In the case of the 4-point bending setup, this corresponded to the load point locations. Unfortunately, due to interference from the loading straps, the rotation meters were not placed exactly at the centreline of the load, but at a nominal distance inwards from the load straps.

Five spring-loaded cable transducers (X1 through X5) were used to measure vertical deflection of the pipe in the constant moment region. From Figure 3.9, it can be seen that transducers X2 through X4 were directly connected to the bottom of the pipe with a thin wire. However, this was not possible with transducers X1 and X5. X1 and X5 were used to measure the deflection of the pipe at the load application points. The loading apparatus attached to the loading straps (see Figure 3.6) made a direct connection from the pipe bottom to the transducer impossible. Also, the transducer wire could not be attached to the bottom of the apparatus, since stretching of the nylon straps would occur, leading to false measurement of the load point displacement. Therefore a rigid lever arm was used. A wire from the transducer on the floor was connected to the tip of the lever. A second wire was then used to connect the pipe to the lever at the load point location. Because of the lever arm, the displacement measured by the transducer was larger than the load point displacement. However, using similar triangles, a reduction factor was determined and used in the data reduction to calculate the load point displacement.

Three LVDT's (L1 to L3) were used to measure longitudinal displacements during the test. In a typical four-point bending test, as curvature is applied, the reaction points will move outwards and the load points will move inwards. This movement changes the length of the shear span, which must be known to calculate the applied moment. LVDT`s L1 and L2 were attached to the reaction points, above the rollers, and measured the longitudinal movement of the pipe ends. LVDT L3 was mounted onto a custom-made frame (shown in Figure 3.10) to measure the movement of the load points. The frame consisted of a steel rod that passed through two sets of linear bearings mounted to a flat bar. The LVDT was mounted to the bar and its core connected to the rod. The assembly was mounted onto the loading straps via two screws on each end. The screws provided a

friction connection to the straps to prevent slippage. Also, the screws allowed the pipe to rotate in plane without placing a rotation onto the measuring frame. As the load points moved inwards, the rod and bar moved closer together. This movement was recorded by L3.

The final measuring device used was a pressure transducer (P1 in Figure 3.9). P1 was placed at the outlet of the water pump that was used to pressurize the pipe. It gave the gauge pressure of the fluid in the pipe during the test.

3.3.5 Test Procedure

3.3.5.1 Pre-Repair Pipe Buckling

The test procedure used in the NPS 6 tests closely resembled the modelling procedure discussed in Chapter 2. Once the specimen had been placed on the test frame and all instrumentation and hydraulic lines connected, a pre-test sequence was conducted. First, the reaction rollers were unlocked. Locks had been placed on the rollers to aid in specimen installation. Second, stabilizing bolts around the reaction load cells (see Figure 3.7) were backed off so that the load cells, not the bolts, would bear the applied load. Finally, zero readings (both manual with the Demec gauge and calliper and electronic) were taken.

Following the pre-test sequence, loading of the specimen began. First, the internal pressure of the pipe was raised to 3,300 kPa. Next, the axial load of 186 kN (or 93 kN per prestressing bar) was applied. During the test, the internal pressure and axial load were kept constant. Third, the stroke of the point load jacks was increased. The test was conducted under stroke control. That is, the stroke of the jacks, rather than the jack load was used to gauge progress of the test. After every 1 mm of jack stroke, an electronic reading or scan, was taken. Manual Demec readings were taken every fifth electronic reading. The stroke of the jack was increased until local buckling was observed and the wrinkle had a height of approximately 6 mm. This wrinkle height occurred at a jack stroke of approximately 50 mm. Figure 3.11 shows the wrinkle height at the end of a typical buckling test.

When the wrinkle had reached a satisfactory height, the pipe was unloaded so that a repair could be made. In the FE model, the load was maintained when the sleeve was installed, but placing a sleeve on a pipe in the lab under load was deemed a safety concern. The load was removed in opposite order it was placed. That is, the point loads were removed first, followed by the axial load and finally the pressure.

3.3.5.2 FRP Repair

After buckling, the FRP sleeve was installed. The first step in the repair phase was the removal of the prestressing bars and any instrumentation that would interfere with the sleeve. Second, the area the sleeve would occupy was marked to show the different sleeve sections (see Figure 3.12). The final step prior to sleeve application was to clean the pipe surface and remove any surface rust, dirt, etc.

The first step in step in FRP application was to apply a thin layer of epoxy onto the pipe. This layer would serve as a base layer and was allowed to become tacky, so that the sleeve could stick easier during placement. Next, epoxy was applied to FRP strips that had been cut to the required length and width. The strips were then wrapped onto the pipe with the fibres orientated in the hoop direction of the pipe exclusively. Because the strips were wrapped over themselves, only one layer of epoxy was necessary between two consecutive layers of fibre. After all the strips had been wrapped onto the pipe, a final layer of epoxy was added. This layer would serve as a protective and saturating layer. A typical FRP repair is shown in Figure 3.13. The sleeve was left for 7 days at room temperature, to insure full curing of the epoxy. After 7 days, the pipe was ready to retest.

3.3.5.3 Post-Repair Testing

During the 7-day curing period, the pipe was readied for testing. The prestressing rods and applicable instrumentation were reconnected to the pipe. It should be noted that Demec points were not replaced, since it would be impossible to place the new points in the exact locations the old ones occupied prior to sleeve installation. After the specified curing time, the same loading procedure followed in Section 3.3.4.1 was repeated. The

test was ended when the curvature of the pipe had reached a sufficient level or jack stroke was exhausted. The end of one NPS 6 test is shown in Figure 3.14.

The same procedure of buckling, FRP repair and post-repair testing was followed for all of the NPS 6 specimens that had sleeves installed.

3.4 Full-Scale Laboratory Tests

3.4.1 Test Matrix

Two NPS 12 pipe tests were conducted in the experimental program. Both were sleeve repairs. No control test was performed, since this pipe size had been tested extensively in previous projects. The same sleeve parameters studied in the NPS 6 pipes were studied in the NPS 12 pipes. Table 3.2 gives the test matrix for the full-scale tests.

Both tests used glass fibre sleeves, however, the fibre and epoxy manufacturer was different for the last test. This accounts for the significantly thicker MBrace sheets. Both glass fibre products were uniaxial fibre sheets.

3.4.2 Test Specimen Preparation

The test specimens used for the full-scale phase of the experimental program were plain NPS 12 pipe sections with an outside diameter of 323.85 mm and a wall thickness of 6.33 mm. This gave a D/t ratio for the full-scale pipe of 51.1. The pipe used in the FE study was a grade X52 pipe. However, due to supply restrictions, X60 pipe, with nominal yield strength of 414 MPa was used. Manufacturer data sheets indicated that the pipe, like the NPS 6 pipe, was fabricated using the ERW process.

Pipe specimens were cut to lengths of approximately 4,070 mm. The NPS 12 specimens were prepared for testing using the same procedure described for the NPS 6 pipe. See Section 3.3.1 for details.

3.4.3 Test Setup

The test setup used for the NPS 12 pipe specimens was the same as the setup for the NPS 6 pipe with only minor modifications. The load-carrying accessories (jacks, rods, straps, transfer beams, end plates) and load cells were sized so that the larger loads that would be present with the larger pipe could be carried safely. In the NPS 6 test series, the hydraulic jacks were operated using hand pumps. Because the hydraulic pressure would be higher for the NPS 12 tests (higher loads), a pneumatically controlled pumping system was used to control the jack stroke. Finally, the reaction points and load points were shifted to accommodate the longer pipe. For the NPS 12 test series, the point loads were located 1,200 mm from the centreline of the reactions, resulting in a constant moment region of 1,370 mm. The L/D ratio for the constant curvature section was 4.25 or approximately half of what was used for the NPS 6 pipe. A greater chance of boundary influence on the wrinkle was possible, but a longer pipe could not be placed in the test setup.

Other than these small changes, the setup remained the same as the one shown in Figure 3.6. A picture of the NPS 12 test setup is shown in Figure 3.15.

3.4.4 Instrumentation

Instrumentation for the NPS 12 test series was essentially the same as the NPS 6 series, shown in Figure 3.9. Three items were modified. First, the redundant strain gauges (S5 and S6, S7 and S8, S11 and S12) were not installed and a new gauge was placed on the FRP sleeve, as was done for the last two NPS 6 tests. Second, Demec points were not installed on the compression face of the pipe due to access difficulties. Finally, for the second NPS 12 test, a third rotation meter was added to measure local curvature in the wrinkle region

3.4.5 Test Procedure

3.4.5.1 Pre-Repair Pipe Buckling

The same general procedure used for pre-repair testing of the NPS 6 pipe was used for the NPS 12 pipe. Following the pre-test sequence, the pipe was pressurized to 3,300 kPa.

Next, the axial load of 710 kN was applied using the two prestressing rods. Third, the stroke on the point load jacks was increased. For the NPS 12 series, it was decided that global curvature was a better indicator of test progress than jack stroke. This decision was made based on observations from the NPS 6 tests. Prior to wrinkling, jack stroke and curvature correlated at a relatively constant rate. However, as buckling began, large increases in curvature occurred for small increases in jack stroke. It was easy to increase the curvature to a level higher than desired if jack stroke was used to gauge progress instead of curvature. Electronic scans were taken at curvature increments of 1×10^{-6} radians/mm.

For the NPS 12 series, the pre-repair test was stopped when the wrinkle had reached a height of approximately 10 mm. This typically occurred at a curvature of 60×10^{-6} radians/mm. The end of a NPS 12 pre-repair test is shown in Figure 3.16.

3.4.5.2 FRP Sleeve Repair

Following the pre-repair test, prestressing rods and instrumentation in the area of the wrinkle were removed, as was done with the NPS 6 pipe. Also, the load straps were moved closer to the pipe ends. This step was done only in the NPS 12 tests, not the NPS 6 tests. As was mentioned in Section 3.4.4.1, the L/D ratio for the NPS 12 tests was half of that for the NPS 6 tests. As such, the load points created a greater overall disturbance to the constant moment region. In addition, the peak load on the NPS 12 pipe was approximately 6 times that of the NPS 6 pipe. These two factors resulted in the formation of the wrinkle immediately adjacent to the loading strap, as seen in Figure 3.16. Insufficient room to apply a sleeve resulted, so it was decided that the shear span would be reduced to 900 mm to accommodate the sleeve. Strap relocation is shown in Figure 3.17.

Once the straps were relocated, the sleeve area was prepared for FRP application. In the first NPS 12 test, the procedure followed for the NPS 6 tests was used. For the second NPS 12 test, a slightly different procedure was used. A primer epoxy was coated onto the pipe around the wrinkle region. Next, a layer of epoxy putty was placed around the pipe

in the wrinkle region to form a smooth surface to which the FRP would bond. The putty was trowelled onto the top half of the pipe and bottom half of a cylindrical cardboard form lined with plastic sheeting. The form was split on one end so that it could be placed around the pipe. The form was clamped together and excess putty scraped from the edges of the form. The formwork used is shown in Figure 3.18. After 1 day of curing time, the formwork was removed and any holes in the putty shell were patched. The completed putty layer is shown in Figure 3.19. With the putty layer constructed, the FRP sleeve was applied in a similar manner as described for the NPS 6 pipe. The FRP repair for the second NPS 12 test is shown in Figure 3.20. The sleeves were allowed to cure for 7 days prior to re-testing.

3.4.5.3 Post-Repair Testing

After sleeve application, the pipe was readied for re-testing. For the NPS 12 tests, it was necessary to move the locations of the rotation meters, since their original locations interfered with sleeve application. They were relocated towards the new strap locations. Figure 3.21 shows typical rotation meter relocation. Once the instrumentation was reattached and the prestressing rods were put back into place, the post-repair testing began. The same loading procedure used for the pre-repair buckling was used for the post-repair testing. As was the case with the NPS 6 tests, the NPS 12 post-repair tests were stopped when the desired curvature had been reached or jack stroke had been exhausted. The end of a typical NPS 12 test is shown in Figure 3.21.

3.5 ANCILLARY MATERIAL TESTS

3.5.1 Steel Tension Coupon Tests

In order to determine accurate material property curves for FE analysis, tension coupons were cut and tested from the NPS 6 and NPS 12 pipe. The coupons were cut in the longitudinal direction of the pipe specimens, from specimens that had not been tested. Since tubular sections are cold rolled, their material property curves differ for the longitudinal and hoop directions. However, previous research (DiBattista *et al.*, 2000) has shown that this difference does not impact FE modelling of behaviour in the

longitudinal direction, i.e. pipe bending and buckling. Therefore, only longitudinal coupons were tested.

Three coupons were cut from the NPS 6 pipe and eight were cut from the NPS 12 pipe. Typically, only three coupons per pipe batch are cut. The reasons for cutting eight NPS 12 coupons will be discussed in Chapter 4. The coupons were machined by a third party and tested at the I.F. Morrison Structural Engineering Laboratory using a MTS 1000 universal testing machine.

The coupons were fabricated and tested according to ASTM Standard A370 (ASTM 2000b). Prior to testing, measurements of cross-sectional dimensions and gauge length were made with a digital calliper and micrometer. Longitudinal strain gauges were mounted onto the coupons at their mid-length.

Measurements of strain were made during the tests with the strain gauges and an extensometer mounted at mid-height. Load and stroke of the test head were measured with the MTS 1000 internal instrumentation. After fracture of the specimen, the two halves were placed together and the gauge length was measured again to determine elongation.

3.5.2 FRP Tension Coupon Tests

The FRP material used consisted of uniaxial fibres in an epoxy matrix. To determine the properties of the material (namely elastic modulus and rupture strain) uniaxial tension coupons were fabricated and tested. Coupons were made in the laboratory at the same time as the FRP sleeves were installed, so that similar epoxy properties would be observed.

Five coupons for each type of FRP material used (1 carbon, 2 glass types) were formed and tested according to ASTM Standard D3039M (ASTM 2000a). Prior to testing, the cross-sectional properties were measured with a digital calliper and micrometer. Two strain gauges were mounted on each specimen at the mid-length, one on each face. One

gauge was mounted in the longitudinal direction, while the other in the transverse direction. The longitudinal and transverse strains were then used to determine the Poisson's ratio for the FRP composite.

After instrumentation had been installed and geometric measurements made, the coupons were tested in the MTS 1000 machine. The test setup is shown in Figure 3.22. The coupons were tested until complete fracture of the fibres occurred (see Figure 3.23).

The results of the experimental program are presented in Chapter 4, along with a comparison of some of the key results with those predicted by the FE model used in Chapter 2.

Table 3.1 - Test Matrix for NPS 6 Pipe Test Series

Specimen ID	Sleeve Material	Sleeve Configuration	Main Sleeve Length (mm)	Sleeve Thickness (mm)	Repair Timing
6-NS	none (control)	-	-	-	-
6-CO-9-M	Replark Carbon	odd	150	0.99	moderate
6-CE-18-E	Replark Carbon	even	75	1.98	early
6-GE-10-L	FTS-GE-30 Glass	even	75	3.00	late

Table 3.2 - Test Matrix for NPS 12 Pipe Test Series

Specimen ID	Sleeve Material	Sleeve Configuration	Main Sleeve Length (mm)	Sleeve Thickness (mm)	Repair Timing
12-GO-12-M	FTS-GE-30 Glass	odd	150	3.60	moderate
12-GO-6-M	MBrace EG 900 Glass	odd	300	4.40	moderate

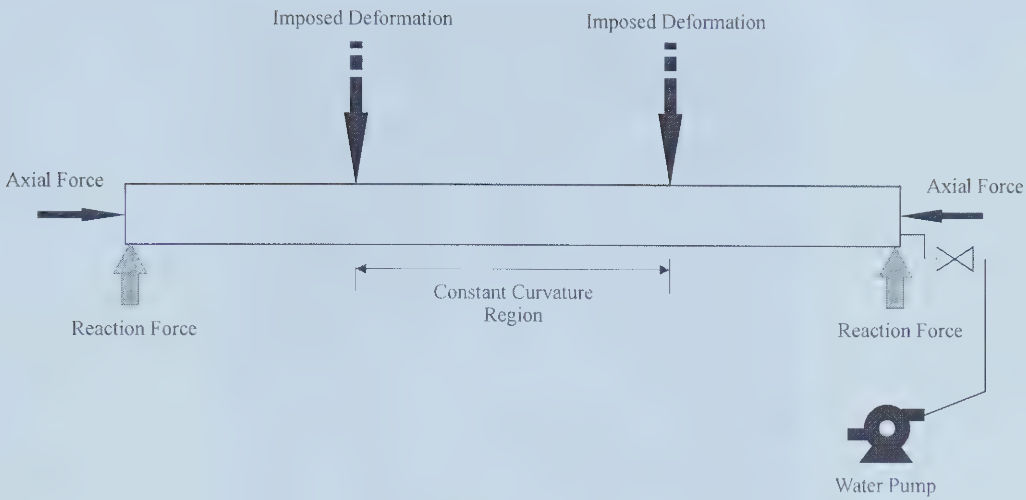

Figure 3.1 - General Schematic of Loads Applied to Pipe Specimens

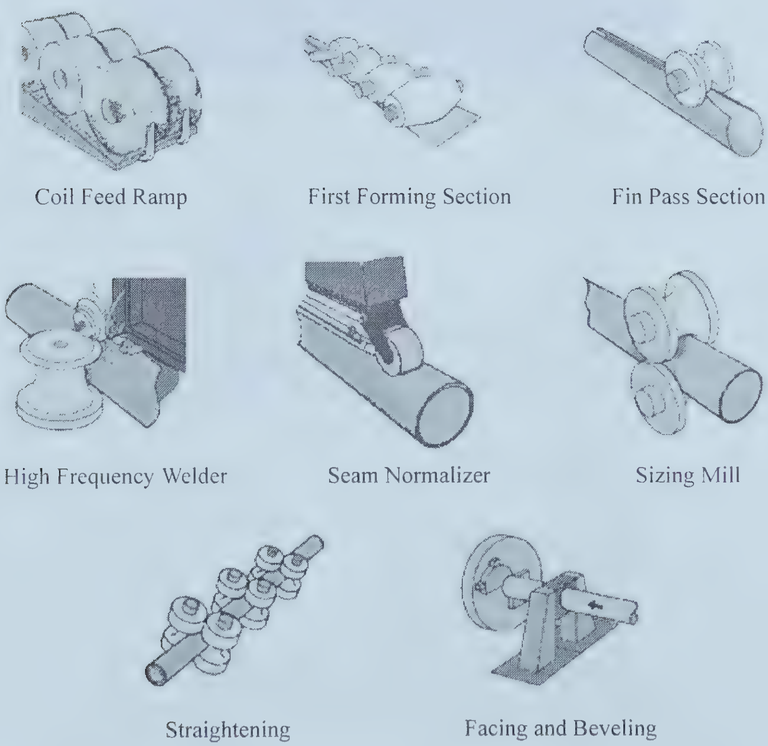

Figure 3.2 - Summary of Electrical Resistance Welding (ERW) Process (U.S. Steel Group, 2000)

Figure 3.3 - End Plate Welding Setup

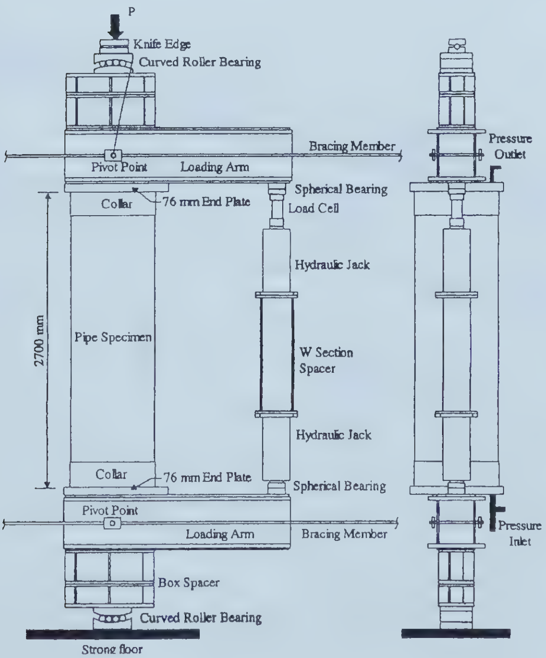

Figure 3.4 - Test Setup for Vertical Pipe Bending Test in MTS 6000 (Dorey *et al.*, 2001)

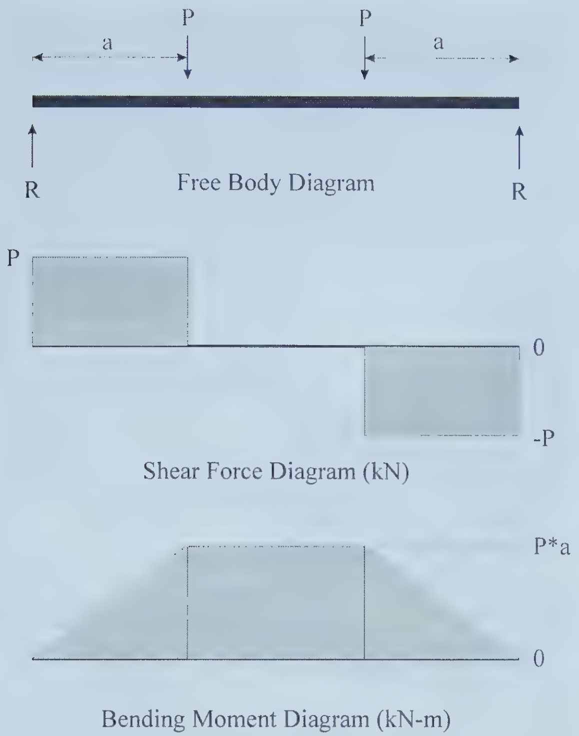

Figure 3.5 - Free Body, Shear Force and Bending Moment Diagrams for 4-Point Bending Setup

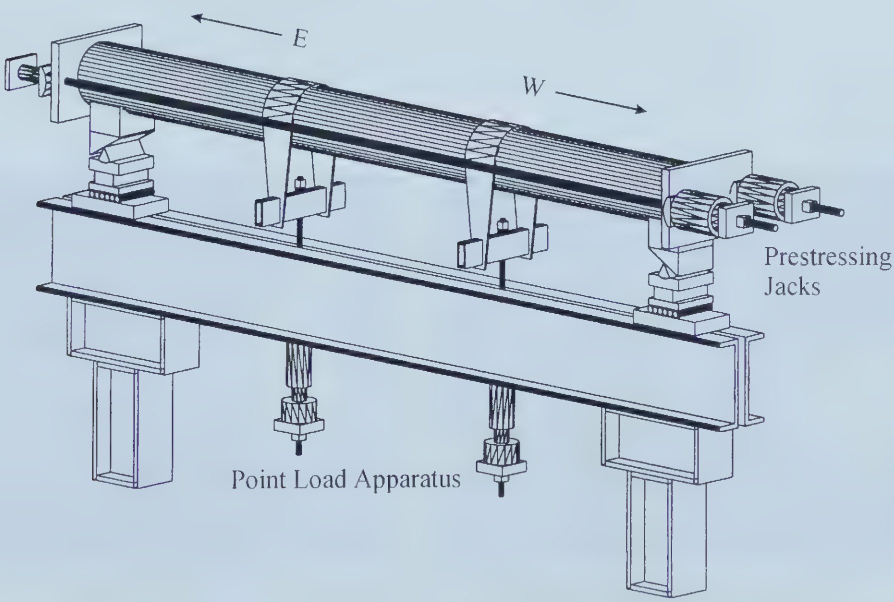

Figure 3.6 - Setup for Horizontal Pipe Bending Test in Independent Test Frame

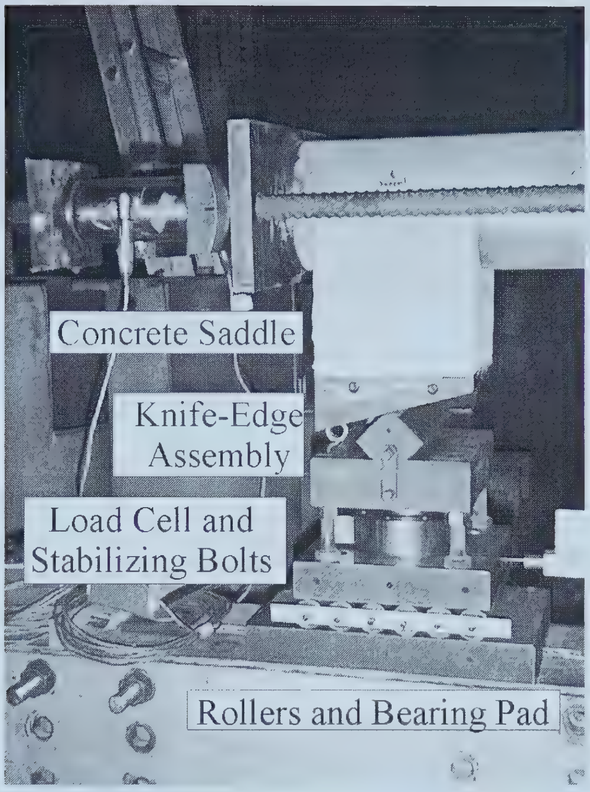

Figure 3.7 - Reaction Setup Components

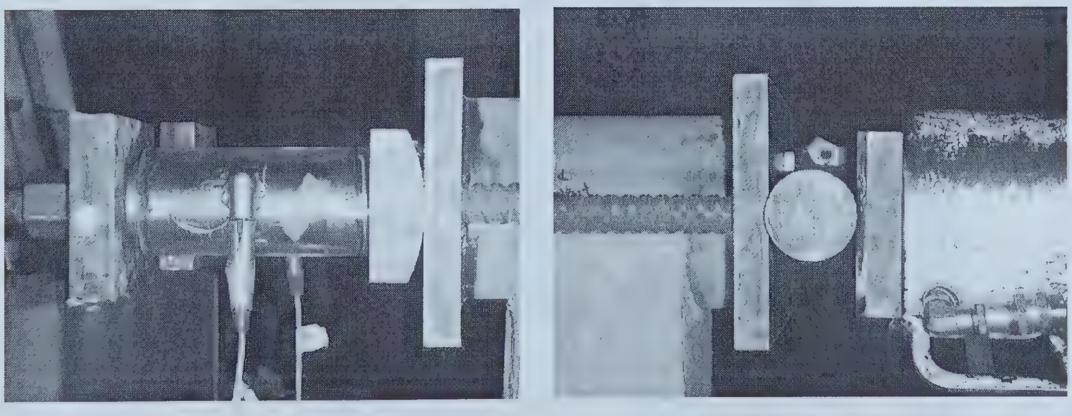

Figure 3.8 - Rockers at End Plate / Prestressing Rod Junction

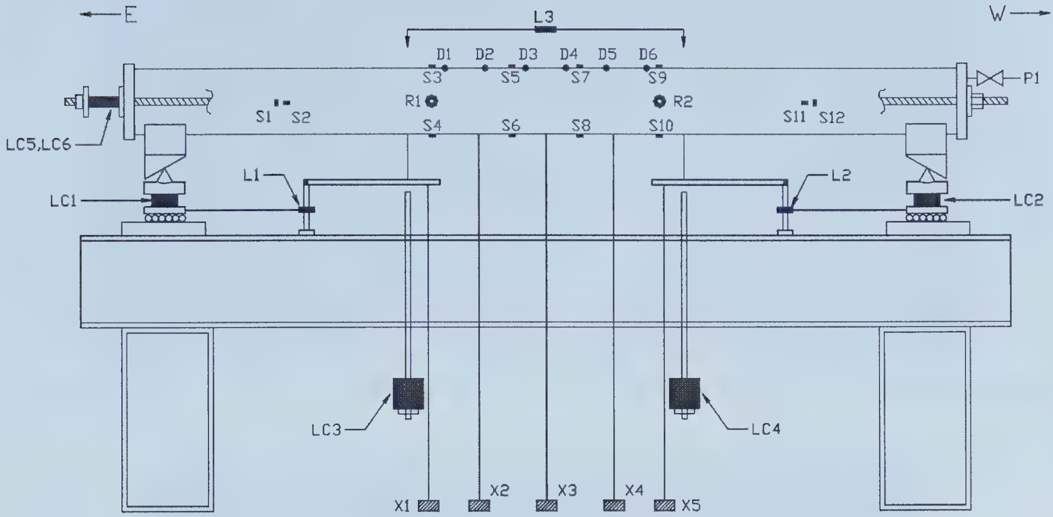

Figure 3.9 - Instrumentation Layout for NPS 6 Pipe Test

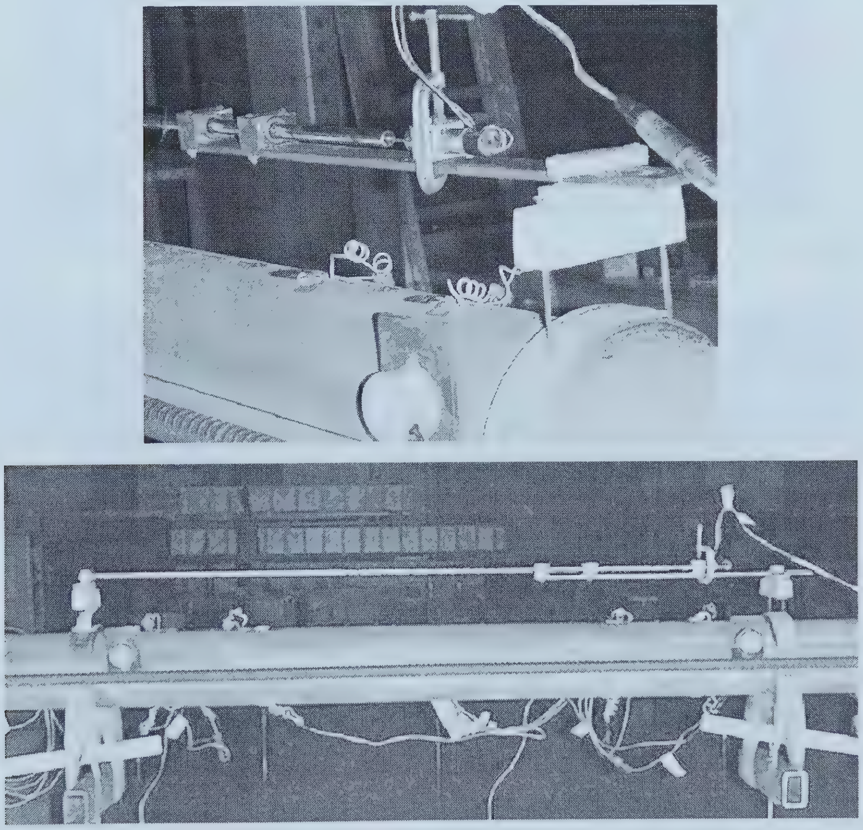

Figure 3.10 - Custom-Built Frame for L3

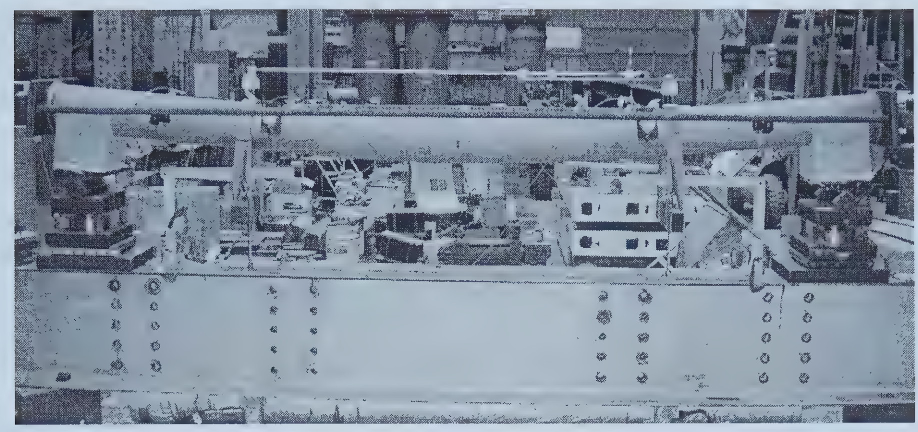

Figure 3.11 - NPS 6 Pipe Deformation at the end of the Pre-Repair Buckling Test

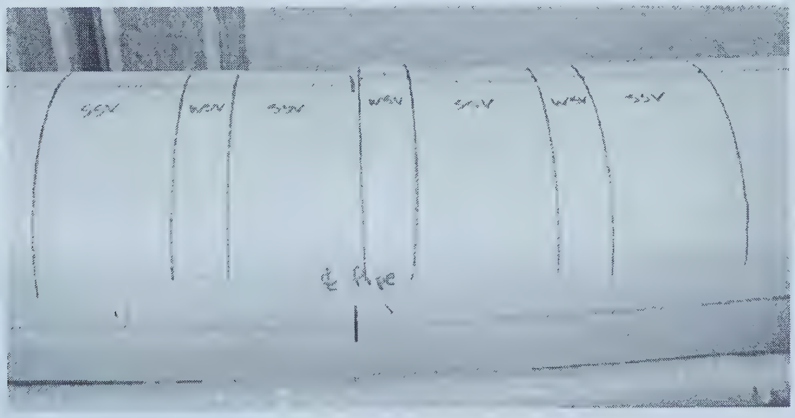

Figure 3.12 - Sleeve Locations are Marked Prior to Sleeve Application

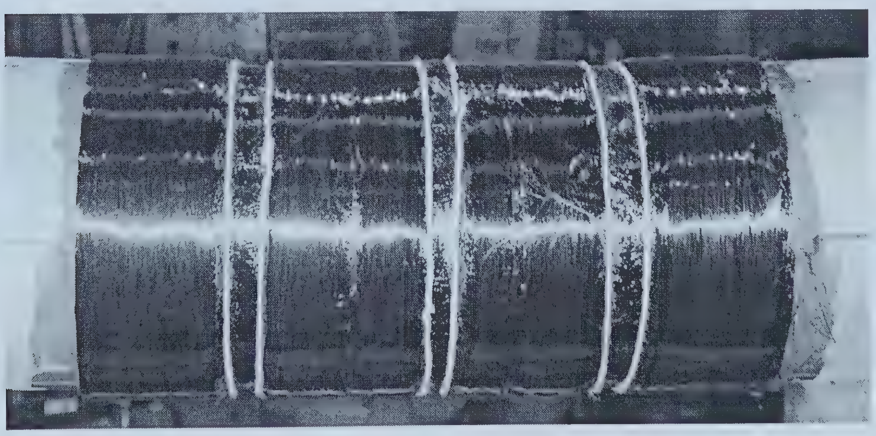

Figure 3.13 - Even Carbon Sleeve is Applied to the Pipe

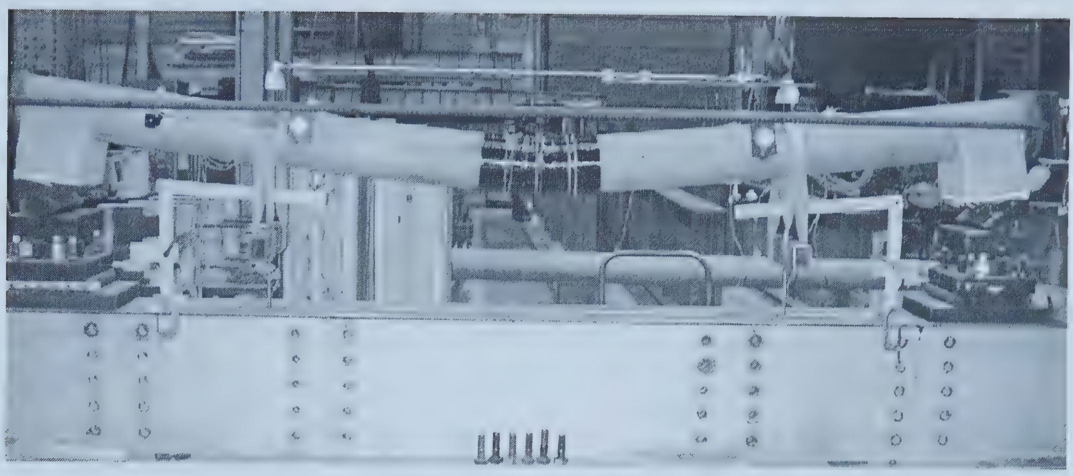

Figure 3.14 - NPS 6 Pipe Deformation at the end of the Post-Repair Test

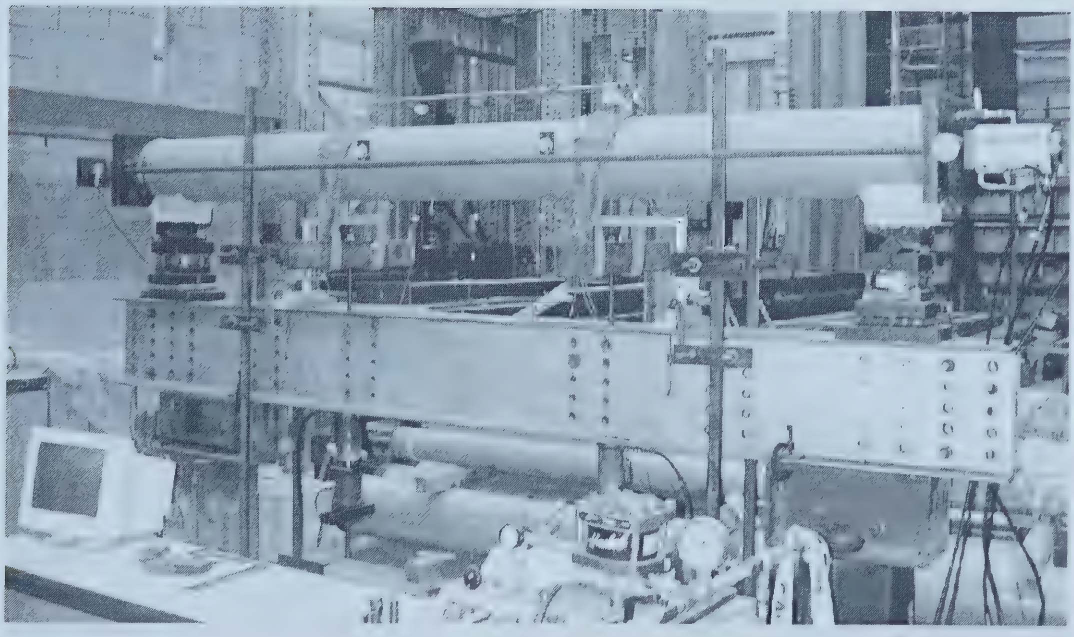

Figure 3.15 - NPS 12 Pipe Test Setup

Figure 3.16 - NPS 12 Pipe Deflection at the end of the Pre-Repair Buckling Test

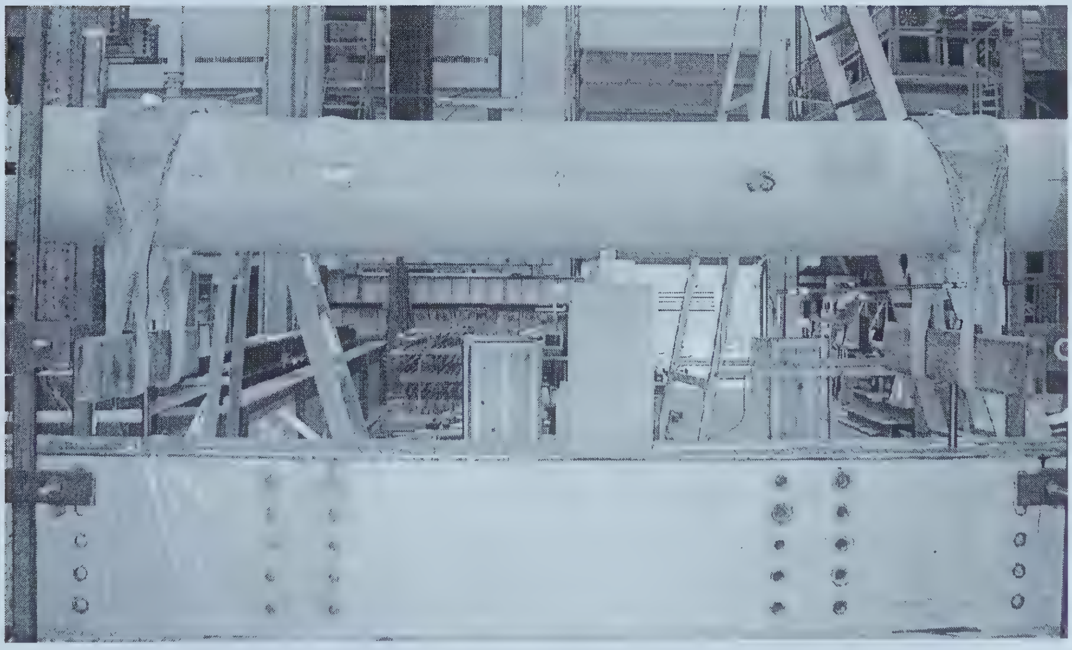

Figure 3.17 - Relocation of Load Straps Following Pre-Repair Buckling Test

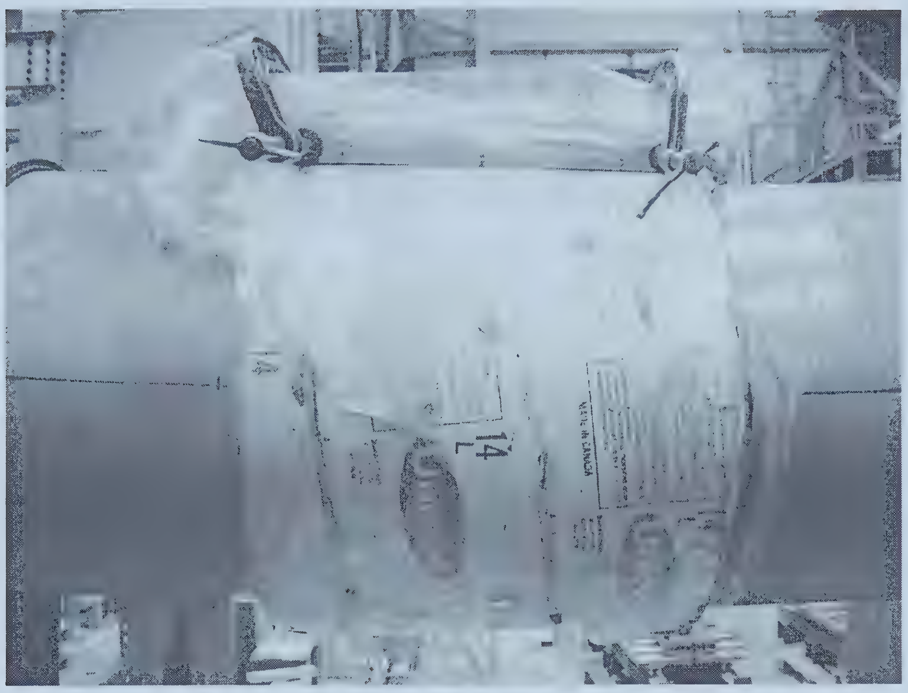

Figure 3.18 - Epoxy Putty Layer is Formed Using Cardboard Formwork Tube

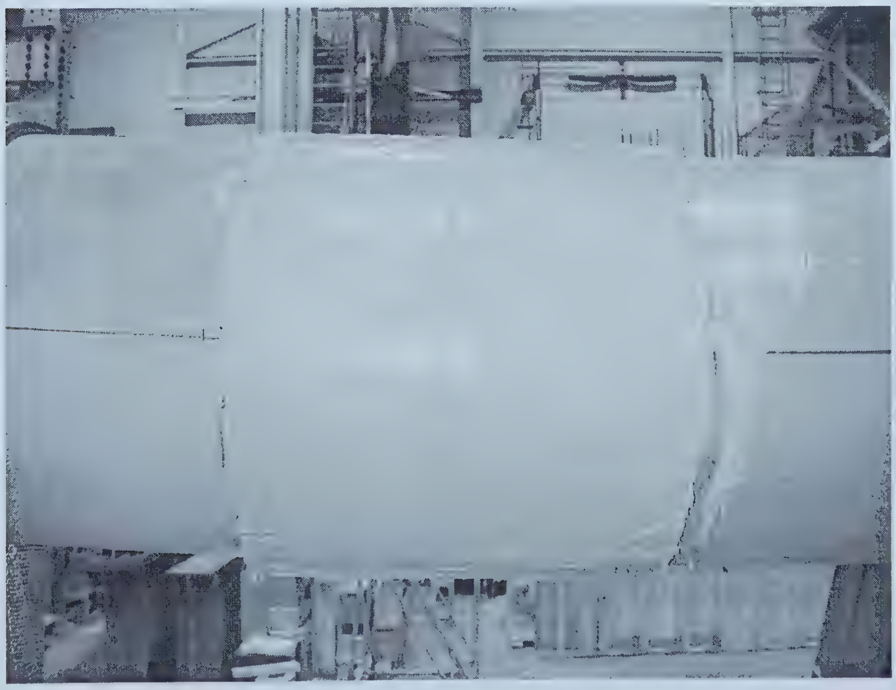

Figure 3.19 - Epoxy Putty Layer After Removal of Formwork

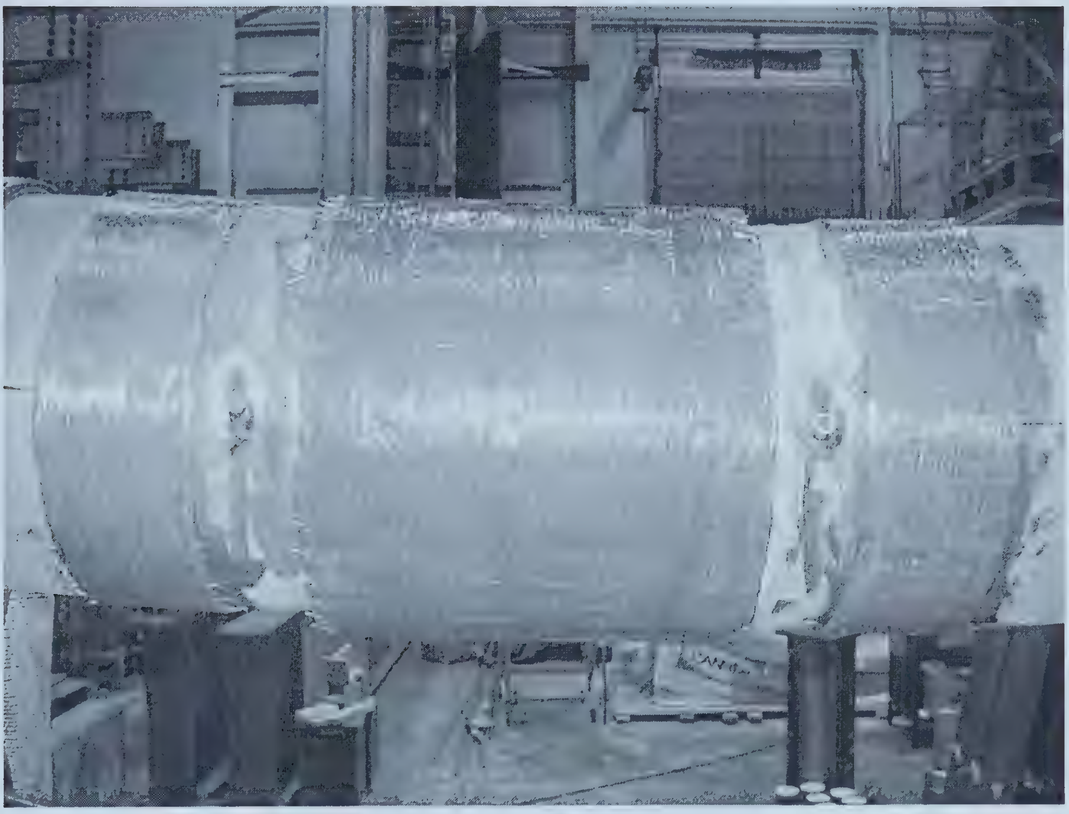

Figure 3.20 - FRP Sleeve Applied to NPS 12 Pipe

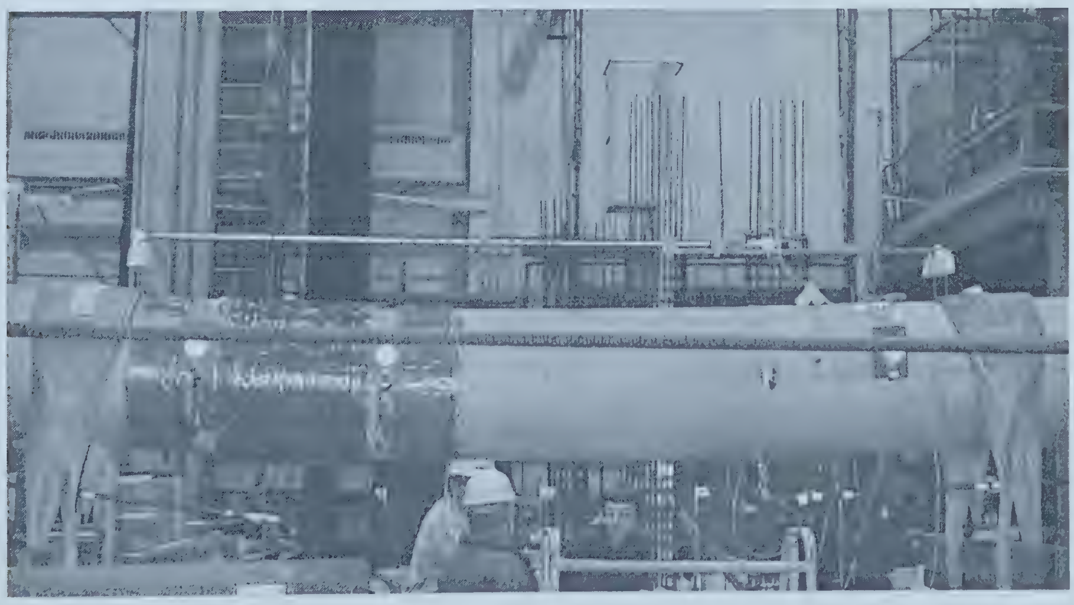

Figure 3.21 – Relocation of Rotation Meters for NPS 12 Pipe Test

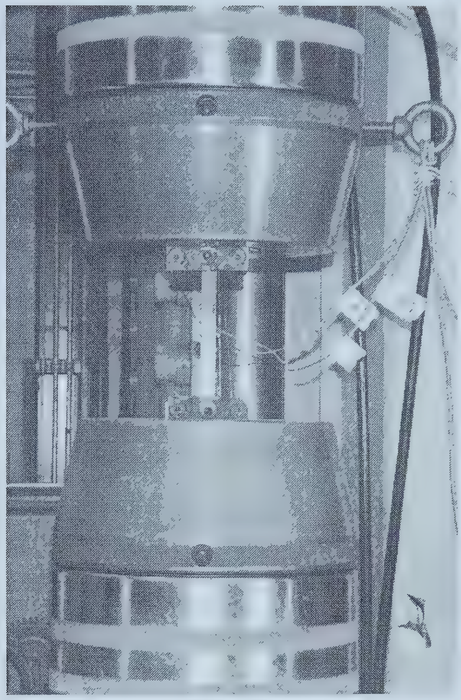

Figure 3.22 - FRP Tension Coupon in the MTS 1000 Universal Testing Machine

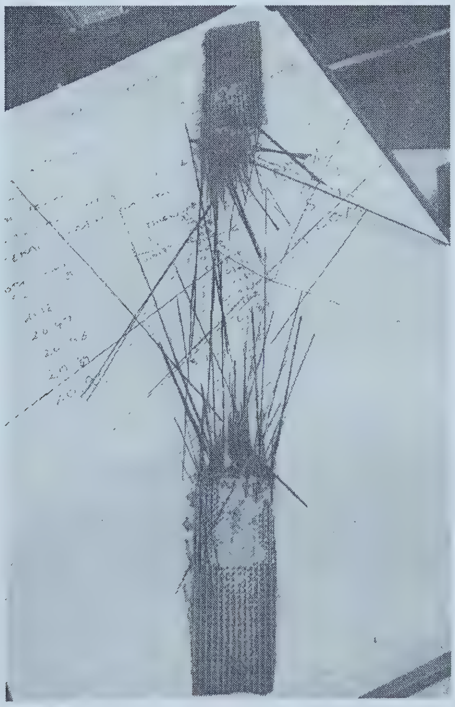

Figure 3.23 - Fracture Pattern for a Typical FRP Tension Coupon

4 EXPERIMENTAL AND FINITE ELEMENT RESULTS

One of the goals of this project was to perform a series of laboratory tests, both half-scale and full-scale; in order to observe the behaviour of wrinkled pipes repaired with FRP sleeves. In Chapter 3, the experimental program designed for the tests was described. The results of the material tests, half-scale pipe tests and full-scale pipe tests are presented in this chapter. Both qualitative results and quantitative results are given in the following sections.

The results of finite element modelling of the NPS 6 and NPS 12 pipe test specimens are also presented in this chapter. These models incorporated the material properties and load histories experienced in the lab tests. The results of the finite element models are then compared to the test results to determine the validity of the model in predicting the behaviour of FRP sleeve repairs on pipe.

4.1 Ancillary Material Test Results

Ancillary material tests were conducted in this project so that actual material properties could be input into finite element models for comparison to test data. Two main groups of materials were used in the experimental program, line pipe steel and uniaxial FRP for the sleeves. As mentioned in Chapter 3, uniaxial tension tests were conducted on both the steel and FRP materials in order to determine their load-deformation response. These results are presented in the following sub-sections.

4.1.1 Steel Material Properties

The NPS 6 and 12 pipes used in the experimental program were manufactured using the ERW process. This process substantially alters the material behaviour of the pipe steel from its parent steel plate through cold working. Therefore, tension coupons were cut from a sacrificial specimen of each pipe size. This insured that the actual properties present in the pipe were measured.

The material properties of interest in this study were the elastic modulus, E, yield stress, σ_y, ultimate stress, σ_{ult} and elongation, $\Delta_{\%}$ of the material. In order to calculate most of

the material properties, the stress-strain relationship had to be determined. This relationship would also be used to define the material behaviour in the finite element model. The stress in the coupon was calculated by dividing the applied load on the coupon by its cross-sectional area. The strain in the coupon was measured directly using an electronic extensometer. Once the stress-strain pairs were plotted using a spreadsheet program, the remaining material properties were determined.

The elastic modulus was calculated by performing a linear regression of the stress-strain data in the linear portion of the stress-strain curve. Data was taken between strains of 500 $\mu\varepsilon$ and 1,500 $\mu\varepsilon$ so that the effects of initial loading were not including in the calculation. The slope of the regression line was taken as the elastic modulus. The yield stress was determined by recording the stress at a strain level of 5,000 $\mu\varepsilon$, in accordance with accepted pipeline standards (API 5L, 1995). The ultimate stress was taken as the peak stress attained by the coupon. It should be noted that two yield and ultimate stress values are reported, a static value and a dynamic value. During plastic straining in a material, the rate of loading affects the apparent load (the dynamic value). Since loading rates amongst different material tests vary, this effect must be eliminated so that a true comparison can be made. Static readings are taken to determine the actual stress level in the coupon, regardless of loading rate. During a static reading, the rate of strain application is reduced to zero for one to two minutes. This pause allows the material to reach a state of static stress. The final material property determined was the elongation. Elongation was determined by measuring two points along the length of the coupon before the test and after. The change in length divided by the original length gave the elongation.

Figure 4.1 shows the stress-strain curves for the three NPS 6 coupons tested. All three specimens displayed similar behaviour prior to strain hardening, but it should be noted that coupon 6-1 showed substantially less ductility. It is not known at this time why this occurred. Since fracture of the pipe specimens is not a concern in the models, this irregularity was ignored. Using the stress-strain behaviour shown in Figure 4.1, the

material properties discussed previously were calculated. Table 4.1 summarizes the calculated material properties for each NPS 6 coupon.

The stress-strain curves for the NPS 12 coupons are shown in Figure 4.2 and the calculated material properties are given in Table 4.2. Originally, only three coupons were tested. However, based on the irregularities in material properties shown in Figure 4.2 and Table 4.2 an additional five coupons were tested. There is an increase in yield stress between consecutive specimens, coupled with a decreased elongation. At first, it was thought that there were errors in the coupon testing. Based on similar results from coupons 12-4 through 12-8, this is not the likely source of the discrepancy. The coupons were fabricated from a single section of the pipe, shown in Figure 4.3. The pattern of hardening in the coupons indicates that the steel used for the pipe may not have been homogeneous in the circumferential direction.

4.1.2 FRP Material Properties

Tensile tests for the FRP materials used in the experimental program were conducted to determine material properties for finite element model input. Since uniaxial FRP materials are essentially linear elastic until failure, only three material properties were determined. Using the measured load and strain values from the tension tests, stress-strain data was calculated. The stress-strain curves were then used to determine the elastic modulus, E_1, ultimate strength, σ_{ult1} and ultimate strain, ε_{ult1}. The "1" subscript indicates that these properties correspond to the 1-direction, or the fibre direction, only. No attempt was made to determine the material properties in the "2" or transverse direction, since only the 1-direction properties were crucial to the FE model.

When calculating material properties for FRP materials, it is important to remember that they are made of two very different components, fibres and matrix. Typically, the measured cross-section area of a coupon is used to calculate its stress. For high-modulus, high-fibre fraction FRP's this is an error. The measured area typically consists of one-third fibre and two-thirds polymer. Since the fibre stiffness is 20 to 80 times that of the matrix, the fibre carries virtually the entire load, if applied in the fibre direction. To

determine the actual stress in the fibre, the thickness of fibres present should be used to calculate the coupon area instead of the entire thickness of the coupon. Since it is very difficult to measure the fibre thickness in the lab, the manufacturer's specified thickness per fibre ply was used to calculate fibre stress.

Using the manufacturer's specified fibre thickness and the measured coupon load, the stress-strain relationships for the FRP materials were determined. Figures 4.4 through 4.6 show the stress-strain curves for the three FRP materials tested. From the stress-strain relationships, the required material properties were calculated. The elastic modulus in the fibre direction, E_1, was calculated by performing a linear regression on each curve between strain levels of 1,000 $\mu\varepsilon$ and 3,000 $\mu\varepsilon$. The slope of the regression line gave E_1. The ultimate stress, F_{ult1}, was determined from the stress-strain plots as the stress level at first fibre fracture. Similarly, the strain level at first fibre fracture was used for the ultimate strain, ε_{ult1}. The calculated material properties are summarized in Tables 4.3 through 4.5.

It should be noted that in many of the coupons, fibre fracture did not occur simultaneously across all the fibres of the coupon. This is shown in Figures 4.4 through 4.6 as the sections of the curves where sharp decreases stress levels occur. In actuality, the fibre stress increases monotonically and the apparent changes are due to loss of fibres in the coupon. When a group of fibres fracture, the effective cross-sectional area of the coupon is reduced and its load carrying capacity drops suddenly. Because the stress calculation is based on a constant area of fibres, the fibre stress also appears to drop. However, as strain is increased, the stress in the remaining fibres increases and a slight increase in load occurs until more fibres fracture. This continues until the ultimate strain in the final group of fibres is exceeded. Because of these actions, it is very difficult to obtain accurate estimates of ultimate stress and strain of the coupon. Therefore, the values given in Tables 4.3 through 4.5 would be considered as lower bound values.

4.2 Half-Scale Laboratory Tests

4.2.1 Test Results

Four NPS 6 bending tests were conducted according to the test matrix presented in Table 3.1. The results of these tests are summarized in this section. Qualitative observations are presented, followed by quantitative moment-curvature and fibre strain results.

4.2.1.1 Observations

The first phase of each test was pre-repair buckling. The procedure described in Section 3.3.5.1 was followed for each of the tests. Figure 4.7 shows a typical deformed pipe in the middle of the pre-repair buckling test. Symmetric deflection of the pipe about its mid-length was observed in all four pre-repair tests, confirming assumptions made in the numerical study. The pre-repair tests were run until a wrinkle formed in the pipe and had grown to a height that was deemed visible by pipeline field personnel. In all four NPS 6 tests, the wrinkle occurred within 50 mm of the mid-length. This was anticipated, since the second order moment would be largest at mid-length. Figures 4.8 shows the magnitude and location of the wrinkle at the end of a typical pre-repair test. For the control specimen, the test was not stopped until the available jack stroke was exhausted. The wrinkle magnitude at the end of the control test is shown in Figure 4.9.

Following each pre-repair test, a FRP sleeve was placed on the pipe in the region of the wrinkle. Figure 4.10 illustrates the geometry of a typical sleeve repair used. Installation of the sleeve over the wrinkle proved to be challenging. The FRP sheets used for the sleeves were not easily contoured to the shape of the wrinkle in the longitudinal pipe direction when they were wrapped circumferentially onto the pipe. The variation in the pipe's diameter along the width of the sleeve section created regions of bulging in the sleeve, where the sleeve was not properly contacting the pipe. Figure 4.11 shows a close-up of a carbon sleeve at the wrinkle crest. The uneven distribution of fibres along the wrinkle crest caused by the changing pipe diameter can be observed. There was some concern at the time that the bond between the sleeve and pipe was not sound. This is addressed in Section 4.3.1.1.

Following curing of the sleeve, the pipe was reloaded. As the curvature of the pipe was increased, the anticipated increase in post-buckling load capacity was observed. After the load was increased above the level at the end of the pre-repair test, fracture of the fibre could be heard. For tests 6-CO-9-M and 6-CE-18-E, occasional fibre fracture at the wrinkle crest was visible along with the fracture sound. For test 6-GE-10-L, no visible fracture occurred when fracture sounds were heard. It was thought that either fibre below the surface was fracturing or delamination of the FRP layers was occurring.

In all three tests, curvature was increased until complete fracture of the fibre had occurred. The deformation of the pipe at end of test 6-CO-9-M is shown in Figure 4.12 as a typical figure. Fracture of the sleeves was limited to the area around the wrinkle crest. Fracture patterns were noticeably different between the carbon and glass fibre sleeves. Figures 4.13 and 4.14 show the fracture of the carbon fibre sleeves. The carbon fibre fractured in a progressive manner, with a steady fracture of the fibres as curvature was increased. Unlike the carbon fibre, the glass fibre fractured in a more sudden fashion. A large group of glass fibres would simultaneously fracture at a distinct location. This fracture pattern is shown in Figure 4.15. There was evidence of significant debonding at the time of fracture for the glass fibre. This confirmed the notion that the bond between the sleeve and pipe established during sleeve application was questionable.

4.2.1.2 Moment-Curvature Behaviour

The primary quantitative measure for the performance of the sleeve repair was its effect on the moment-curvature performance of the pipe. Two aspects of moment-curvature performance were of interest: the effect of the sleeve on the moment capacity of the pipe and the effect of the sleeve on the ductility of the pipe. Both of these aspects were considered equally important in assessing the sleeve repair.

In the finite element study presented in Chapter 2, the global moment along the pipe length was determined. Due to second order effects, this moment was calculated at the mid-length of the pipe, the location of maximum second order moment. The total

moment, M_T, applied to the test specimen was calculated from the electronic data gathered at every load step using the following formula:

$$M_T = \frac{N_{LC1}\left(l_{S1} + \Delta_{R1} + \frac{\Delta_{LOAD}}{2}\right) + N_{LC2}\left(l_{S2} + \Delta_{R2} + \frac{\Delta_{LOAD}}{2}\right)}{2} + \left(P_{LC5} + P_{LC6}\right)\Delta_{CL} \quad (4.1)$$

where: $N_{LC1(2)}$ = east (west) reaction loads (kN)

$l_{S1(2)}$ = initial length of east (west) shear span (m)

$\Delta_{R1(2)}$ = longitudinal movement of east (west) reaction (m)

Δ_{LOAD} = relative longitudinal movement of load points to each other (m)

$P_{LC5(6)}$ = north (south) axial load in prestressing rod (kN)

Δ_{CL} = vertical deflection of pipe at mid-length (m)

The global curvature in the preliminary FE study was determined by measuring the rotations of the pipe ends. In the NPS 6 tests, rotation was measured only in the area of constant span moment, the region where the moment would be calculated. Global curvature was calculated at every data scan using Formula 4.2:

$$\Phi_{GLOBAL} = \frac{|\theta_1| + |\theta_2|}{l_{\theta1-\theta2}} * 1x10^6 \quad (4.2)$$

where: Φ_{GLOBAL} = global curvature (μrad/mm)

$\theta_{1(2)}$ = rotation of east (west) RVDT (radians)

$l_{\theta1-\theta2}$ = initial gauge length between rotation meters (mm)

The moment-curvature plots for the NPS 6 tests are given in Figure 4.16. As one can expect, the behaviour of each test is similar up until the point of sleeve application. The curves follow a general pattern prior to sleeve application. Behaviour is linear up to 20 μrad/mm. The pipe is still in the elastic range in this region. Between 20 and 80 μrad/mm yielding of the cross-section occurs and the slope of the curve decreases as yielding progresses through the cross-section. At a curvature of approximately 80 μrad/mm, the slope of the curve is essentially zero. This indicates that pipe cross-section has fully yielded and the plastic moment capacity of the pipe has been achieved. The ability for the pipe to reach its plastic moment prior to local buckling is consistent with

observations of other low D/t ratio pipes (Dorey *et al.,* 2001). Local buckling occurs shortly afterwards, at 100 μrad/mm, followed by a rapid drop in moment capacity.

An anomalous drop in moment capacity seems to occur for the 6-NS specimen at around 70 μrad/mm. In fact, this reading is akin to a static reading taken in the material coupon tests. In the first pipe test, the nylon straps used to transfer load from the point jacks to the pipe were permanently stretched. The magnitude of stretching was not known prior to testing, so at this point in the test, the stroke of the jacks was exhausted. It was necessary to recover the jack stroke in order to continue the test. A reading was taken prior to and following reset of the jacks. The static response, measured after resetting of the jacks gives an indication of the loading rate used during the test. Because the straps were permanently stretched after the first test, it was not necessary to reset the jacks in subsequent tests until sleeve application; thus, no drops are seen in the three repair tests.

At the point of buckling, a rapid drop in moment capacity of the pipe occurs. Again test 6-NS gives some misleading results. Between curvatures of approximately 120 and 140 μrad/mm, the capacity of the pipe seems to be constant. This was not true in reality. Following buckling, it was very difficult to maintain the axial load due to large axial deformations in the pipe. After a curvature of 120 μrad/mm was reached, it was decided that axial load would no longer be maintained and the curvature would be increased via vertical displacement at the load points only. When the jack stroke was increased, the corresponding increase in curvature caused the axial load to drop due to axial shortening of the pipe. The system reacted to the drop in axial load by increasing the span load to keep the total moment constant. This problem was avoided in subsequent tests by increasing the strokes on the axial and point load jacks simultaneously. Looking at the moment level when test 6-GE-10-L is stopped for sleeve application, it is indeed less that what was observed with 6-NS, indicating that the moment capacity does drop at higher levels of curvature.

Examining Figure 4.16 further, the effects of the sleeve repairs on the moment capacity and ductility of the pipe are shown. In all cases, the post-buckling moment capacity of

the pipe is increased following sleeve repair. A drop in moment capacity follows the peaks in all three tests. This same drop was observed in Chapter 2, when secondary wrinkling occurred. In the case of the lab tests, however, this drop is due to fracture of the fibre sleeve (something that was not examined in the FE study).

Several trends are present in Figure 4.16. First, the earlier the pipe is repaired, with reference to curvature, the larger the recover of capacity is. Second, comparing tests 6-CO-9-M and 6-CE-18-E, the even sleeve design seems to provide more ductility to the system. That is, the drop in moment capacity after fibre fracture is much less in the even sleeve repair than the odd sleeve. Finally, the glass fibre sleeve, although the latest repair, provides very good ductility to the pipe; the rate of moment capacity decrease for 6-GE-10-L is much less than that of 6-CE-18-E.

4.2.1.3 FRP Strain

In Figures 4.13 through 4.15, fracture of the sleeve directly over top of the wrinkle crest was illustrated. When the preliminary FE study was conducted, it was not believed that fracture of the fibre would be a problem, since the ultimate strength of the fibres was 3 to 10 times that of the pipe and pipe fracture was never observed in monotonically loaded bending tests under normal operating pressures. However, after fibre fracture in test 6-CO-9-M, it was decided that the behaviour of the fibres in the sleeve should be looked at more closely.

Since fibre fracture had occurred near the crest of the wrinkle a strain gauge was placed on the outer surface of the sleeve at the centreline of the wrinkle. The gauge was orientated in the hoop direction of the pipe, which corresponded to the fibre direction in the sleeve.

Figure 4.17 shows the strain in the fibre versus global curvature in the pipe for tests 6-CE-18-E and 6-GE-10-L. Both curves display similar behaviour. Each has three distinct sections. There is an initial jump in fibre strain immediately after application of load. This jump is due to the application of internal pressure to the pipe, which creates hoop

strain in the pipe (longitudinal strain in the fibre) with very little change in global curvature. The second segment of the curve corresponds to initial reloading of the pipe. This is the elastic re-loading segment of the moment curvature curves shown in Figure 4.16. The final segment of the curve corresponds to growth of the wrinkle and the increase in moment capacity seen in Figure 4.16.

Although the two materials exhibit similar strain at fracture, fracture in the carbon sleeve was initiated much earlier than the glass fibre sleeve (as mentioned in Section 4.2.1.1). This is to be expected, since the ductility of carbon fibre is approximately 50% that of glass fibre. Fracture initiated in 6-CE-18-E at a strain level of approximately 0.3 % with significant fracture occurring at 1.1%. When the gauge was lost at 1.9%, there was virtually no fibre left intact over the wrinkle crest. Conversely, in 6-GE-10-L, there was no evidence of fracture occurring until a strain of 1.2%. Even at this point, no fracture was visible, only fracture sounds were heard. Fracture of the glass fibre came suddenly at a strain of 2.0%. At this point all the fibres at the wrinkle crest fractured and the strain gauge was lost. From these observations, the ductility of the glass fibre, compared to carbon, is evident.

4.2.2 Comparison to Finite Element Results

Results of the FE analysis of the four NPS 6 bending tests are presented in this section and compared to the results observed in the laboratory tests. The FE analysis and test results are compared both visually, via the deformed shape of the pipe at different stages in the test, and graphically, via plots of global moment and fibre strain versus global curvature.

4.2.2.1 FE Model Used in the Comparison

In Chapter 2, a FE model for the NPS 12 pipe was developed and tested. This model consisted of elements approximately 25 mm x 25 mm in dimension with a total pipe length of 2,438 mm. To model the NPS 6 pipe used in the laboratory testing, the NPS 12 model was reduced in dimensions to match that of the NPS 6 pipe. The length of the NPS 6 model was taken as the length between the two load points in the testing, 1,524 mm. By using the same L/D ratio for the model as the test specimen, between load

points, the maximum moments of the two would be comparable. It was determined, however, that several other modifications to the original FE model were required.

Originally, no attempt was made to reduce the mesh size of the NPS 6 model because the moment-curvature behaviour of the model agreed well with that observed in the 6-NS test. However, the geometry of the wrinkle was considerably different between the two. The coarse mesh used was not able to predict the smaller wrinkle dimensions of the NPS 6 pipe. Because it would be important in sleeve repair design to have a good estimate of the wrinkle geometry, it was decided that the mesh needed to be refined. A two-step refinement was chosen and is shown in Figure 4.18. Elements at the ends of the model were reduced from 25 mm x 25 mm to 12.5 mm x 12.5 mm and immediately in the vicinity of the wrinkle area, the elements were again reduced to 6.25 mm x 6.25 mm. This type of stepped refinement allowed the geometry of the wrinkle to be properly modelled, without adding an excessive number of elements to the model.

The initial imperfection pattern was modified from the original FE model. Based on work by Dorey *et al.* (2001), a "blister" imperfection was used instead of the "bulge" imperfection shown in Chapter 2. The blister imperfection had the same profile in the longitudinal direction as the bulge, a cosine curve. However, in the hoop direction, the blister imperfection did not encompass the entire circumference of the pipe. It was limited to an arc of equal length as its longitudinal dimension. A cosine shape in the circumferential direction was also chosen to give a smooth transition between the peak imperfection magnitude and the nominal pipe diameter. A typical blister imperfection is shown in Figure 4.19. The amplitude of the imperfection was also modified, to reflect the smaller pipe. A maximum height of 1.5% of the wall thickness, or approximately 0.045 mm was chosen.

The final modification to original FE model was with regards to the material model used. Equations 2.1 and 2.2 were used to convert measured engineering stress – strain data shown in Figure 4.1 to true stress – logarithmic plastic strain data required by ABAQUS. When this material model was used in the analysis, buckling of the pipe occurred at

significantly lower levels than observed in the experiments. This phenomenon has been observed in FE analysis of pipe buckling when the material model used contains a yield plateau (Dorey *et al.*, 2001). Examining Figure 4.1 closely, a yield plateau is evident. Normally, line pipe that has been hydrotested does not exhibit a distinct yield plateau (Zhou *et al.*, 1996). Yielding is more gradual and a smooth rounded stress – strain curve results. An accepted method for developing a true stress – strain curve for pipeline steel is to use a modified Ramberg-Osgood formulation (DeGeer and Cheng, 2000) as shown in Equation 4.3:

$$\varepsilon_{true} = \frac{\sigma_{true}}{E} + \left(\varepsilon_{py} - \frac{\sigma_y}{E}\right)\left(\frac{\sigma_{true}}{\sigma_y}\right)^n \tag{4.3}$$

where: ε_{true} = true strain (mm/mm)

ε_{py} = engineering strain at yield, 0.005 mm/mm

σ_{true} = true stress (MPa)

σ_y = yield stress (MPa)

E = Young's modulus (MPa)

n = strain hardening parameter

Values for σ_y and E were taken from averages of the values reported in Table 4.1. The dynamic yield stress was used in Equation 4.3, since, as was seen in Figure 4.16, there was some dynamic component to the global moment. The strain hardening parameter, n, was chosen so that the slopes of the calculated true stress – strain curve and the measured true stress – strain curve (shown in Figure 4.20), in the strain-hardening region, were similar. A value of n = 10 was used in the material model.

4.2.2.2 Wrinkle Geometry

The geometry of the wrinkle in the model and test results can be compared to determine the validity of the model. Figures 4.21 through 4.24 compare the wrinkle geometry predicted by the model to that observed in the lab tests for the four NPS 6 tests. Figure 4.21 shows the wrinkle at the end of the test, while Figures 4.22 through 4.24 show the wrinkle prior to sleeve application. These figures show that the model does a very good job predicting the failure mode of the pipe with the refined mesh.

Figures 4.25 through 4.27 show the wrinkle development at the conclusion of each test. The model predicts secondary wrinkle growth for the carbon fibre sleeves, when it does not actually occur in the lab. As was mentioned previously, the model did not account for fibre fracture, which allowed the primary wrinkle to be stopped. In Figure 4.27, continued growth of the primary wrinkle is shown. While this did occur in the lab, it occurred along with fibre fracture. Again, the model does not assume fracture of the fibre.

4.2.2.3 Moment-Curvature Behaviour

The global moment – curvature histories of lab tests 6-NS, 6-CO-9-M, 6-CE-18-E and 6-GE-10-L and their respective FE models are plotted in Figures 4.28 through 4.30. Very good agreement between the test data and the model data prior to sleeve repair is observed. At the early stages following the repair, the model does a reasonable job predicting the moment – curvature response. However, all the repair models then begin to diverge from the test data. The point of divergence corresponds to the approximate point of fracture in the laboratory sleeves. Since the model does not account for fracture, it can't be used to compare to test data after this point. However, if fracture of the sleeve is prevented, one can assume that the model should be able to predict the response of the pipe to the repair. This possibility will be further discussed in Chapter 5.

4.2.2.4 FRP Strain

Fibre strain – global curvature behaviour for specimens 6-CE-18-E and 6-GE-10-L shown in Figure 4.17 is compared to FE model data in Figure 4.32. Specimen 6-CE-18-E shows very good agreement for strain levels below 1%. Below this level there was limited fibre fracture observed, so the model predicts behaviour well. Above 1% strain, fibre fracture became prevalent and the sleeve could not slow down the wrinkle as predicted in the model (indicated by a decrease in the strain growth in the fibre) and strains elevated. For specimen 6-GE-10-L excellent agreement at all levels of strain is shown. The sudden fracture of the glass fibre sleeve mentioned in Section 4.2.1.3 manifests itself in Figure 4.32 through the agreement between FE and test data. For the carbon fibre sleeve, as fracture progressed in the sleeve, the behaviour of the model and

test data progressively diverged. In the case of the glass fibre, progressive failure was absent, thus the model was able to predict behaviour very well prior to fracture.

4.3 Full-Scale Laboratory Tests

4.3.1 Test Results

Two repair tests were conducted on the full-scale, NPS 12, pipe. The test variables were given in Table 3.2 in Chapter 3. In this section, as was done for the NPS 6 pipe, both qualitative and quantitative results of the experiments are presented.

4.3.1.1 Observations

Since the NPS 12 test setup used was essentially the same as the NPS 6 test setup, it was anticipated that pipe behaviour during the pre-repair testing would be very similar to previous observations from the NPS 6 tests. During the first part of the pre-repair test for 12-GO-12-M the pipe behaved much like expected. The deformed shape of the pipe during the pre-repair test is shown in Figure 4.33. During the last part of the pre-repair test, however, the behaviour of the pipe changed from previous tests. In Chapter 3 it was mentioned that due to the smaller L/D ratio of the constant moment region for the NPS 12 test setup, the disturbance caused by the loading strap might have more influence on the location of wrinkle formation. This was indeed the case for test 12-GO-12-M. In Figure 4.34, the wrinkle forming immediately adjacent to the east load strap can be seen.

In order to accommodate a repair sleeve for 12-GO-12-M, the load points and rotation meters were relocated as described in Section 3.4.5.2. Once the load straps were relocated, a FRP sleeve was installed onto the pipe. The sleeve, shown in Figure 4.35, was composed of a glass fibre section over the wrinkle and two carbon fibre sections away from the wrinkle. Originally, a sleeve system consisting entirely of glass fibre was planned, but due to material shortages, there was only enough glass fibre to cover the critical section over the wrinkle. If one examines Figure 4.35 closely, the fibre in the vicinity of the wrinkle crest appears to undulate. The inability of the fibre sleeve to form to the contours of the pipe around the wrinkle created the undulations. As was the case with the NPS 6 tests, the bond of the 12-GO-12-M sleeve was questionable.

Upon reloading of the 12-GO-12-M specimen after sleeve curing, the same behaviour seen in the 6-GE-10-L test occurred. Popping noises could be heard, but no fibre fracture was apparent. The popping was likely debonding occurring in the undulating regions of the sleeve. The fibre fracture, shown in Figure 4.36, appeared suddenly, followed by a rapid drop of pipe elevation.

To avoid wrinkle formation near the load strap for test 12-GO-6-M, steel collars were placed around the pipe in the vicinity of each load strap (see Figure 4.37). The purpose of the collars was to stiffen the pipe locally, forcing the wrinkle to form closer to the mid-length of the pipe. The collars were kept hand-tight during the 12-GO-6-M pre-repair test so that no additional imperfections would be created in the pipe wall. Early in the 12-GO-6-M pre-repair test the collar solution appeared to be work. Figure 4.38 shows the very early stages of a wrinkle forming near the mid-length of the pipe. As additional curvature was imposed onto the pipe, the wrinkle in Figure 4.38 did not grow. This did not make sense until a second wrinkle was seen growing under the collar adjacent to the east load strap.

The steel collars were not effective in stiffening the pipe in the hoop direction when only hand tight. The result was the formation of a wrinkle at the same location it formed in the 12-GO-12-M test. As the wrinkle grew, it placed the collar bolts into tension, creating a stiffer collar. The stiffened collar was able to slow the wrinkle growth and force inward deformation of the pipe wall adjacent to the wrinkle toe. This is shown in Figure 4.39. As was required in the 12-GO-12-M test, the loading straps and rotation meters had to be relocated to accommodate the repair sleeve.

The fibre sleeve was installed according to the revised procedures discussed in Chapter 3. The sleeve was shown in Figure 3.20. During reloading of the pipe, the debonding sounds observed in previous tests were absent. This indicated that the revised sleeve application technique had provided a good bond between the sleeve and pipe. Very little outward growth of the wrinkle was observed during reloading. Once elastic reloading

was completed, the capacity of the pipe increased, as anticipated. As plastic deformation was increased, the sleeve began to move inwards adjacent to the wrinkle crest. The inward "dents" in the sleeve diagonally symmetric about the wrinkle crest can be seen in Figure 4.40. The pattern was very similar to the diamond buckling shape observed in previous buckling tests of pipe under zero internal pressure (for example Dorey *et al.*, 2001). It became apparent that the sleeve had stopped the outward growth of the bulge buckle and forced secondary wrinkling to occur, as predicted in earlier FE models. Secondary wrinkling, however, took the form of inward buckles immediately adjacent to the outward buckle.

4.3.1.2 Moment-Curvature Behaviour

The global moment and global curvature of the NPS 12 pipe specimens were calculated from the measured test data using Equations 4.1 and 4.2. Figure 4.41 gives the moment-curvature histories for the 12-GO-12-M and 12-GO-6-M tests. The shapes of the curves are similar to those seen in Figure 4.16 for the NPS 6 pipe tests. This was expected, since the D/t ratios of the two pipe sizes were very similar. Initially the curve is linear, when the pipe is still in the elastic range. Yielding of the cross-section begins at a curvature of approximately 10 μrad/mm. For specimen 12-CO-12-M, the plastic moment is reached prior to local buckling at a curvature of 55 μrad/mm. Specimen 12-CO-6-M appears to have significantly higher amounts of ductility prior to local buckling (buckling at 81 μrad/mm). The increase in ductility was actually due to the collar located over top of the wrinkle.

Figure 4.38 showed the appearance of a very small bulge near the mid-length of the pipe. That picture was taken at a curvature of approximately 58 μrad/mm, very close to the buckling curvature of 12-CO-12-M. In previous pipe buckling tests, it has been observed that multiple wrinkles form at the onset of buckling and shortly after, one wrinkle dominates. It can be assumed that this same phenomenon was occurring in the 12-CO-6-M specimen and the wrinkle shown in Figure 4.38 was only one of these wrinkles. In all likelihood, a second wrinkle had been simultaneously growing under the collar and began to dominate. The collar then slowed its growth. This increased the ductility of the pipe in

a similar manner as observed in the FE modelling done by Yao and Murray (2000). One can recall that in their analysis, the sleeve was placed onto the pipe immediately after the peak moment was reached and subsequently a gain in ductility occurred. If the effect of the collar is ignored, it can be hypothesized that the two tests performed similarly prior to sleeve application.

When the post-repair behaviour of the NPS 12 specimens is examined, similarities to the NPS 6 tests are observed. For specimen 12-GO-12-M an increase in the ductility of the pipe occurs, similar to what was seen with 6-GE-10-L. This increase appears to be indicative of the glass fibre used. The same relative rise in moment capacity after sleeve installation for 12-GO-12-M compared to 6-GE-10-L is absent. This may be largely due to the very questionable bond of the fibre to the pipe. Looking at 12-GO-6-M, a more significant increase in moment capacity following sleeve installation occurs, similar to 6-GE-10-L. However, the ductility increase seen with the other glass fibre sleeve repairs is noticeably absent. The abrupt change in buckling mode from outwards bulging to inwards diamond buckling likely caused the limited ductility gain.

4.3.1.3 FRP Strain

The FRP strain at the wrinkle crest was monitored for the NPS 12 test series. Figure 4.42 shows the longitudinal fibre strain at the wrinkle crest versus global pipe curvature. For specimen 12-GO-12-M, the same type of behaviour that was observed in the NPS 6 series is present, with fracture of the fibre occurring at a strain of 1.7%. The behaviour of 12-GO-6-M is somewhat different. A peak strain of 1.2% is reached in the fibre, followed by a rapid drop in strain. Since fibre fracture in the 12-GO-6-M test was not observed, the drop in strain can be attributed to secondary wrinkling occurring immediately adjacent to the wrinkle crest, the diamond buckling. The strain in the primary wrinkle was rapidly shed to the secondary wrinkles.

4.3.2 Comparison to Finite Element Results

The results of FE analysis based on the test parameters of the NPS 12 laboratory tests are presented in this section. As was done with the NPS 6 FE models, comparisons of the

observed wrinkle geometry and moment and fibre strain – curvature behaviour to model predictions will be made.

4.3.2.1 FE Models Used in the Comparison

Similar modifications as those discussed in Section 4.2.2.1 were applied to the original NPS 12 FE model, to create the NPS 12 FE model used to compare to test results. The length of the model was reduced from 2,438 mm to 1,372 mm, to reflect the distance between the load points used in the laboratory tests. A mesh refinement was then implemented (shown in Figure 4.43). The entire mesh of the model was refined from 25 mm x 25 mm elements to 12.5 mm x 12.5 mm elements. The blister imperfection, shown in Figure 4.19, was also implemented into the model. An imperfection with amplitude of 1.5% of the wall thickness (or 0.095 mm) was used. It should be noted that the imperfection was still introduced at the mid-length of the model, even though wrinkling did not occur at mid-length in the test specimens. It was anticipated that the exact location of the wrinkle would not impact the behaviour of the pipe. The Ramberg-Osgood material model was implemented into the pipe model. In Figure 4.2, the yield plateau for the 12-1 coupon is not a prevalent as was the case with the NPS 6 coupons. However, for consistency between the NPS 6 and NPS 12 models, Equation 4.3 was used to determine the true stress – strain curve for input into ABAQUS (see Figure 4.44). Because of the variable material properties observed between the NPS 12 coupons, values for σ_y, E and n were determined from the stress – strain curve for coupon 12-1, considered a lower bound of the material properties. Unlike the NPS 6 tests, the NPS 12 tests were conducted under lower load rates. Therefore the static yield stress was used in Equation 4.3 to calculate true strain.

Two final modifications were made to the original FE model for the 12-GO-6-M specimen, for comparison purposes only. To simulate the effects of the collars on development of the wrinkle, temporary elements were added to the model immediately after the peak moment was reached to simulate the collars. These elements had the geometry of the collars, but with variable material stiffness. In the 12-GO-6-M test, the collars were not effective until the wrinkle had begun to grow underneath one and tension

the collar bolts. This was simulated in the model by varying the stiffness of the collar elements from 0 to 200,000 MPa as the elements were strained. The collar elements were then deactivated prior to sleeve application.

For test 12-GO-6-M, wrinkling occurred in an unsymmetrical fashion, as shown in Figure 4.39. This occurred because the collars were not symmetric about the location where the wrinkle formed. Unsymmetrical behaviour was modelled by rotating the pipe ends unequally. By rotating one end of the pipe 90% of the rotation at the other end, unsymmetrical behaviour was achieved.

4.3.2.2 Wrinkle Geometry

Figures 4.45 and 4.46 show the wrinkle geometry predicted by the FE models and those observed in tests 12-GO-12-M and 12-GO-6-M. In the case of 12-GO-12-M, very good prediction by the model occurs. Again, the mesh refinement allows the geometry of the wrinkle to be captured smoothly. For 12-GO-6-M, the prediction is reasonable, but not excellent. This can be expected, given the difficulty in modelling the complex interaction between the wrinkle and the collars.

Figures 4.47 and 4.48 show the wrinkle geometry at the end of each NPS 12 test. The FE model predicts the growth pattern of the wrinkle for test 12-GO-12-M, although the two differ after fibre fracture. In Figure 4.48, it is shown that the model does predict the inwards buckling that was observed. The model appears to predict more inwards growth than observed in the test, but it should be noted that the model does not include the putty filler (see Section 3.4.5.2) that was used between the pipe and the FRP sleeve. While the test sleeve moved inwards only slightly, one should add the inwards growth prior to sleeve repair, which was filled with putty, to make a correct comparison.

4.3.2.3 Moment-Curvature Behaviour

Moment – curvature plots of model and test data for 12-CO-12-M and 12-CO-6-M are shown in Figures 4.49 and 4.50. For test 12-CO-12-M, the FE model predicts behaviour very well, until fibre fracture, which occurs at a curvature of 94 μrad/mm. The FE model for test 12-CO-6-M does a reasonable job predicting the behaviour of the pipe prior to

sleeve repair. During reloading, following sleeve repair, the model predicts the test well. This was anticipated, since this was elastic reloading. After reloading, the model diverges from the test data. This is most likely due to the complexity of the transition from outwards to inwards buckling.

4.3.2.4 FRP Strain

Figure 4.51 shows the plots of fibre strain versus global curvature for tests 12-CO-12-M and 12-CO-6-M and their respective models. Both models predict fibre strain well in the initial reloading stages. Following reloading, both models begin to diverge from test data. The FE model for test 12-CO-12-M is similar to test data, except that strain is accumulated more quickly in the FE model than seen in the test. This may be due to debonding that was heard occurring during the test, causing a softer response by the fibre as strains were relieved. For test 12-CO-6-M, the FE model does not accurately predict the behaviour of the fibre. The general shape is somewhat similar, but the rapid relief of strain observed in the test is absent in the model, although the model does show a slow stress relief. The large discrepancies shown in the 12-CO-6-M model are not typical of the other models shown in this chapter. However, given the complexity of the 12-CO-6-M test, this is acceptable.

Several patterns of behaviour of FRP sleeve repairs on buckled line pipe have been observed in Chapter 2. In this chapter, several of these patterns have been verified through laboratory tests. These patterns and their potential towards optimizing FRP sleeve repairs on line pipe will be discussed in Chapter 5.

Table 4.1 - Engineering Properties Determined from NPS 6 Pipe Coupons

Specimen	t (mm)	$\sigma_{y\ stat.}$ (MPa)	$\sigma_{y\ dyn.}$ (MPa)	$\sigma_{ult\ stat.}$ (MPa)	$\sigma_{ult\ dyn.}$ (MPa)	E (MPa)	Elong. (%)
6-1	3.220	413	428	463	488	188883	26.5
6-2	3.220	410	424	468	493	195018	30.2
6-3	3.229	417	434	483	508	196571	32.9
Average	3.223	413	429	471	496	193491	29.9
Std. Dev.	0.005	4	5	10	10	4065	3.2
Co. Var. (%)	0.2	0.9	1.2	2.2	2.1	2.1	10.6

Table 4.2 - Engineering Properties Determined for NPS 12 Pipe Coupons

Specimen	t (mm)	$\sigma_{y\ stat.}$ (MPa)	$\sigma_{y\ dyn.}$ (MPa)	$\sigma_{ult\ stat.}$ (MPa)	$\sigma_{ult\ dyn.}$ (MPa)	E (MPa)	Elong. (%)
12-1	6.276	497	507	537	569	195071	27.3
12-2	6.311	525	547	555	583	196493	24.8
12-3	6.417	537	564	559	587	188678	22.4
12-4	6.438	525	539	532	563	197736	27.1
12-5[1]	6.498	547	561	553	584	188585	7.2
12-6[1]	6.473	541	561	544	580	190853	5.8
12-7[1]	6.426	527	543	534	567	191218	7.1
12-8[1]	6.379	486	505	526	556	188393	14.3
Average	6.402	523	541	543	574	192128	25.4
Std. Dev.	0.077	21	23	12	11	3780	2.3
Co. Var. (%)	1.2	4.1	4.3	2.2	2.0	2.0	9.1

[1] Specimens 12-5 through 12-8 fractured outside gauge marks and therefore were not included in the calculation of the elongation average and standard deviation.

Table 4.3 - Engineering Properties Determined from Carbon Fibre Coupons

Specimen	t (mm)[1]	E_1 (MPa)	$\sigma_{ult\ 1}$ (MPa)	$\varepsilon_{ult\ 1}$ (%)
C-1	0.110	229207	3443	1.38
C-2	0.110	197338	3249	1.60
C-3	0.110	233653	3728	1.56
C-4	0.110	233864	3802	1.56
C-5	0.110	232073	3392	1.50
Average	0.110	225227	3523	1.52
Std. Dev.	0.000	15701	234	0.09
Co. Var. (%)	0.0	7.0	6.6	5.6

[1] Manufacturer's specified thickness for 1 layer of fibre sheet

Table 4.4 - Engineering Properties Determined from FTS-GE-30 Glass Fibre Coupons

Specimen	t (mm) [1]	E_1 (MPa)	$\sigma_{ult\,1}$ (MPa)	$\varepsilon_{ult\,1}$ (%)
G1-1	0.149	74049	1060	1.54
G1-2	0.149	69642	883	1.69
G1-3	0.149	70857	1029	1.66
G1-4	0.149	81469	1077	1.35
G1-5	0.149	80550	1235	1.61
Average	0.149	75313	1057	1.57
Std. Dev.	0.000	5453	125	0.13
Co. Var. (%)	0.0	7.2	11.9	8.5

[1] Manufacturer's specified thickness for 1 layer of fibre sheet

Table 4.5 - Engineering Properties Determined from MBrace EG900 Glass Fibre Coupons

Specimen	t (mm) [1]	E_1 (MPa)	$\sigma_{ult\,1}$ (MPa)	$\varepsilon_{ult\,1}$ (%)
G2-1	0.353	61530	696	1.77
G2-2 [2]	0.353	65270	170	0.29
G2-3	0.353	70882	891	1.23
G2-4 [2]	0.353	49990	292	0.54
G2-5	0.353	82497	924	1.19
Average	0.353	71636	837	1.39
Std. Dev.	0.000	10504	123	0.32
Co. Var. (%)	0.0	14.7	14.7	23.2

[1] Manufacturer's design thickness for 1 layer of fibre sheet

[2] Specimens G2-2 and G2-4 fractured prematurely at the tension grips and therefore were not included in the calculation of the average values.

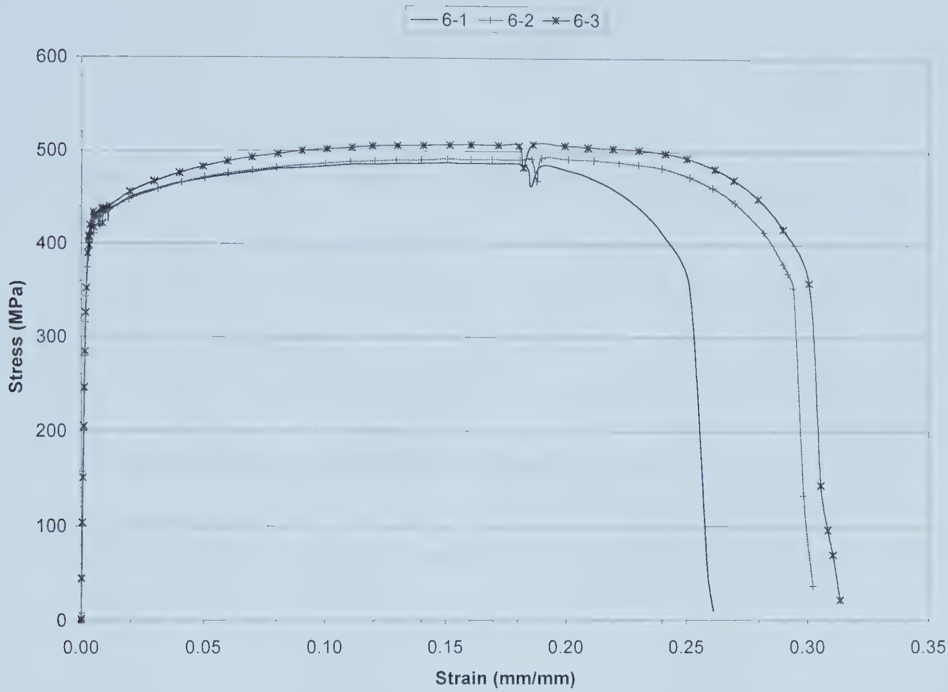

Figure 4.1 - Engineering Stress vs. Engineering Strain for NPS 6 Coupons

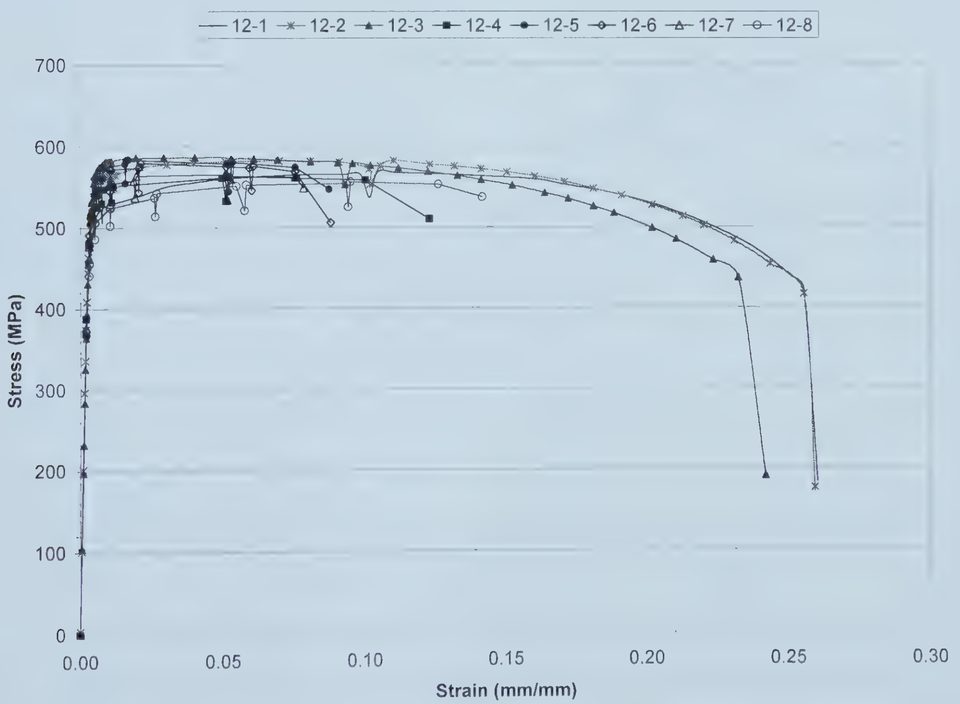

Figure 4.2 - Engineering Stress vs. Engineering Strain for NPS 12 Coupons

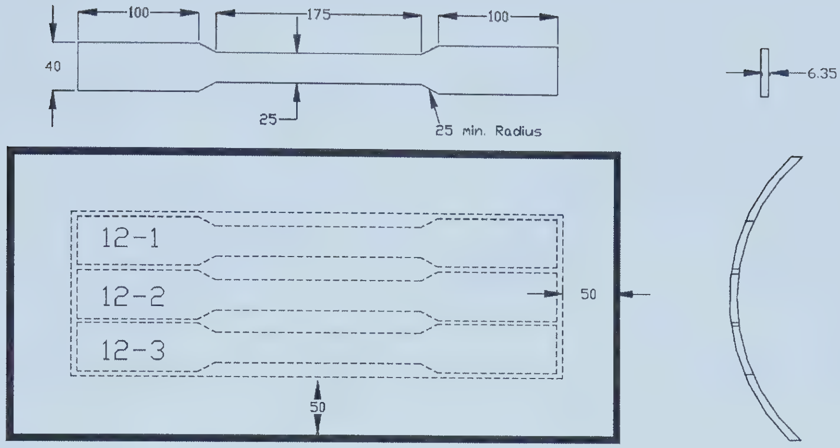

Figure 4.3 - Fabrication Schematic for NPS 12 Pipe Coupons

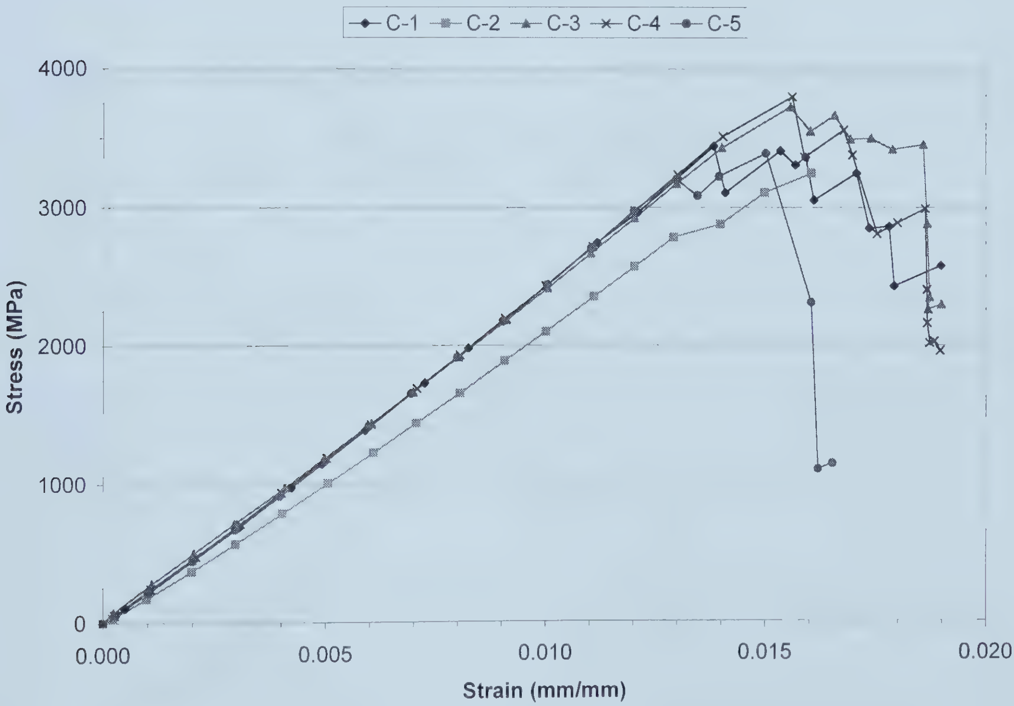

Figure 4.4 - Engineering Stress vs. Strain for Carbon Fibre Coupons

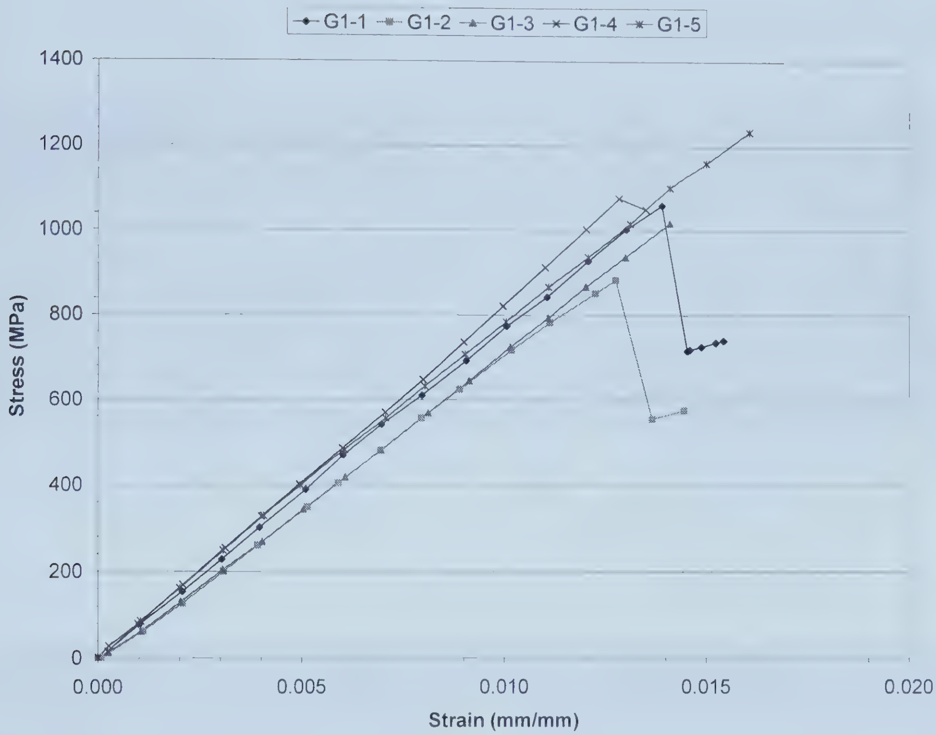

Figure 4.5 - Engineering Stress vs. Strain for FTS-GE-30 Glass Fibre Coupons

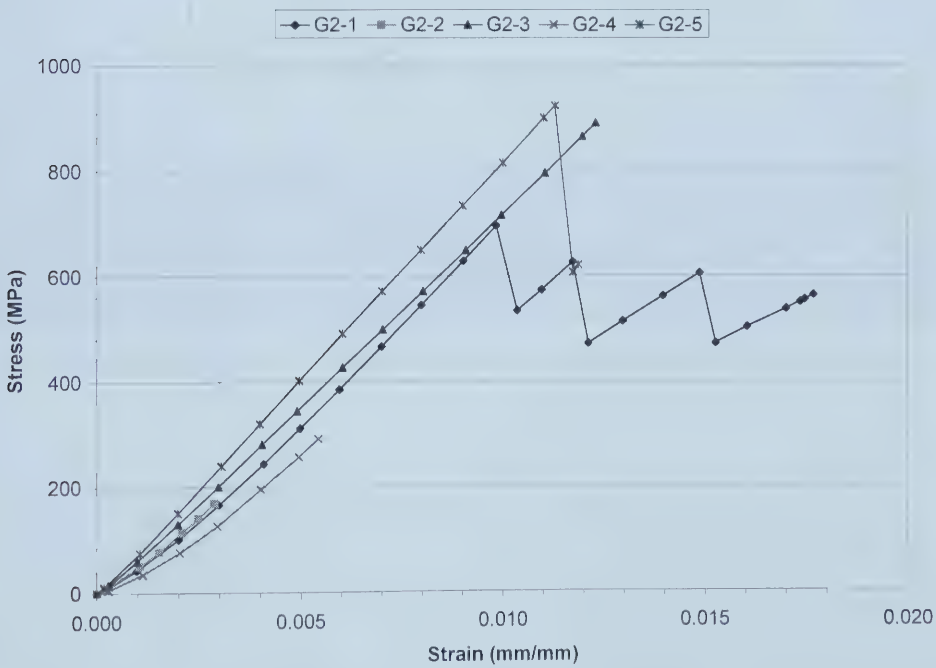

Figure 4.6 - Engineering Stress vs. Strain for MBrace EG900 Glass Fibre Coupons

Figure 4.7 - Deflected Shape of NPS 6 Pipe During Pre-Repair Buckling

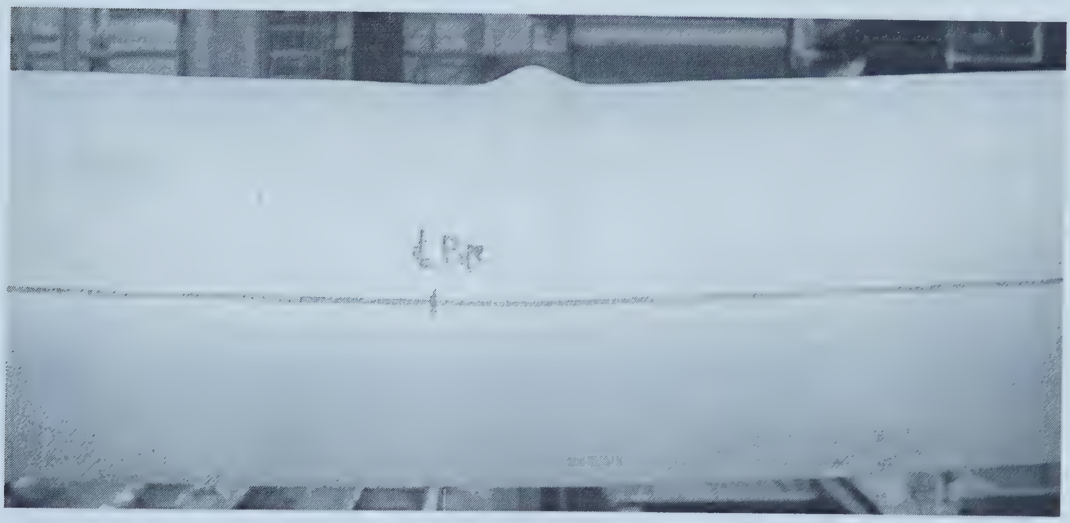

Figure 4.8 - Typical Wrinkle Height at end of Pre-Repair Buckling

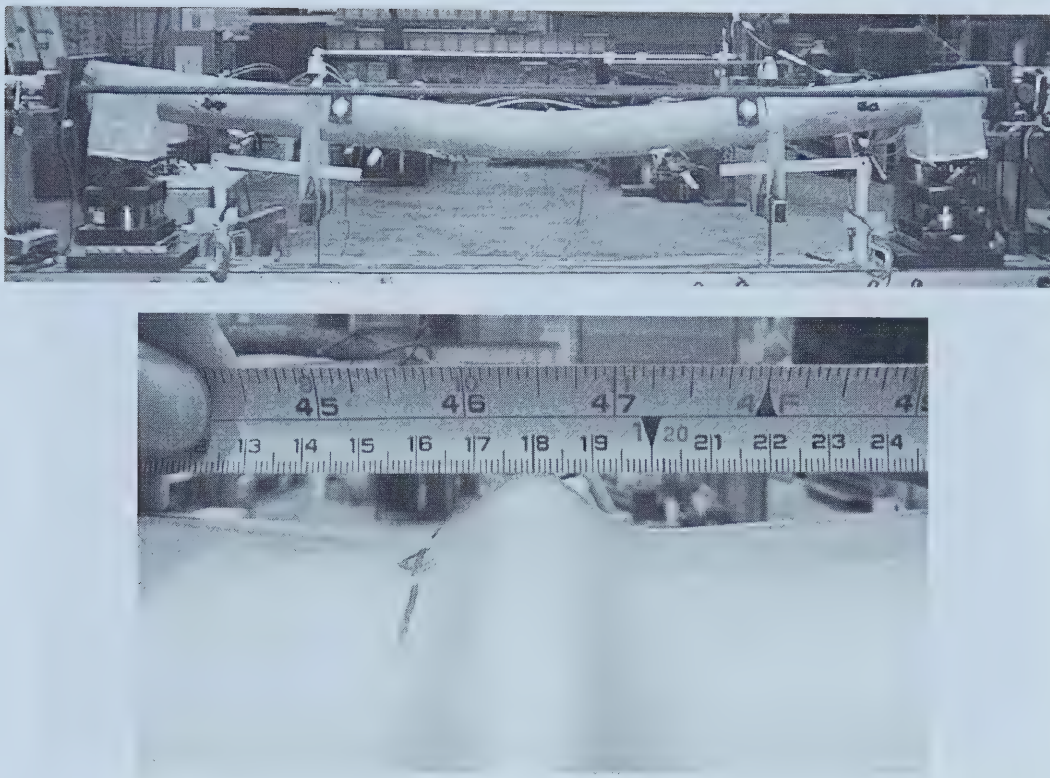

Figure 4.9 - Pipe Deflection and Wrinkle Magnitude a the end of Test 6-NS

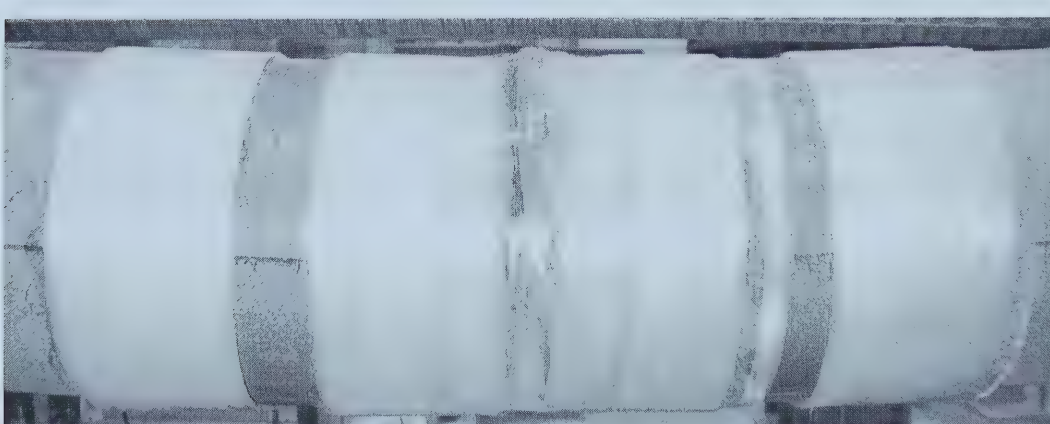

Figure 4.10 - Typical FRP Sleeve Repair on NPS 6 Pipe (6-GE-10-L Specimen)

Figure 4.11 - Difficulty in Insuring Proper Bond and Fibre Distribution at the Wrinkle Crest

Figure 4.12 - Deflected Shape at the end of a Typical Sleeve Repair Test (6-CO-9-M Specimen)

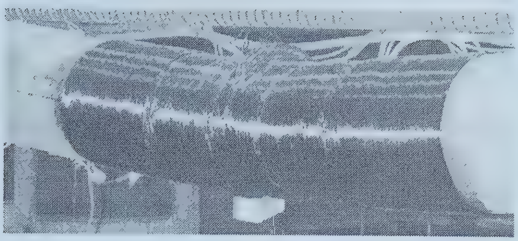


Figure 4.13 - Fracture Pattern for Specimen 6-CO-9-M

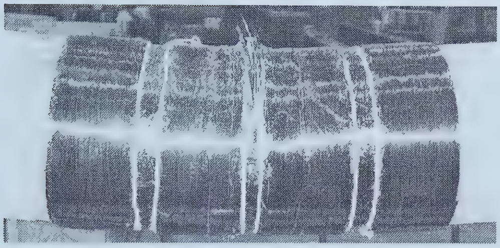


Figure 4.14 - Fracture Pattern for Specimen 6-CE-18-E

Figure 4.15 - Fracture Pattern for Specimen 6-GE-10-L

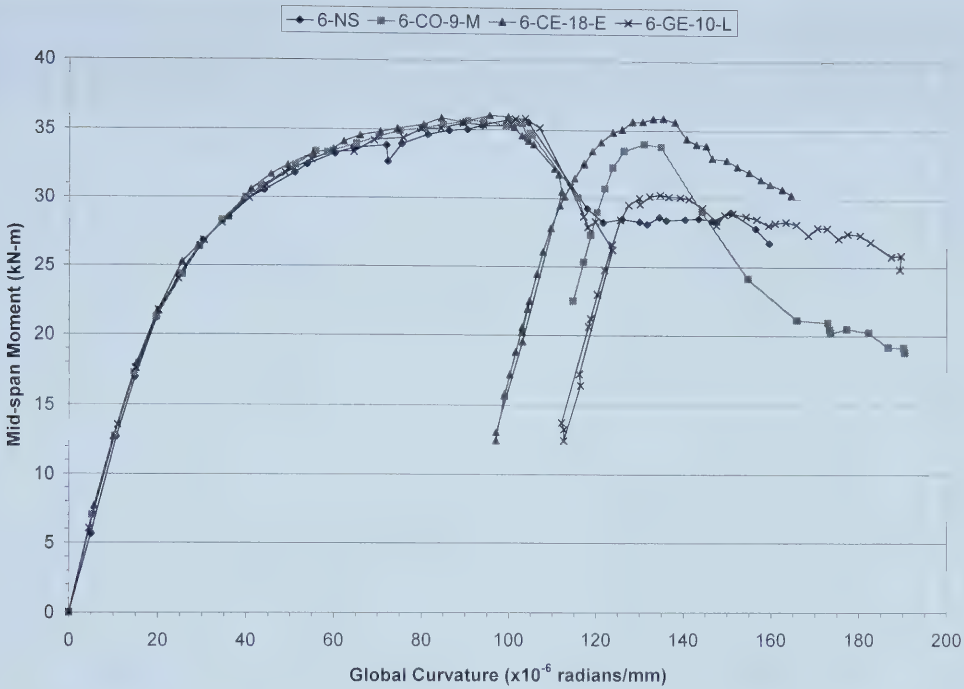

Figure 4.16 - Global Moment vs. Global Curvature for NPS 6 Test Series

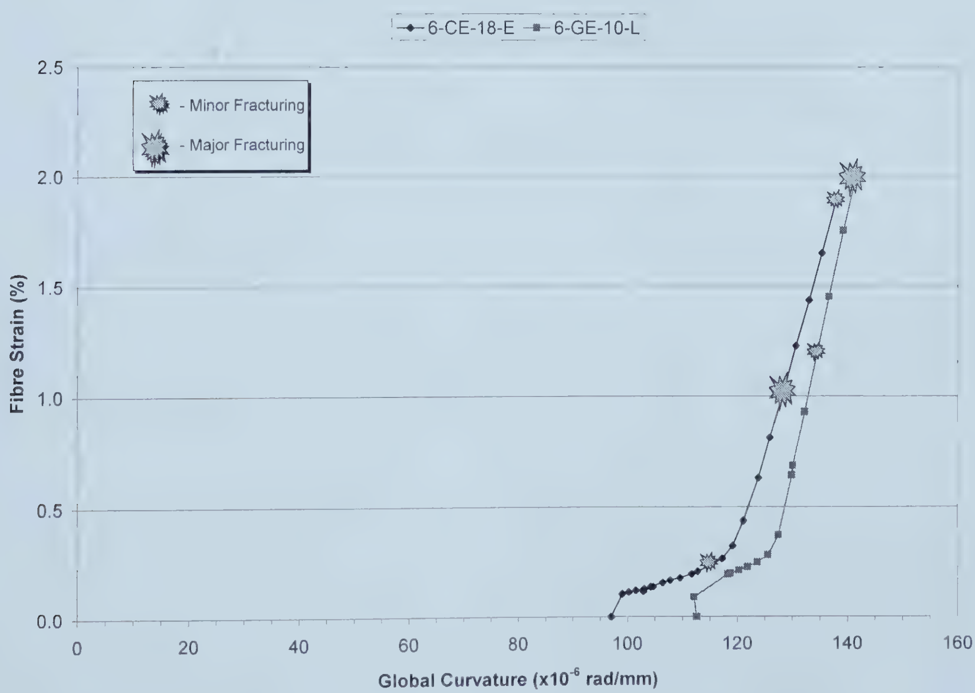

Figure 4.17 - Fibre Strain vs. Global Curvature for NPS 6 Test Series

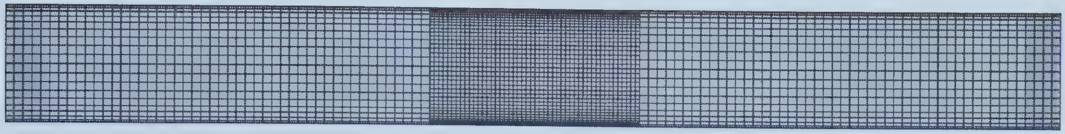

Figure 4.18 - Refined Mesh for NPS 6 FE Model

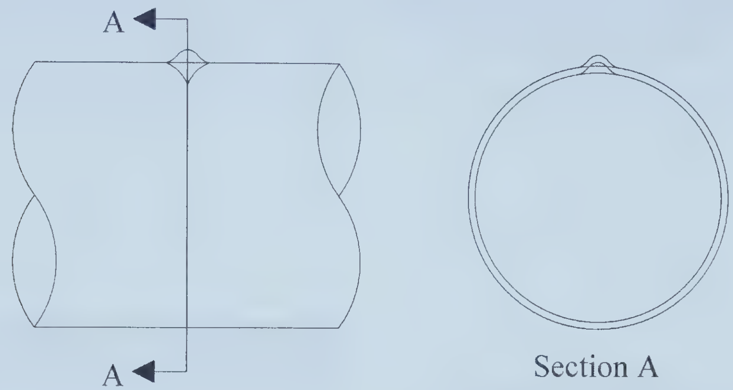

Figure 4.19 - General Schematic of "Blister" Initial Imperfection

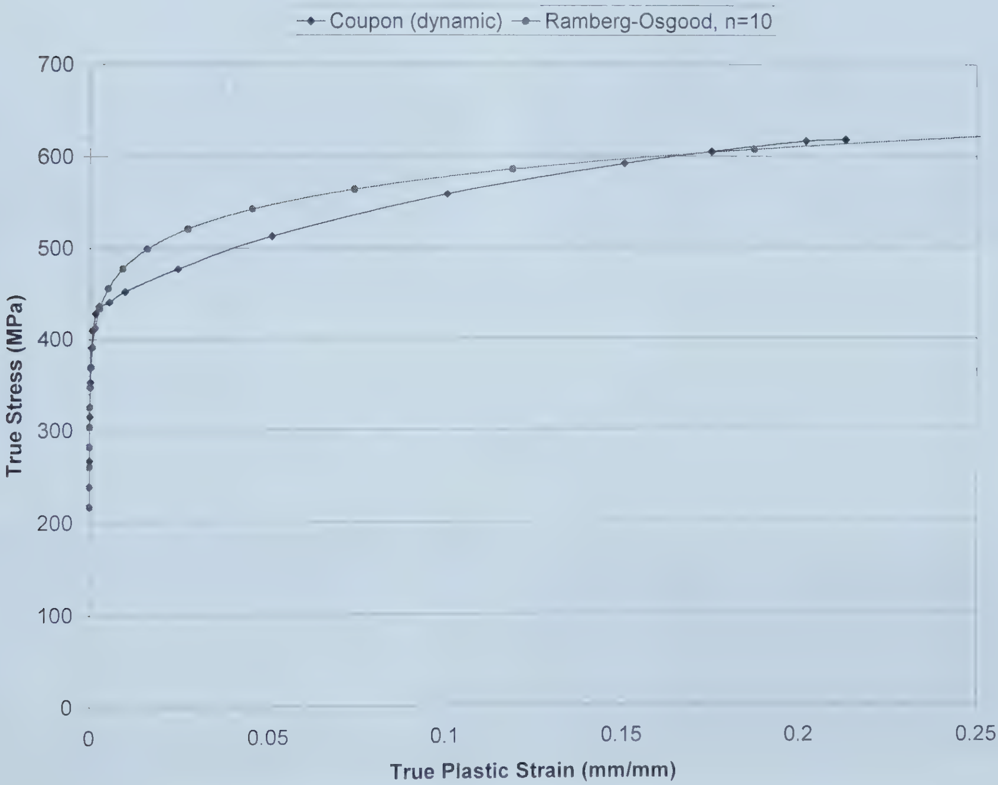

Figure 4.20 - Ramberg-Osgood Fit of True Stress - True Strain for NPS 6 Coupons

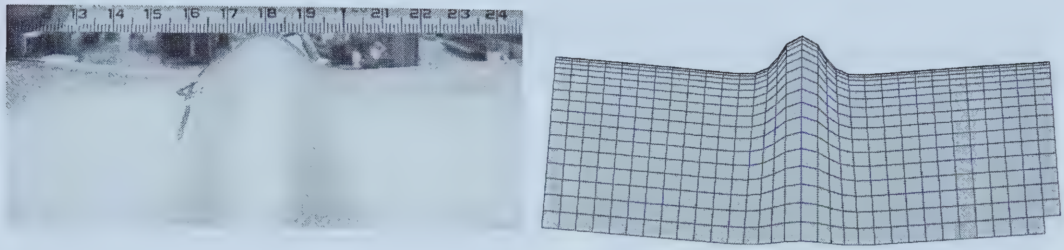

Figure 4.21 - Comparison of Wrinkle Geometry at end of Test 6-NS

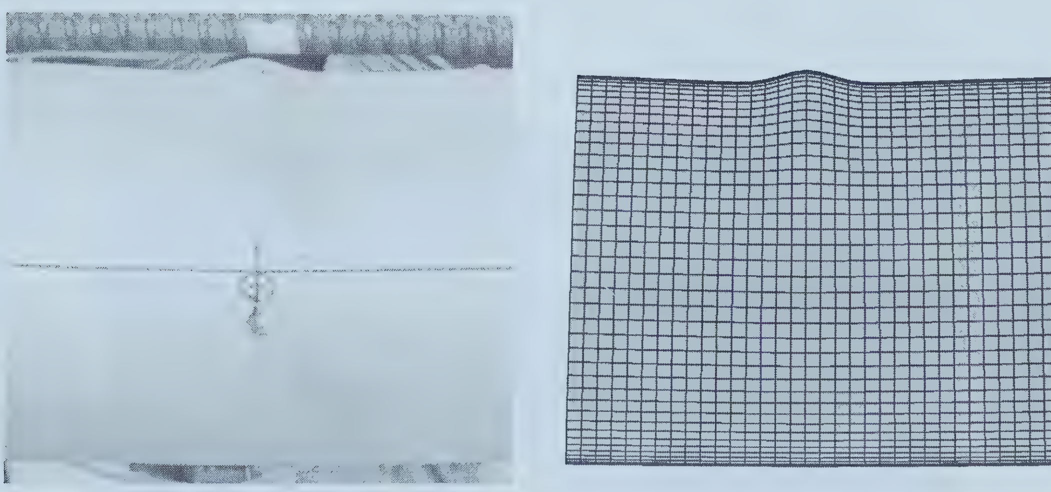

Figure 4.22 - Comparison of Wrinkle Geometry After 6-CO-9-M Pre-Repair Test

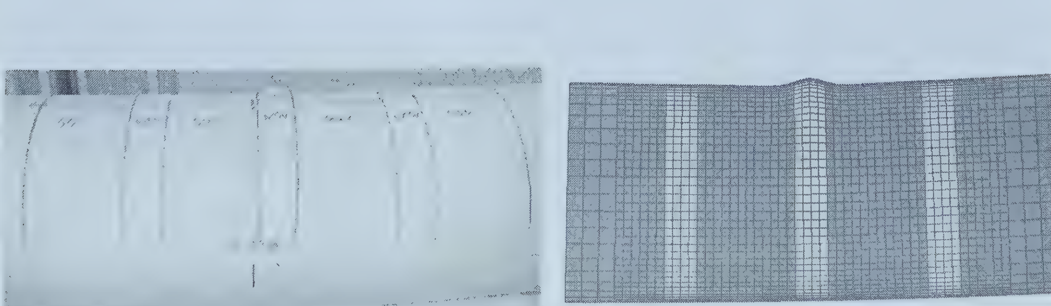

Figure 4.23 - Comparison of Wrinkle Geometry After 6-CE-18-E Pre-Repair Test

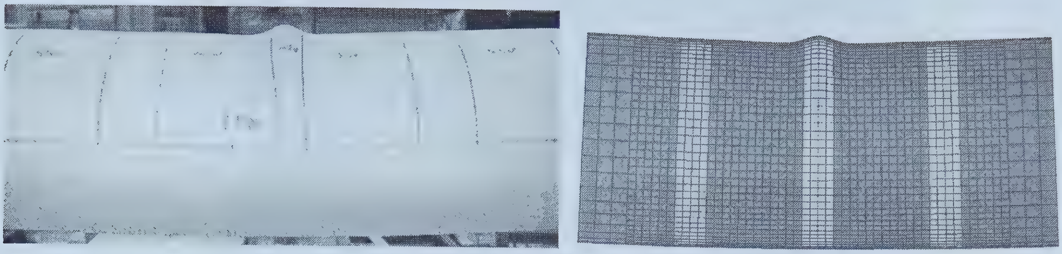

Figure 4.24 - Comparison of Wrinkle Geometry After 6-GE-10-L Pre-Repair Test

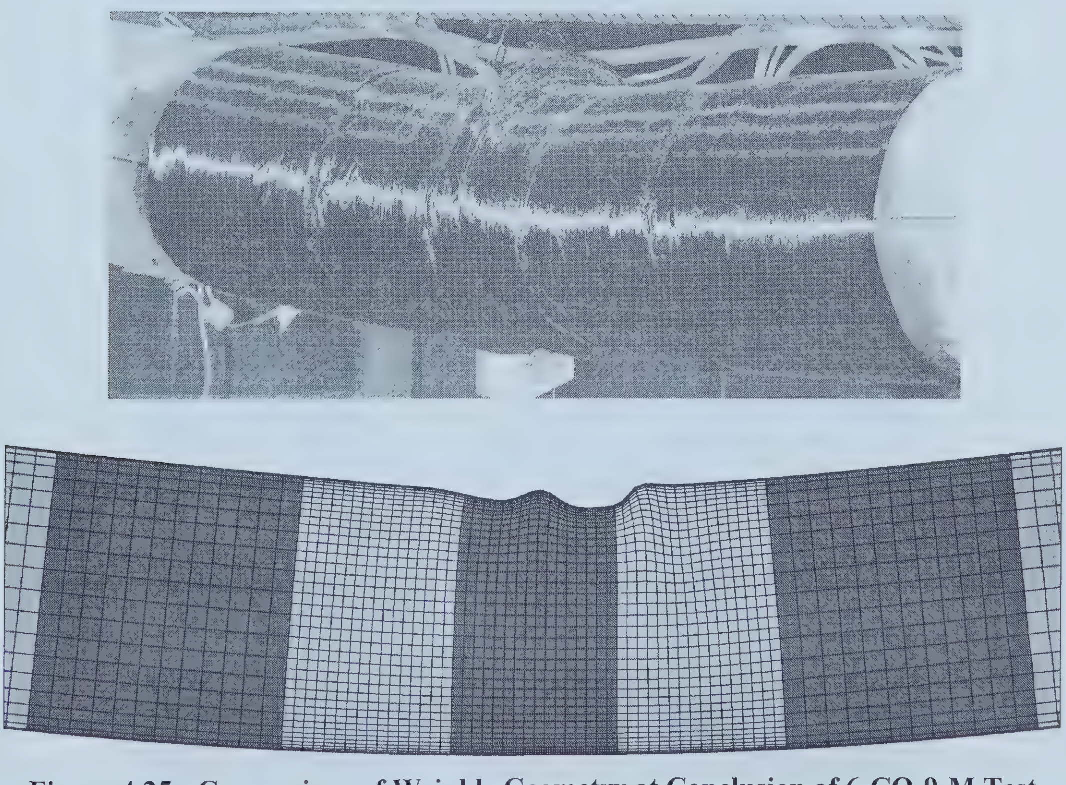

Figure 4.25 - Comparison of Wrinkle Geometry at Conclusion of 6-CO-9-M Test

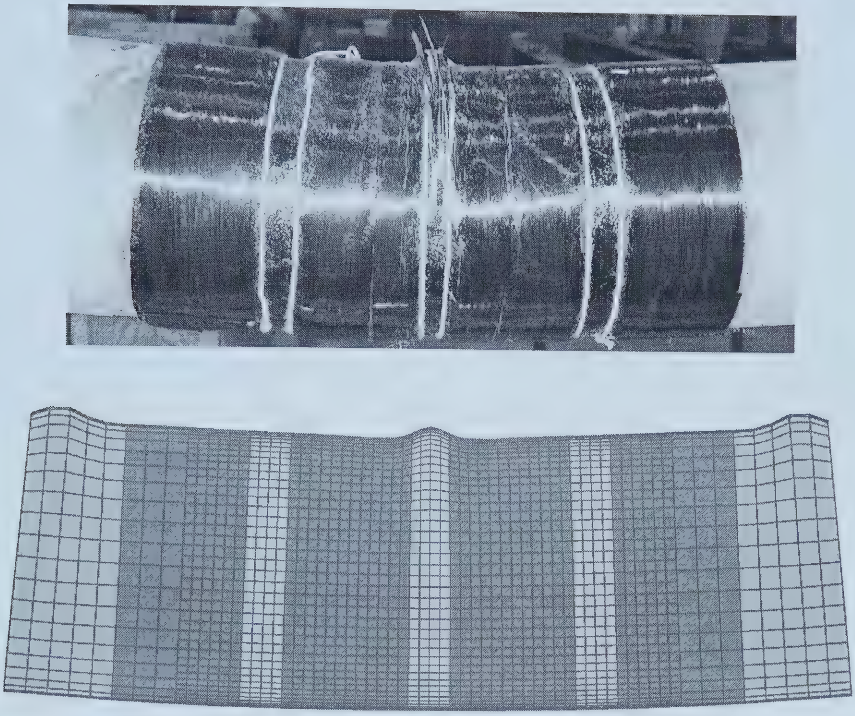

Figure 4.26 - Comparison of Wrinkle Geometry at Conclusion of 6-CE-18-E Test

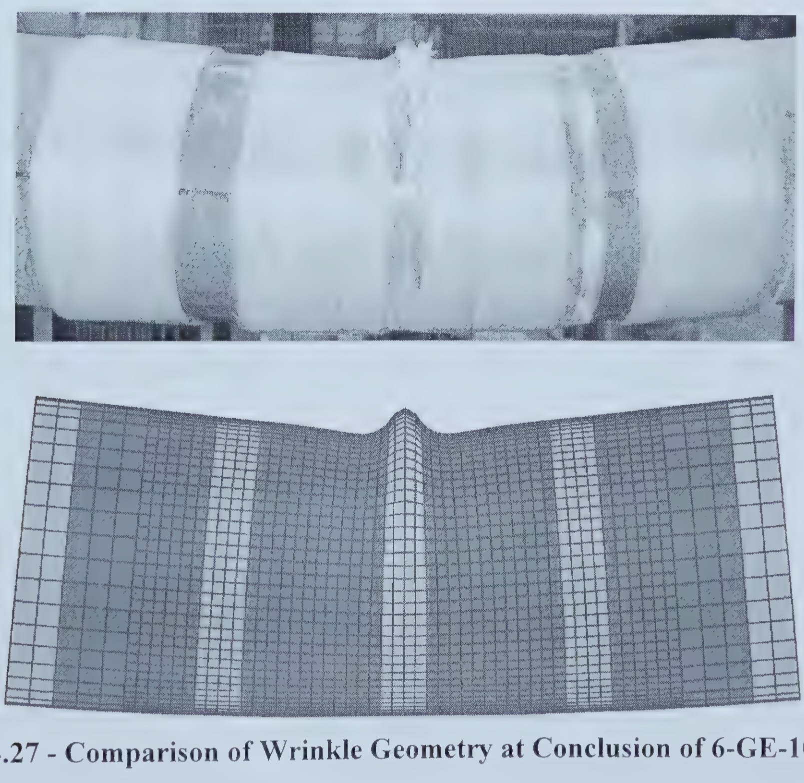

Figure 4.27 - Comparison of Wrinkle Geometry at Conclusion of 6-GE-10-L Test

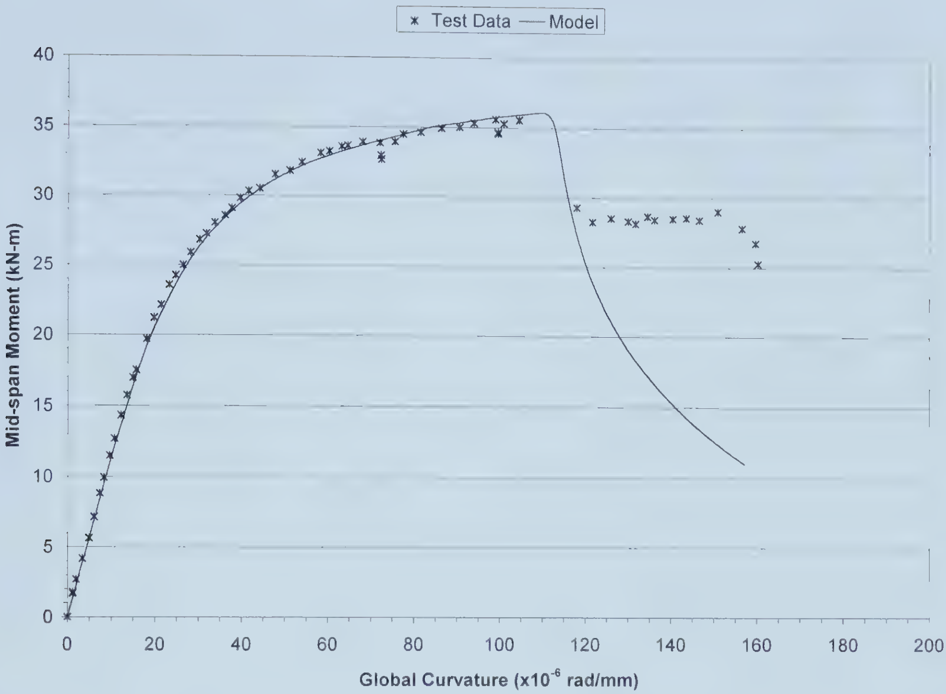

Figure 4.28 - Global Moment vs. Curvature for 6-NS (Test and FE Model)

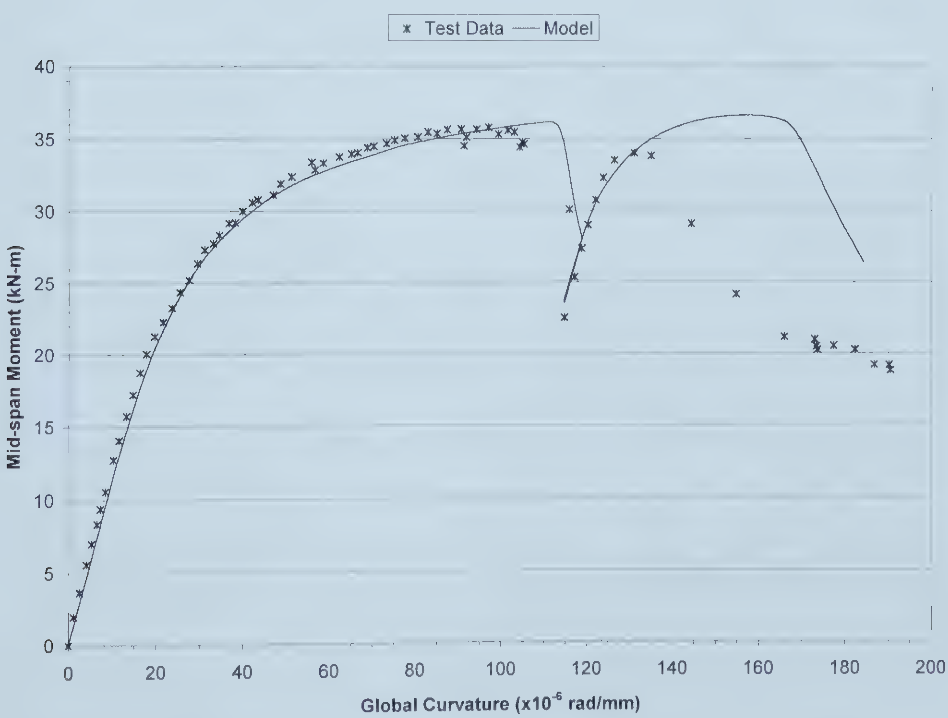

Figure 4.29 - Global Moment vs. Curvature for 6-CO-9-M (Test and FE Model)

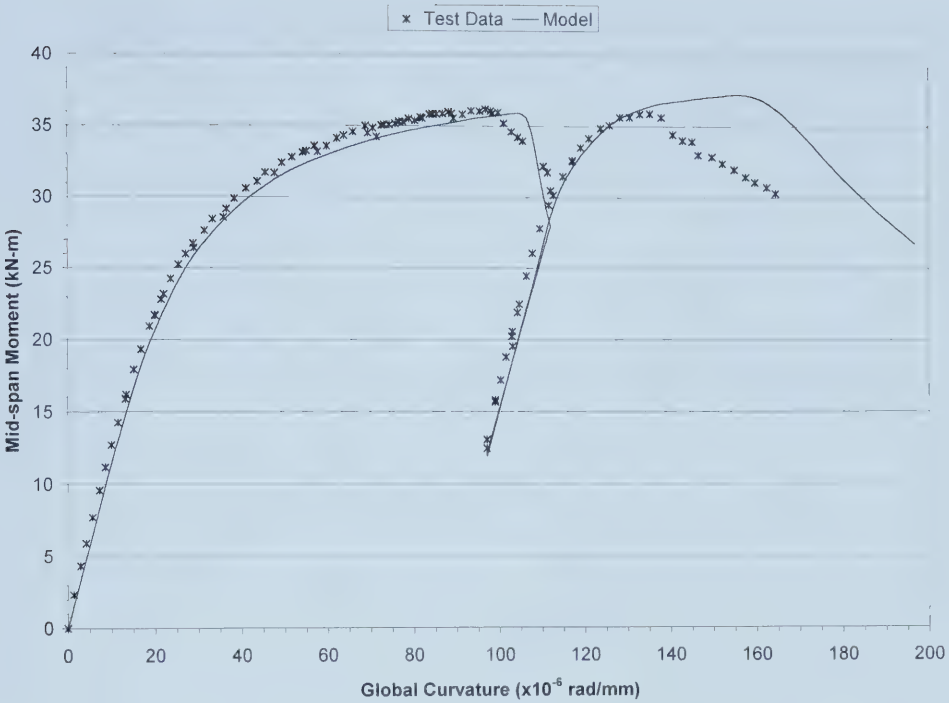

Figure 4.30 - Global Moment vs. Curvature for 6-CE-18-E (Test and FE Model)

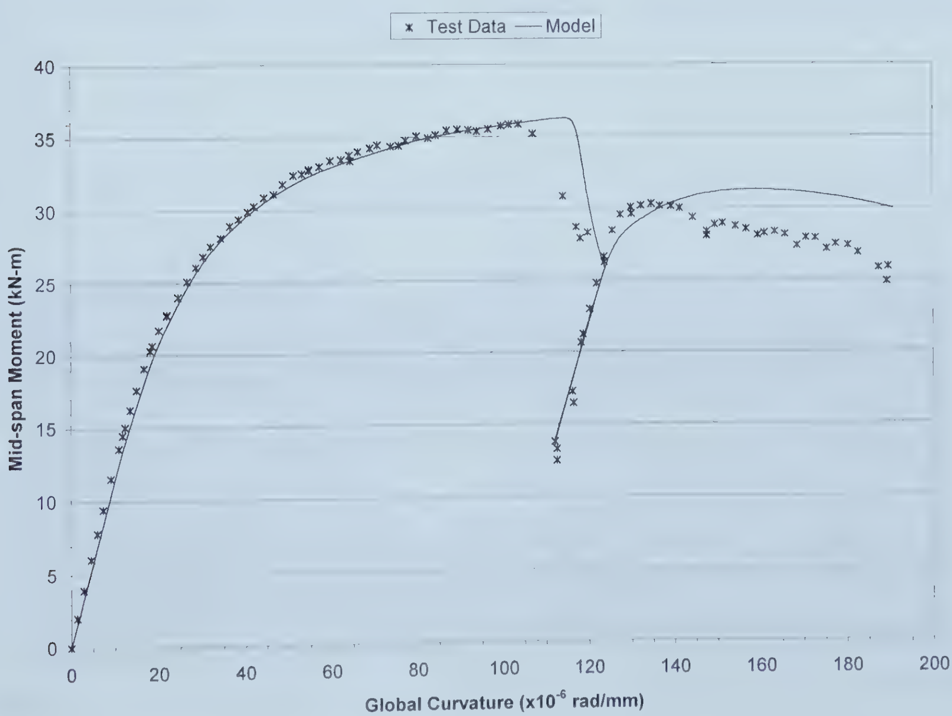

Figure 4.31 - Global Moment vs. Curvature for 6-GE-10-L (Test and FE Model)

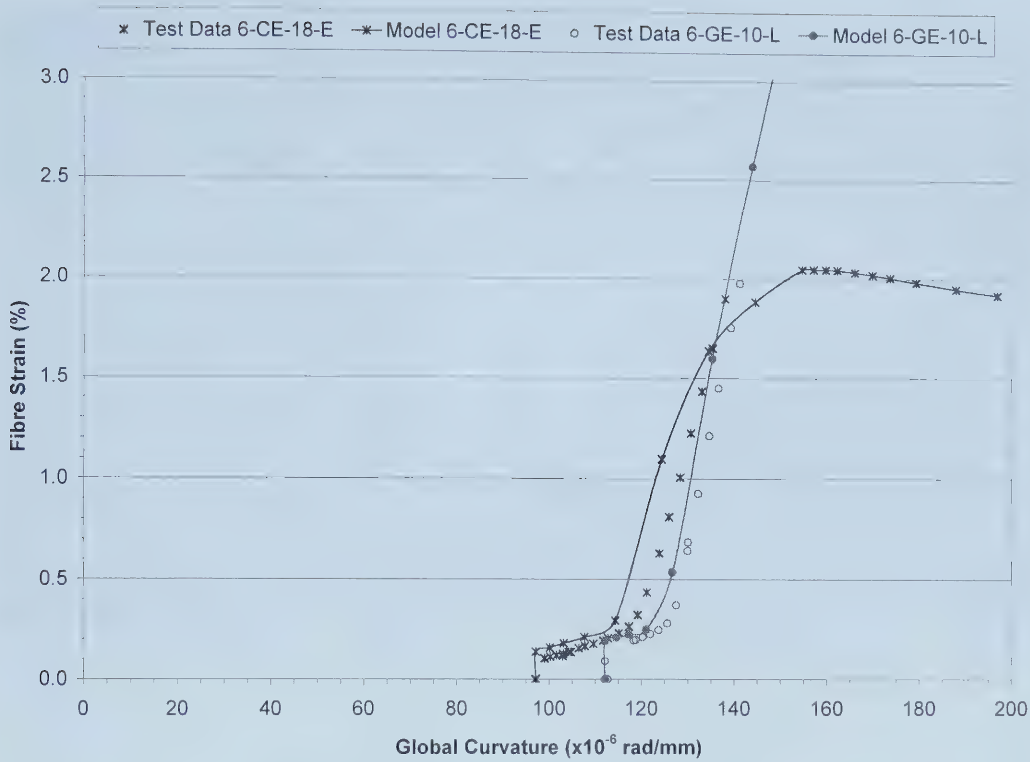

Figure 4.32 - Fibre Strain vs. Global Curvature for 6-CE-18-E and 6-GE-10-L (Test and FE Model)

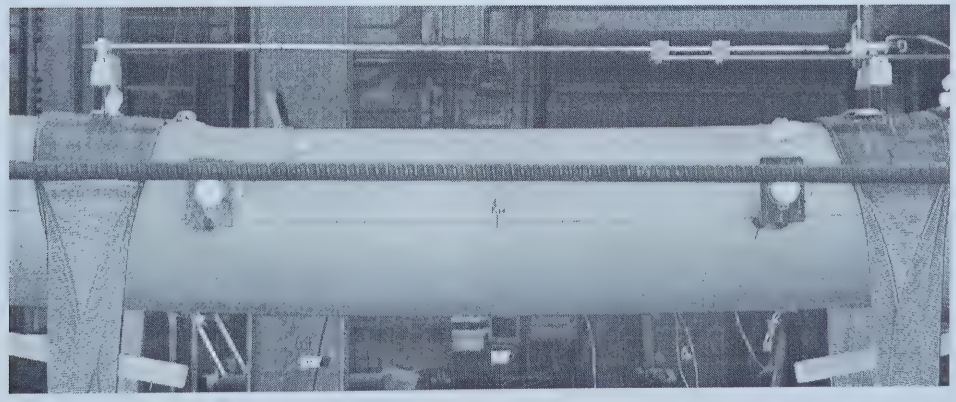

Figure 4.33 - Deflected Shape of 12-GO-12-M Specimen at the end of Pre-Repair Buckling

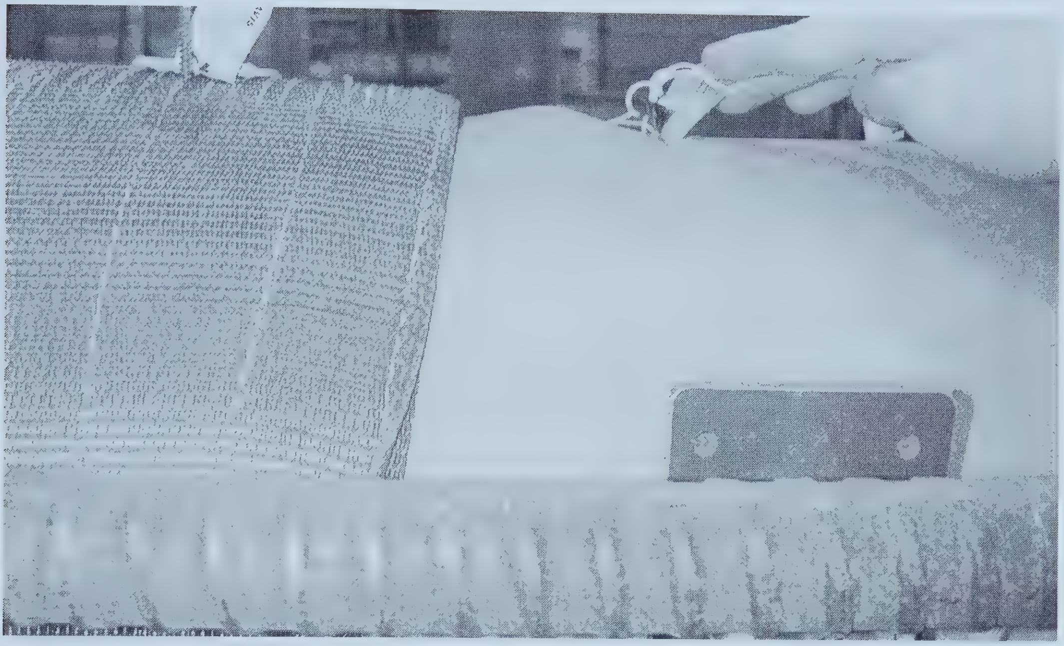

Figure 4.34 - Wrinkle Geometry of 12-GO-12-M Specimen Prior to Sleeve Repair

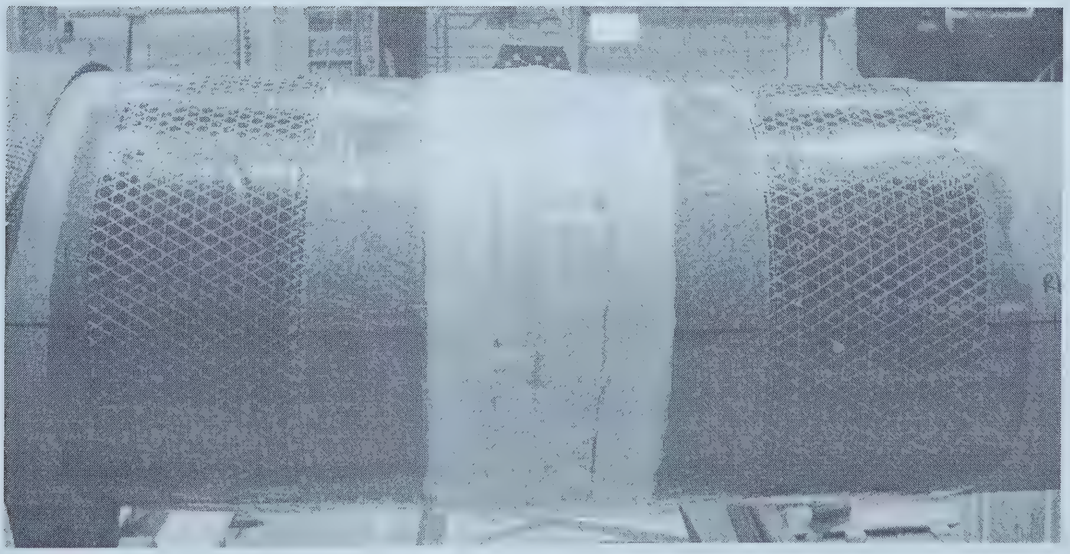

Figure 4.35 - 12-GO-12-M Specimen Following Sleeve Repair

Figure 4.36 - Fracture Pattern for 12-GO-12-M Sleeve Repair

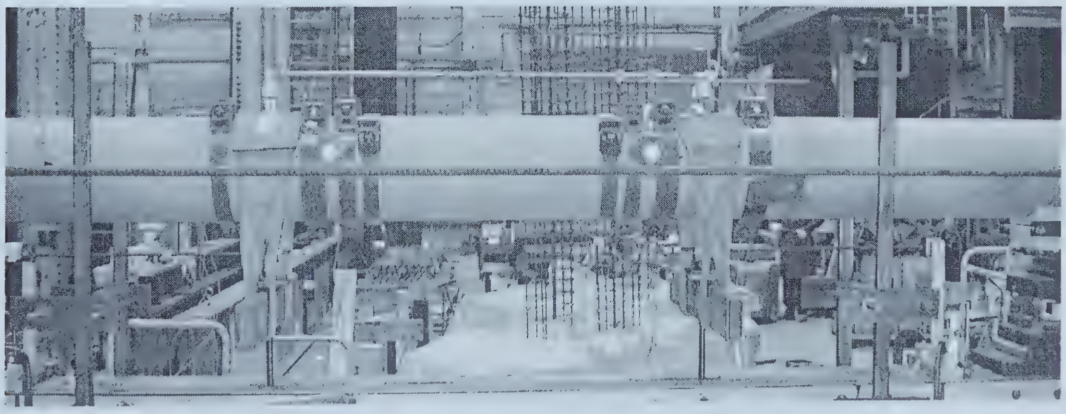

Figure 4.37 - Stiffening Collars Used for Pre-Repair Buckling of 12-GO-6-M Specimen

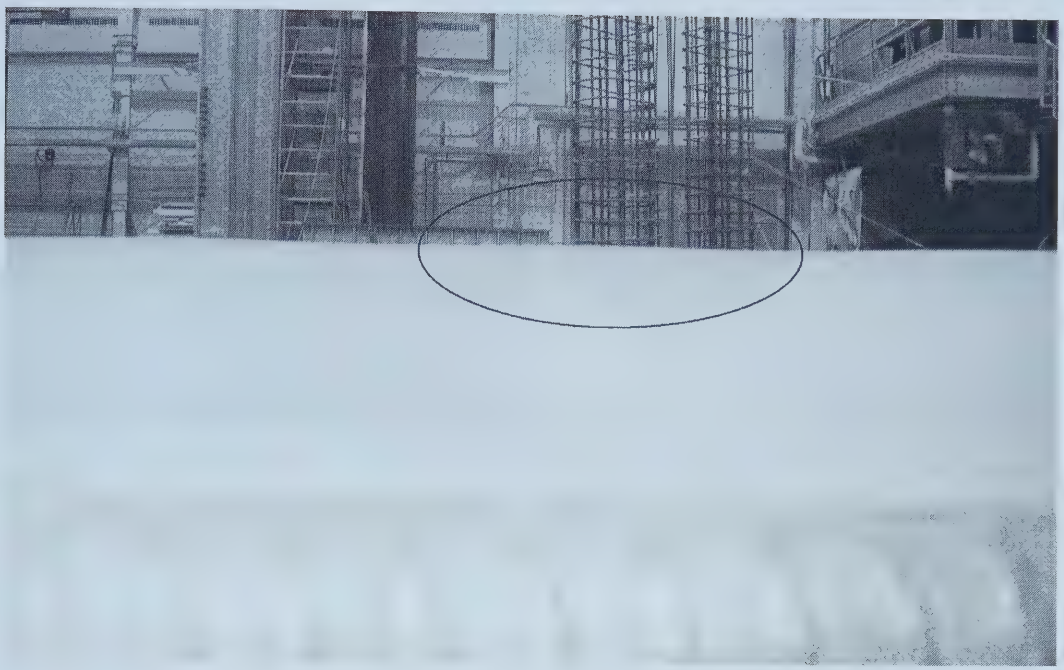

Figure 4.38 - First Appearance of Wrinkling Near Mid-Length for 12-GO-6-M Specimen

Figure 4.39 - Wrinkle Geometry of 12-GO-6-M Specimen Prior to Sleeve Repair

Figure 4.40 - "Diamond" Secondary Buckling of 12-GO-6-M Specimen Following Sleeve Repair

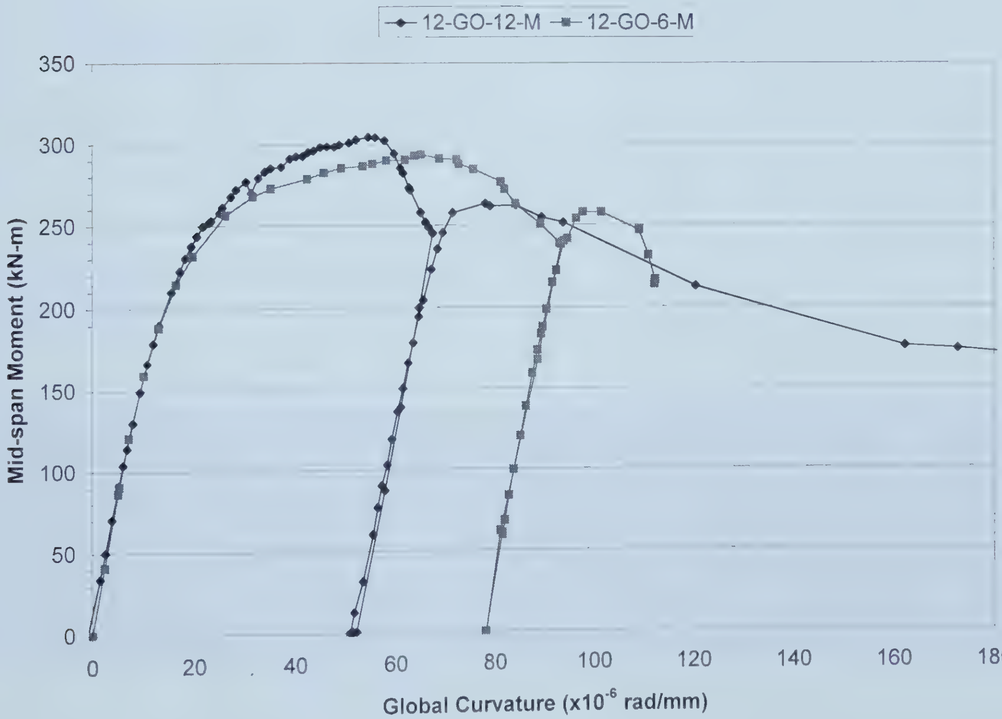

Figure 4.41 - Global Moment vs. Global Curvature for NPS 12 Test Series

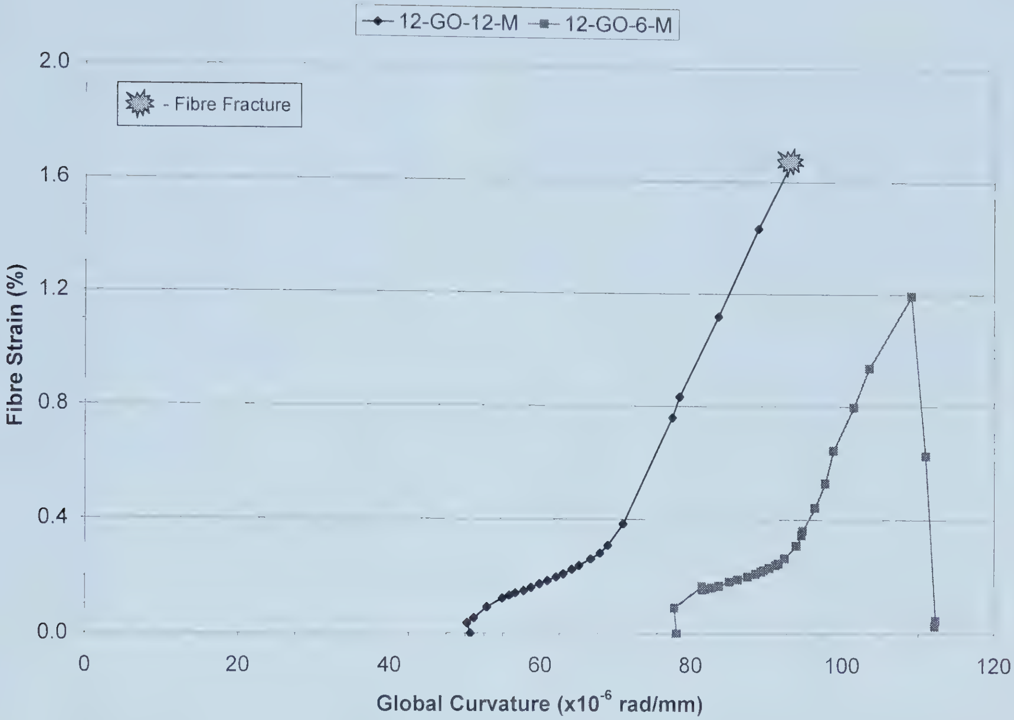

Figure 4.42 - Fibre Strain vs. Global Curvature for NPS 12 Test Series

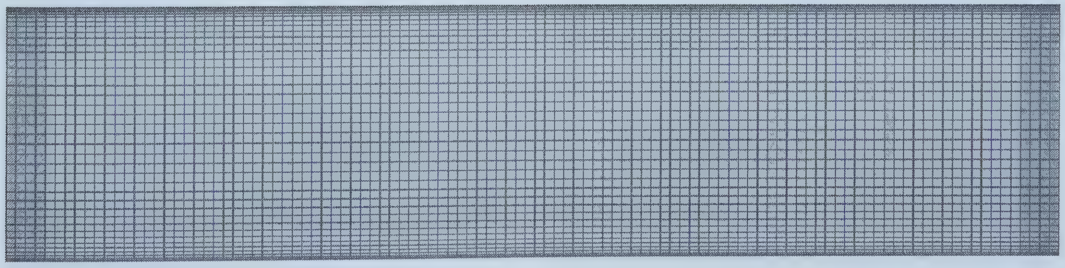

Figure 4.43 - Refined Mesh for NPS 12 FE Model

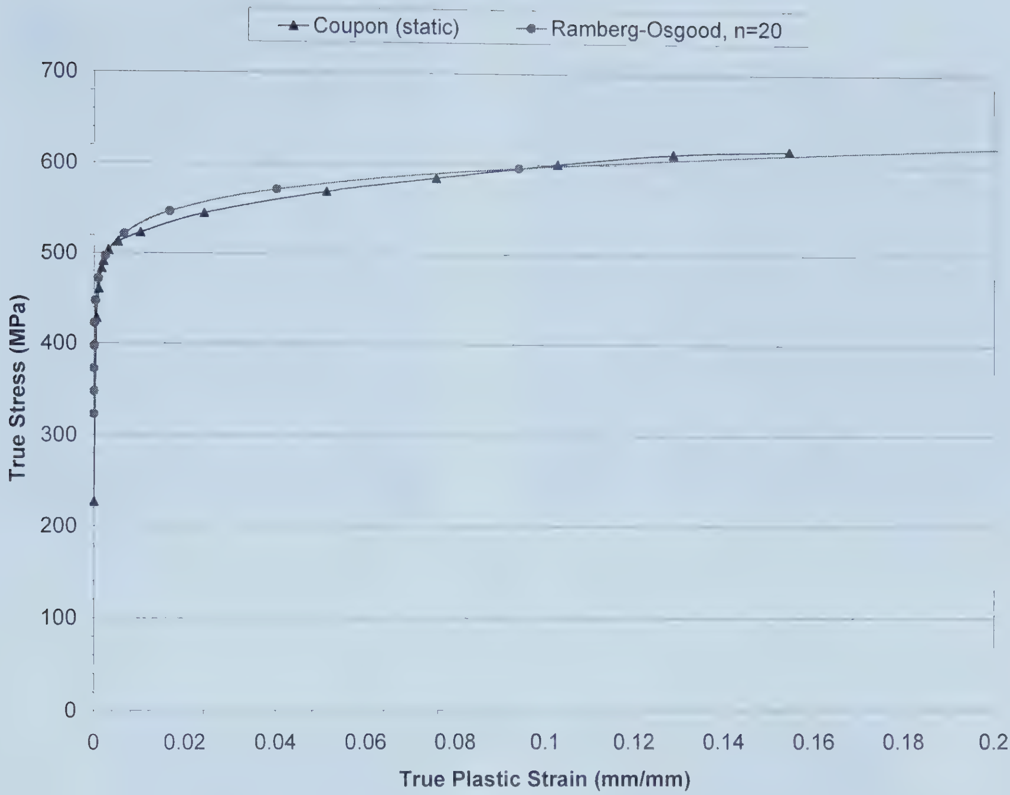

Figure 4.44 - Ramberg-Osgood Fit of True Stress - True Strain for NPS 12 Coupon

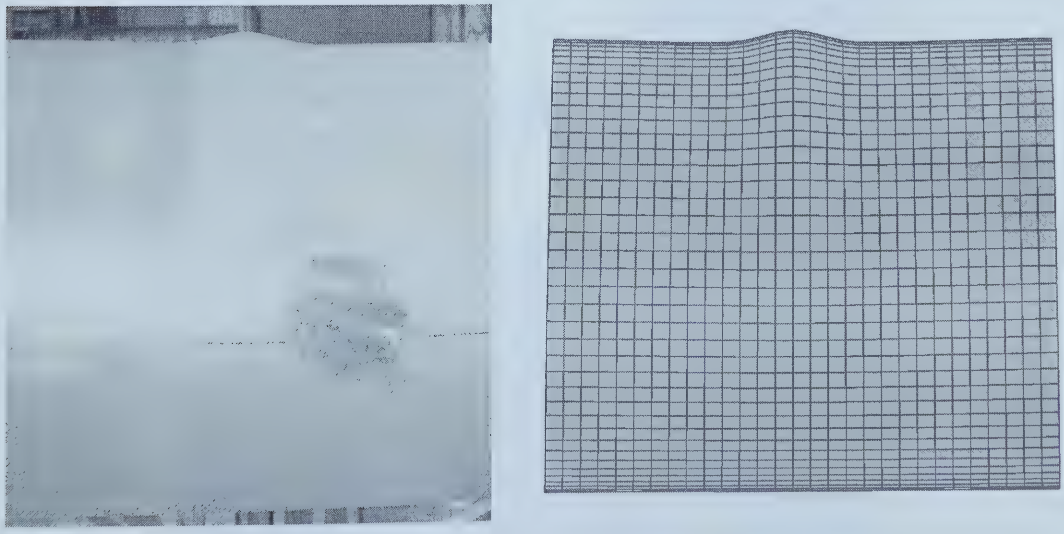

Figure 4.45 - Comparison of Wrinkle Geometry Following 12-GO-12-M Pre-Repair Test

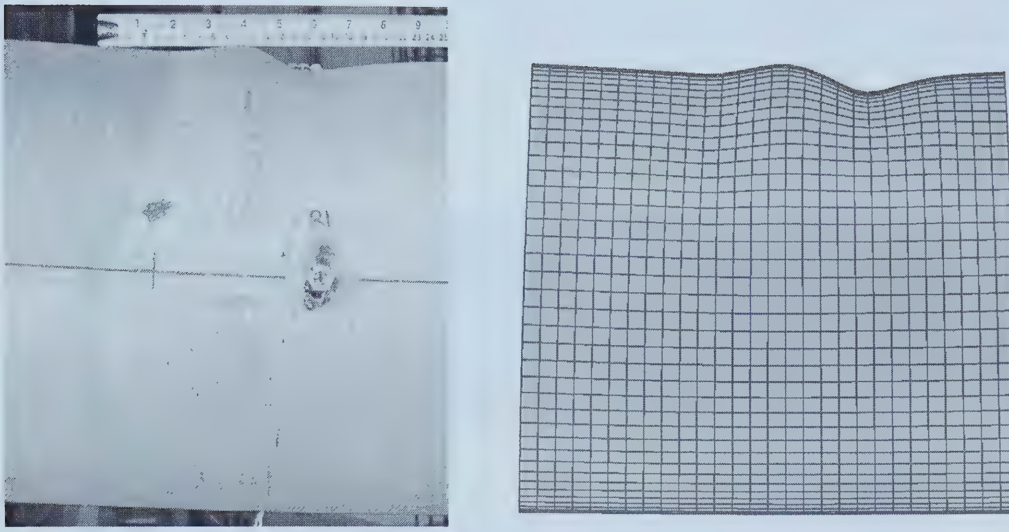

Figure 4.46 - Comparison of Wrinkle Geometry Following 12-GO-6-M Pre-Repair Test

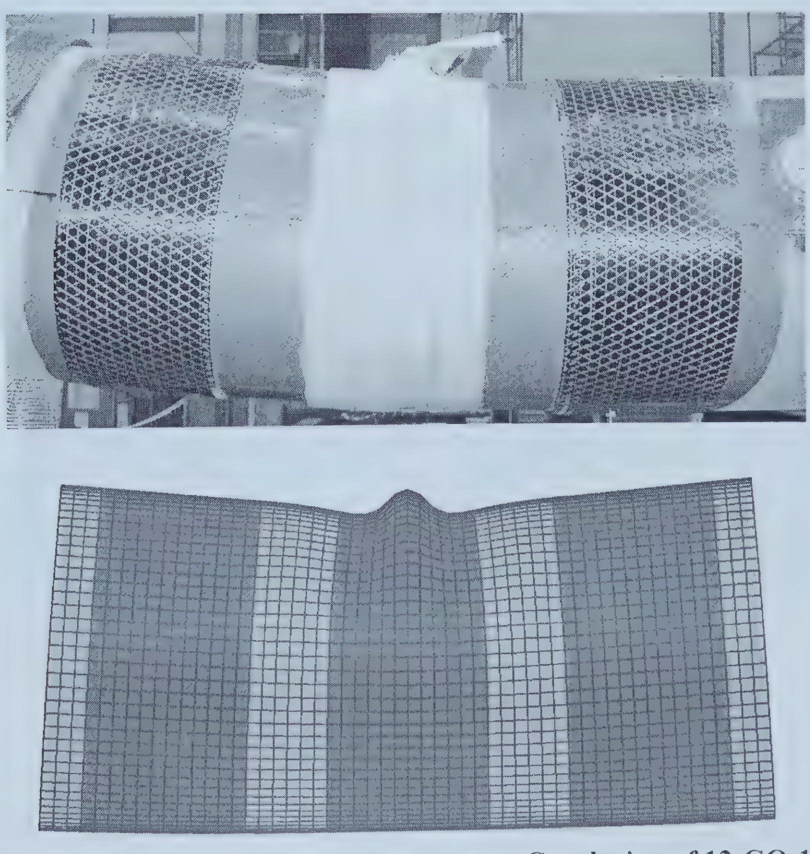

Figure 4.47 - Comparison of Wrinkle Geometry at Conclusion of 12-GO-12-M Test

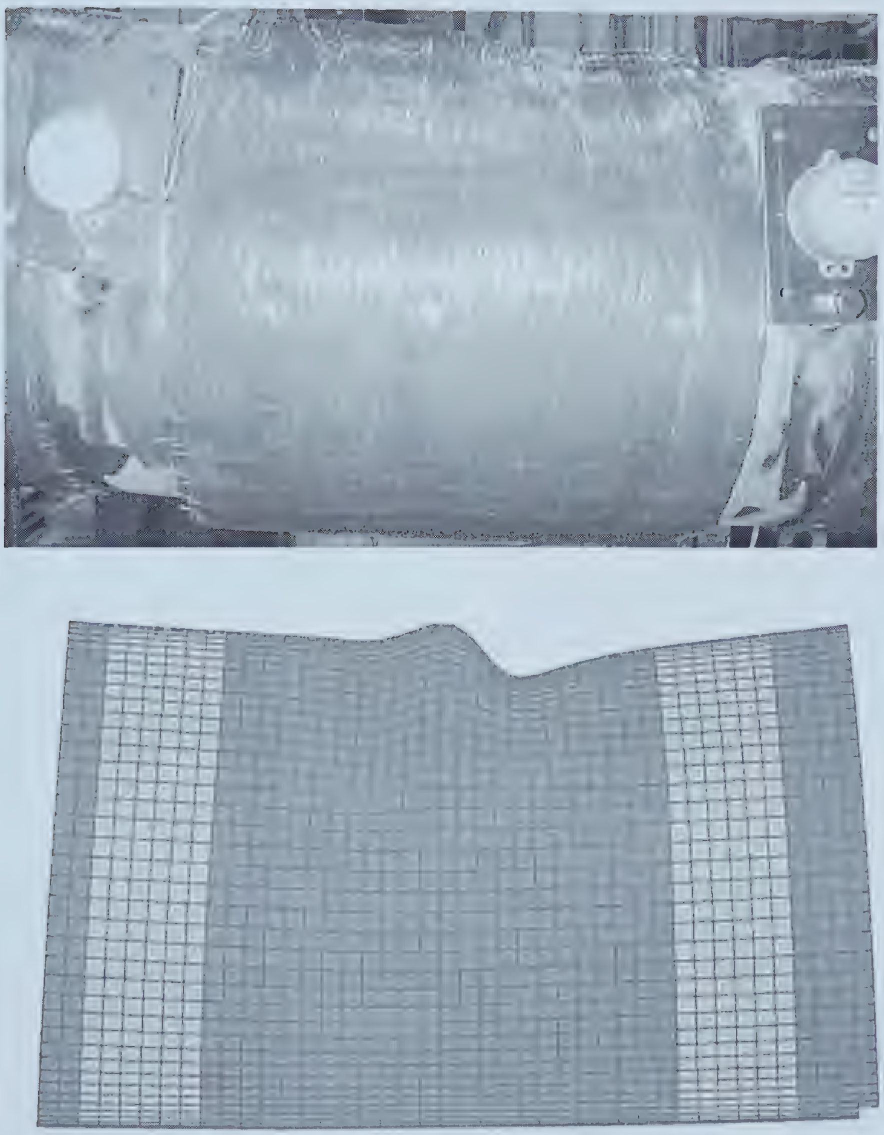

Figure 4.48 - Comparison of Wrinkle Geometry at Conclusion of 12-GO-6-M Test

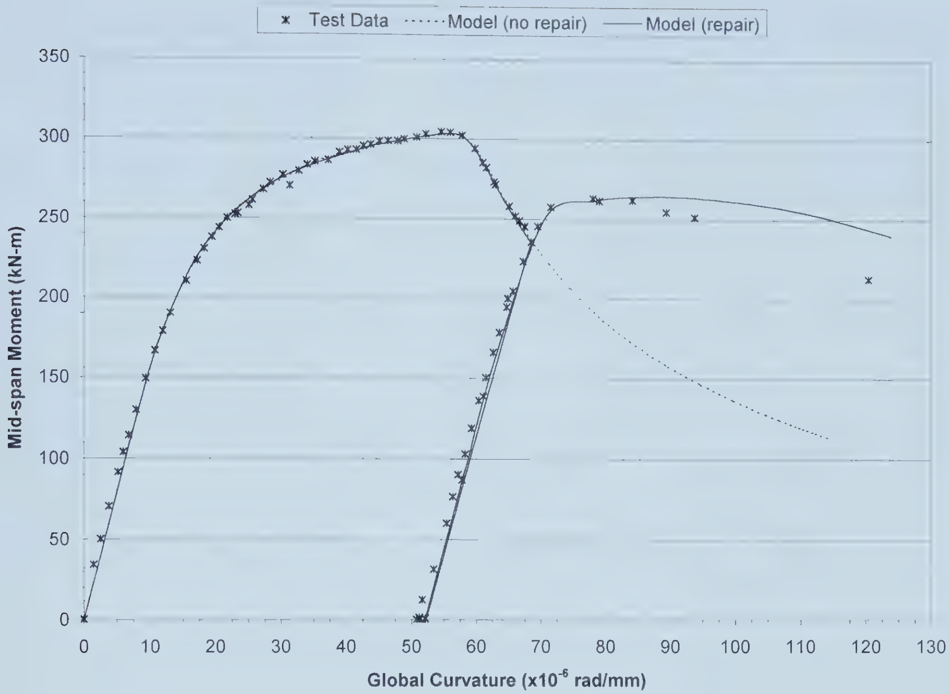

Figure 4.49 - Global Moment vs. Curvature for 12-GO-12-M (Test and FE Model)

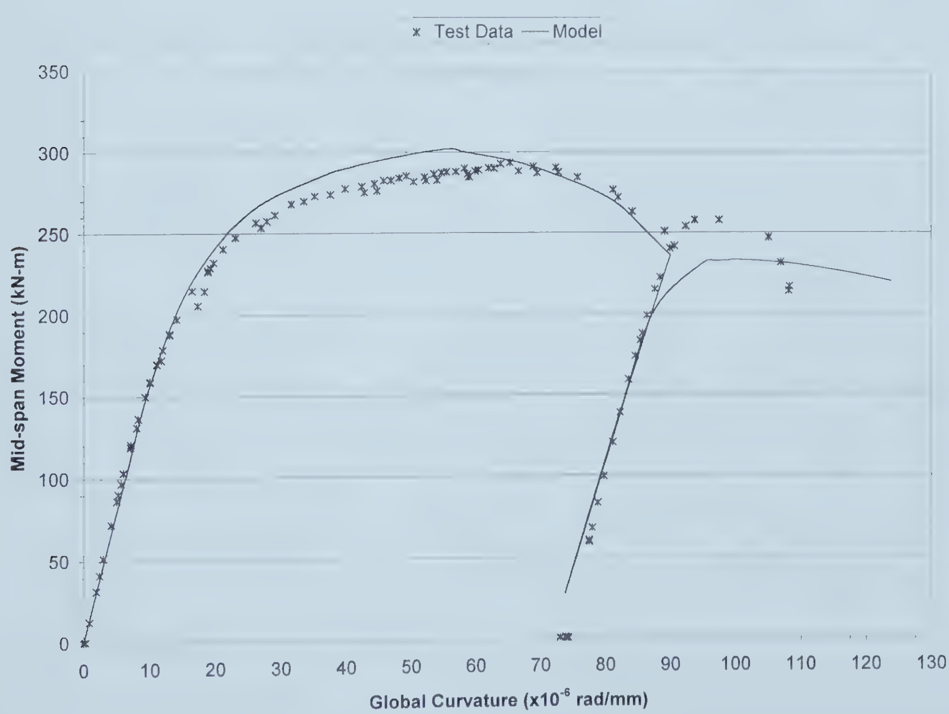

Figure 4.50 - Global Moment vs. Curvature for 12-GO-6-M (Test and FE Model)

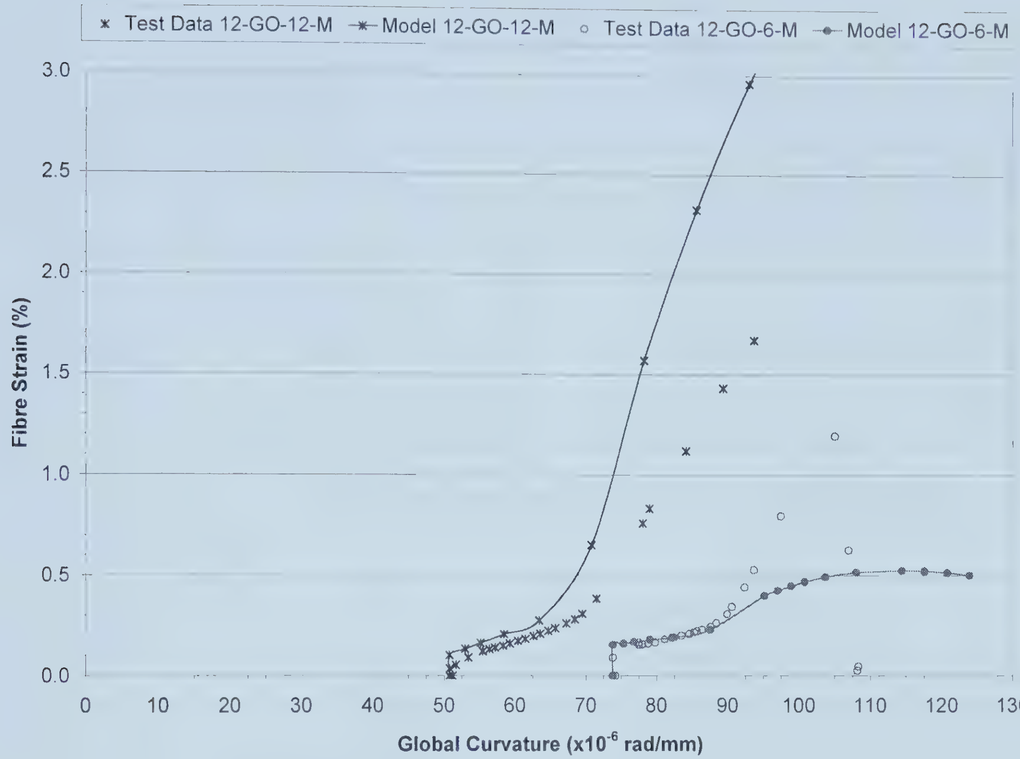

Figure 4.51- Fibre Strain vs. Curvature for 12-GO-12-M and 12-GO-6-M (Test and FE Model)

5 DISCUSSION OF KEY FINDINGS

In Chapters 2 and 4 the behaviour of sleeve repairs on steel line pipe was examined, both through finite element analysis and laboratory study. The focus of the numerical study presented in Chapter 2 was on the effects of the sleeve repair on the overall moment – curvature behaviour of the pipe. The results of the experimental program, detailed in Chapter 4, were intended to verify the assumptions made in the FE analysis. In addition to verifying the overall impact of sleeve repair on pipe behaviour, experimental work also showed that the design of the sleeve impacted the behaviour of the sleeve itself. That is, from fracturing of sleeves observed in testing, it became apparent that the sleeve had to be designed not only to optimize pipe behaviour, but also to resist strains imposed onto it without losing integrity.

In this chapter, several of the key effects of sleeve design parameters on the behaviour of the sleeve – pipe system will be discussed. Results shown in the preliminary FE analysis and experimental program will be used to illustrate these key effects. The response of the two components of the sleeve – pipe system to the sleeve design parameters will be discussed separately in the following sections.

5.1 Effects of Sleeve Repair Design Parameters on Pipe Behaviour

The primary goal of this project was to study the global flexural behaviour of a wrinkled pipe repaired with an external sleeve. Three groups of sleeve design parameters were found to interact in optimizing the sleeve repair. Geometric and material properties of the sleeve, along with repair timing acted together in altering the flexural behaviour of the pipe. These parameters were explored in detail in the numerical study and partially validated with a limited number of laboratory tests. A discussion of the effects of these parameters is given in this section.

It should be noted that although both steel and FRP sleeves were examined for sleeve repairs in Chapter 2, only FRP sleeves were examined in the experimental program presented in Chapters 3 and 4. Therefore, the discussion in this section will be limited to FRP repair sleeves.

5.1.1 Sleeve Geometry

Three aspects of sleeve geometry contribute to performance of the repair. First, the sleeve configuration has been shown to have a major impact on flexural behaviour of the pipe. The configurations explored in this project were the single sleeve, even sleeve and odd sleeve. The second important aspect of sleeve geometry is the spacing of the multiple sleeve sections, the gap size. Third, the length of the sleeve sections has been shown to affect the performance of the repair in specific cases.

5.1.1.1 Sleeve Configuration

The configuration of the repair has been observed to have a profound impact of the flexural behaviour of the pipe. The single, even and odd sleeve configurations were extensively explored in the FE analysis. Examining moment – curvature plots for the three configuration types in Figures 2.21, 2.23 and 2.26, general pattern in the behaviour of the pipe, following repair, is seen. Moment capacity increases after the sleeve is applied and eventually declines. However, it is apparent that the even and odd sleeve configurations provide a wider range of behaviour patterns than the single sleeve. The moment recovery of the pipe and the ductility of the pipe can be designed by the engineer, to a greater extent than in the single sleeve case, by adjusting certain parameters of the sleeve design. This makes FRP the ideal material for the repair, since many of its properties can be custom-designed.

The behaviour of the two "multiple" sleeve configurations (even and odd sleeves) can be compared to each other. Figures 2.23 and 2.26 showed that although the even and odd sleeve repairs behaved somewhat similarly, the even sleeve showed more range in types of behaviour than the odd sleeve. The even sleeve design was able to add significantly more ductility to the pipe, in some cases, than the odd sleeve. This is very important, since in many instances, it is the ductility of the pipe that is of concern, rather than its flexural strength. The ductility of the even sleeve repair over the odd sleeve repair was also observed in the experimental tests. In Figure 4.16 it is shown that even sleeve repairs 6-CE-18-E and 6-GE-10-L provide substantially more ductility than the odd sleeve repair 6-CO-9-M. This pattern of behaviour observed in the tests verifies that the

trends seen in the FE analysis are correct. To explain the different behaviours of the even and odd sleeve designs, one must zoom in on the pipe and examine the development of the wrinkle.

The growth pattern of the wrinkle over time (or as curvature is increased) has been shown to be a key factor in improving flexural behaviour of the pipe. The results of Chapter 2 showed that if the wrinkle is slowed, the moment capacity and subsequently the ductility of the pipe could be improved. It is the sleeve's ability to control the wrinkle growth rate that determines its effectiveness as a repair. The odd sleeve design places a large amount of sleeve material over the top of the wrinkle. This makes it more challenging to slow the wrinkle growth to a level that shows larger improvements in moment capacity at high levels of curvature, without causing secondary wrinkling and a subsequent drop in ductility. The inherent design of the even sleeve helps alleviate this problem.

The even sleeve design shifts the material concentration from directly over top of the wrinkle to the edges of the wrinkle. By doing this, the growth rate of the wrinkle can be manipulated, to a greater extent than the odd sleeve design, by modifying the stiffness of the sleeve. This point is illustrated clearly in Figures 5.1 and 5.2. Figure 5.1 shows the wrinkle height for two repair schemes, one odd and one even scheme. Both repairs have identical material properties, sleeve lengths, etc. The odd sleeve stops the wrinkle (and creates secondary wrinkling) while the even sleeve allows it to grow. The result, shown in Figure 5.2, is that the even sleeve repair substantially increases the ductility of the pipe compared to the odd sleeve design. While the even repair is superior in this perspective, it does have drawbacks. These drawbacks will be discussed in later sub-sections.

5.1.1.2 Sleeve Spacing

One of the keys to success of the multiple sleeve repairs, the even sleeve design especially, is the spacing of the sleeves, also referred to as the gap size. Figure 2.22 showed the effect of the gap size on a typical even sleeve repair. Very small changes in the gap size (relative to the diameter of the pipe for example) transformed the behaviour of the sleeve drastically. If the gap was too small, the two sleeves would essentially act

as a single sleeve, eliminating the advantages of multiple sleeves. If the sleeves were placed too far apart, the wrinkle would not be constrained and sleeve would have little, if any effect on the flexural behaviour. It becomes apparent that detailed knowledge of the geometry of the wrinkle is necessary in order to properly implement the even sleeve design. If a FE model is used to design a sleeve, the model mesh must be fine enough to accurately predict the geometry of the wrinkle, otherwise, the sleeve could be ineffective. Initial FE modelling of the NPS 6 pipe in this study did exactly that. The mesh used was not fine enough to accurately portray the wrinkle. The even sleeve designs created with this model would have been ineffective when applied to test specimens. Fortunately, the mesh size was decreased after observations of wrinkle geometry from specimen 6-NS made it apparent that the original mesh was too coarse.

The effect of the gap size on odd sleeve repairs was shown to be less drastic than the effect on even sleeve, but present nonetheless. The purpose of the gap, for odd sleeves, was to capture secondary wrinkling, instead of allowing secondary wrinkling outside the sleeve zone. Figure 2.28 showed the effect of the gap size for the odd sleeve repair. It was found that a certain gap size was required to allow secondary wrinkling in the gap. This is intuitively obvious, since the wrinkle would need a certain amount of unrestricted space before it would grow. As the gap size was decreased, the wrinkle was forced outside the gap, but surprisingly, the repair performed slightly better. After closer examination, it appeared that as the gap size was reduced, the three sleeve components began acting as one long sleeve, thus increasing the overall stiffness of the pipe. However, the effect of the gap size was not as dramatic as was observed for the even sleeve. Because of this, the odd sleeve design could be considered more robust. One likely has a better chance of improving the capacity of the pipe with an odd sleeve than an even sleeve, when the exact geometry of the wrinkle is not known.

5.1.1.3 Sleeve Length

The length of the sleeve segments had different effects on the behaviour of the pipe for the even and odd sleeves. The performance of the even sleeve design, as will be discussed in the following section, is highly dependant on the hoop stiffness of the sleeve.

One could surmise that because of this, the length of the sleeve would not have a major impact on performance. In Figure 2.25, for a low E_1 sleeve, the performance was virtually independent of sleeve length. It is understood that if E_1 is increased, the length of the sleeve would have a slightly larger impact on performance, but compared to other factors in sleeve design, length is a minor contributor.

In the case of the odd sleeve, sleeve length plays a slightly larger role. It was mentioned in the previous section that as the sleeve spacing of the odd sleeve segments was decreased, the sleeves appeared to act as a longer sleeve, increasing moment capacity. This trend is consistent with longer sleeve segments as well. Figure 2.29 showed that as the sleeve length increased, the moment recovery was larger. This behaviour is consistent with the notion that as more of the pipe is reinforced with external sleeving, the higher its strength will be.

5.1.2 Sleeve Stiffness

One of the greatest advantages of using FRP as a material for repair sleeves is the wide range of sleeve stiffness that can be implemented. The stiffness of the sleeve is a product of the sleeve's material stiffness (the elastic modulus) and its thickness. The designer can vary both of these parameters quite easily for FRP sleeves, compared to steel sleeves. Because the sleeve stiffness is a product of the modulus and thickness, only one of these parameters need to be varied in order to study effects of sleeve stiffness on the pipe. By choosing to vary the modulus, the effects of sleeve stiffness can be examined in both pipe directions, something that cannot be done with the thickness.

In Chapter 2 it was shown that by varying the stiffness of the sleeve in the principle pipe directions (E_1 being longitudinally and E_2 being circumferentially/hoop) the behaviour of the pipe could be significantly modified to suite design guidelines. For both even and odd sleeve designs, as the stiffness of the sleeve is increased, the moment recovery and ductility are improved. There are limits, however. When the sleeve stiffness approaches that of the pipe steel, ductility is sacrificed for the gain in moment capacity. This is especially evident when the longitudinal stiffness of the sleeve is large. In Figures 2.23

and 2.26, it can be seen that in all cases where the value of E_l is high, the multiple sleeves act much like a single sleeve, eliminating the benefits of the multiple sleeves. When E_l is high, the sleeve contributes significantly to the flexural stiffness of the pipe. The increase in flexural stiffness at the wrinkle location is sufficient to force a new wrinkle to form in the next weakest area, adjacent to the sleeve. When the longitudinal modulus is decreased to very low levels, the flexural stiffness of the sleeve becomes negligible. Despite this, ductility and moment capacity gains are prevalent. This is due to the influence of the hoop stiffness of the sleeve on the pipe.

The stiffness of the sleeve in the hoop direction has a major impact on the behaviour of the pipe, because of its influence on the growth rate of the wrinkle. A sleeve with little longitudinal stiffness interacts with the pipe by constraining the radial growth of the wrinkle. By constraining the radial growth of the wrinkle, strain in the pipe is transferred from the plastic hinge to areas with higher stiffness. The result is increased flexural capacity and ductility. As the hoop stiffness of the sleeve is increased, the wrinkle's growth is constrained further and the strength of the pipe increases. This was clearly observed in the experimental work conducted in this project. Figure 4.16, shows substantial increases in the moment recovery between the carbon fibre sleeve repairs and the glass fibre repair. The glass fibre repairs shown in Figure 4.41 follow this trend, with smaller moment capacity gains resulting from the lower modulus glass fibres.

Numerical and experimental work conducted in this project has shown that by focussing the stiffness of the sleeve in the hoop direction of the pipe, the post-buckling flexural behaviour of the pipe can be significantly altered. This is not to say that sleeves with longitudinal stiffness have no function. If it is deemed necessary to achieve the highest possible moment capacity recovery with the sleeve repair, a sleeve with a large longitudinal stiffness is necessary. However, the ductility of the pipe would then be reduced. In any event, the FRP materials available today, from uniaxial fibre sheets to more complicated multiaxial laminates, are capable of providing the designer with the necessary sleeve stiffness in both the hoop and longitudinal directions.

5.1.3 Timing of Sleeve Repair

The final sleeve design parameter studied in this project that impacted the behaviour of the pipe was the timing of the sleeve repair. One should be aware that although the timing of the repair has been considered a design parameter in the laboratory setting, it might not always be a design parameter in the field. That is, one does not have very much control over the magnitude of the wrinkle when it is discovered.

The effects of repair timing were briefly studied in Chapter 2. Looking at Figure 2.31, one sees that as the repair is made sooner, the peak post-repair moment approaches the buckling moment of the pipe. This result is anticipated, since at lower levels of deformation, the pipe can recover its plastic moment prior to secondary buckling. At higher levels of deformation, ovalization of the cross-section in the bending plane reduces the plastic moment capacity of the pipe. This leads to a lower post-repair peak moment. A similar pattern is seen in the NPS 6 pipe tests. Examining specimens 6-CO-9-M and 6-CE-18-E in Figure 4.16, the earlier repair allows the pipe to reach its plastic moment, while the later repair does not. To make a true comparison, like sleeve repair geometries would have to be compared at different repair times, but due to limited test specimens and time constraints, this was not possible in this project. However, based on agreement between numerical and experimental results in this project, it is appropriate to assume that two like geometries, applied at different times, would herald a similar result.

It is clear that the timing of the repair has an impact on its ability to recover the peak moment of the pipe. An earlier repair is inherently more effective than a later repair. However, as mentioned earlier, the timing of the repair is likely to be out of the hands of the pipeline company. An optimum design for that particular timing, whatever it was, would have to be made. Factors not yet considered in the design of the repair, factors relating to the integrity of the sleeve itself, but dependant on the timing of the repair, must be discussed. These factors will be presented in the following section.

5.2 Effects of Sleeve Repair Design Parameters on Sleeve Integrity

In the previous section the effects of sleeve design parameters (geometric, material, timing) on the overall flexural behaviour of the wrinkled pipe were discussed. These effects, which were first studied in the preliminary FEA, were validated in the experimental program. The experimental program also provided results that were not considered in the preliminary FEA. In all NPS 6 repairs and the first NPS 12 repair test, fracture of the fibre sleeve occurred. Because sleeve fracture was not incorporated into the FE model, the model could no longer predict the behaviour of the pipe after fracture had occurred. While it is possible to incorporate fracture into the FE model for better prediction of flexural behaviour of the pipe, it is beyond the scope of this study. In field applications of sleeve repair, it would be necessary to avoid fracture of the sleeve. In order to insure that fracture of the sleeve does not occur, the effects of the design parameters, discussed previously, on sleeve integrity must be determined.

A primary measure for the integrity of the sleeve is the maximum strain in the fibres. By setting limits on the fibre strain in the sleeve, fracture can be avoided, insuring sleeve integrity. In Chapter 4 it was shown that the FE model was able to accurately predict the strain in the sleeve at the wrinkle crest (the location of maximum tensile straining of the fibre). Thus, the model can be used with confidence to examine the effects of sleeve design parameters on the maximum strain.

Because of the immense number of combinations of sleeve material, thickness, geometry and timing that are possible, certain variables discussed in Section 5.1 will be held constant in the examination. The geometry of the sleeve is held constant. An odd sleeve repair for a NPS 12 pipe is modelled, with sleeve segment lengths of 100 mm and gap sizes of 100 mm. This model is shown in Figure 5.3. While the even sleeve design has been shown to produce more superior results, from a flexural aspect, it was also shown to be very sensitive to geometry (gap size especially). For this reason, a more robust odd sleeve design was chosen in order to eliminate the effects of geometry.

Four parameters are examined for their effects on the fibre strain in this section. The timing of the repair and the modulus of the sleeve (in the hoop direction) are re-examined. The effects of sleeve thickness, held constant in previous FE modelling, are explored. Finally, the angle of the fibre, with respect to the hoop direction of the pipe, is varied. By changing the angle of the fibre to the direction of extreme straining in the pipe, it is be possible to change the strains imposed onto the fibres.

Through experimental work, it was found that the method in which the sleeve is applied to the pipe has a major impact on the integrity of the sleeve. Although installation is not a true design variable, it is key to a successful repair and must be considered when designing a sleeve. Therefore, findings relating to sleeve installation will also be discussed in this section.

5.2.1 Sleeve Design Parameters

The follow sub-sections discuss the results of FE modelling of the sleeve design parameters discussed previously. A new model designation was adopted to reflect these parameters and will be used in the discussion. The general format of the designation is **VW-X-Y-Z**, where:

- **V** = sleeve material; C – carbon fibre (E_1 = 230 GPa, E_2 = 10.3 GPa), G – glass fibre (E_1 = 73.5 GPa, E_2 = 8.3 GPa),
- **W** = sleeve configuration; O – odd sleeve,
- **X** = angle of fibres with respect to hoop direction of pipe in degrees,
- **Y** = timing of repair; a – 0.0315 radians, b – 0.0350 radians, c – 0.0420 radians,
- **Z** = thickness of sleeve in millimetres.

5.2.1.1 Repair Timing

The first parameter studied was the timing of the repair. In Section 5.1.3 it was postulated that the earlier a repair is made, the less the amount of energy that must be absorbed by the sleeve in order to regain moment capacity. Following this reasoning, one would assume that this would also result in less strain accumulated in the sleeve. Examining the plot of fibre strain versus global curvature for three different repair

timings in Figure 5.4, this is seen. When the sleeve is applied earlier, less strain occurs in the sleeve prior to secondary wrinkling (the drop in the curves) and the sleeve integrity is maintained. Looking at the plot of moment versus curvature for these repairs (shown in Figure 5.5) the same trend displayed in Figure 2.31 appears. It is interesting to note that as the timing of the repair is increased, the ductility of the pipe increases. This trend indicates that a later repair is not necessarily detrimental to the pipe.

The trends seen in Figure 5.4 warn the designer that if a sleeve repair is applied too late, fracture of the sleeve becomes more likely. In the case of the repair GO-0-c-5.6 shown in Figure 5.4, fibre strain levels reach approximately 75% of the typical fracture strain of the glass fibre. This margin is likely to be considered unsafe in field applications. While it would be advantageous to perform the repair earlier, this is not likely to be an option in the field. In this case, the other design parameters would have to be modified to achieve a safer strain level. The first parameter that could be changed is the fibre modulus (in other words the type of fibre).

5.2.1.2 Fibre Modulus

A set of glass fibre repairs was shown in Figure 5.4. Figure 5.6 plots the results of the same set repairs, except with carbon fibre. The higher modulus sleeve is able to reduce the fibre strain by more than 50%, to levels well within the average CFRP fracture strain of 1.5% (observed in the ancillary material tests of this project). As an added bonus, when comparing moment – curvature behaviour of the glass and carbon fibres (in Figures 5.5 and 5.7, respectively), the carbon fibre provides slightly higher peak post-repair moments as well.

The fibre modulus is a major contributor to the equivalent stiffness of the sleeve. It has become apparent that a stiffer sleeve not only improves peak post-repair moments, it also dramatically reduces the strain in the fibres. However, there is a second contributor to the sleeve stiffness, the sleeve thickness. The effect of this parameter on sleeve integrity is discussed next.

5.2.1.3 Sleeve Thickness

The impact of sleeve thickness on sleeve integrity has yet to be explored. Because the equivalent stiffness of the sleeve is a product of fibre modulus and sleeve thickness, one should expect that a change in thickness would have the same effect on fibre strain that a change in fibre modulus had. Figure 5.8 illustrates that as the thickness of the sleeve is reduced, the peak strain increases. This is consistent with a reduction in effective stiffness of the sleeve. Figure 5.9 shows the effects of thickness on the same repairs, using glass fibre however. The same trends are observed, with much larger strains. The larger strains are consistent with the use of a lower modulus fibre.

Interlaminar stresses and stress concentrations at the sleeve – pipe boundary will also be affected by sleeve thickness. A thicker sleeve will have greater amounts of shear lag between the fibres on the top surface and those nearest the pipe. In addition, as the sleeve thickness increases, the stress concentration at pipe surface is decreased. One can expect that these factors will affect the integrity of the repair. However, they are considered to be outside the scope of this project and have not been explored further.

It has been shown that both the thickness and modulus of the sleeve can be changed in order to significantly lower strain levels in the sleeve. These are two major advantages of the FRP sleeve over sleeves made of conventional materials. A third advantage of FRP's, the ability to use different fibre orientations, is explored next.

5.2.1.4 Fibre Orientation

Up to this point in the discussion of FRP sleeve repairs, only two configurations of fibres have been proposed: fibres placed in the hoop direction of the pipe (as was done in numerical and laboratory study) or fibres placed in the longitudinal direction of the pipe. The fibres, however, can be placed at any angle to the principal axes of the pipe as desired. Placement of the fibres at angles has two effects. First, an angled lamina will have different global material properties than a lamina with its fibres orientated in-line with the global axis (in the case of sleeve repair, the global 1 and 2 axes are aligned with the hoop and longitudinal directions, respectively). This feature allows the global

stiffness of the sleeve to be altered without having to change materials or sleeve thickness.

It is intuitive that by changing the angle between the fibres and the direction of extreme straining in the pipe (in the hoop direction for example), the strain imposed onto the fibres in their local directions will change. The magnitude or direction of the change in strain, however, is not intuitively obvious. Therefore, the FE model was used to study the effects of angled fibres. The COMPOSITE shell feature of ABAQUS was used to simulate the angled laminate. The laminates were constructed using fibres at positive and negative angles to the hoop direction. For example, a laminate with fibres at 30° was constructed of equal layers at +30° and –30°. In actual construction of angle-ply laminates, the layers would be of alternate +/- angles (+30, -30, +30, -30, etc.). For simplicity in modelling, only three layers were used (+30, -30, +30). The top and bottom layers of the laminate were half the thickness of the middle layer. The result was an equal thickness of fibres at positive and negative angles and a laminate symmetric about its mid-thickness. The thickness used for each layer was greater than the actual thickness of a typical unidirectional sheet. Therefore any number of actual fibre layers could be modelled using the three-layer laminate by adjusting the thickness of each layer. Since interaction between the layers was not in the scope of this study, this simplification was deemed reasonable.

In Figure 5.10, the effects of different fibre orientations on the maximum fibre strain of the sleeve are shown. A general trend of increased fibre strain with increased fibre angle occurs. It is apparent that angled fibres are not beneficial to the integrity of the sleeve for a given thickness. While this may be true, the magnitudes of the strains shown in Figure 5.9 are somewhat misleading. One must remember that as the angle between the fibres and hoop direction increases from 0° to 90°, the global modulus of the sleeve in the hoop direction decreases, even though the local fibre moduli remain constant. As observed previously, lower modulus sleeves accumulate more strain than higher modulus sleeves. To make a better comparison for different fibre angles, the sleeve thickness would have to be modified to keep the overall sleeve stiffness somewhat constant. Even then, a true

comparison would be difficult, since the sleeves with angled fibres also have some degree of longitudinal stiffness that the 0° sleeve does not. This comparison has not been made, since it appears that even with the correction for sleeve stiffness, placing the fibres at angles would have little, if any, benefit over the much simpler 0° fibre repair.

5.2.2 Sleeve Installation Procedure

Up until now, the discussion of key findings has focussed on quantitative aspects of sleeve design; how sleeve design impacts flexural behaviour of the pipe and strain in the sleeve. Of equal importance to the design of a successful sleeve repair, especially with respect to sleeve integrity is the way in which the sleeve is installed onto the pipe. In numerical modelling conducted throughout this project it has always been assumed that the sleeve would be perfectly bonded to the pipe at all times and its geometry would match that of the pipe exactly. These assumptions were necessary in order to develop a workable model of the pipe without excessive complications. However, laboratory testing has shown that these assumptions are not automatically satisfied and certain measures must be taken to approximate them as closely as possible.

The geometry of a wrinkled pipe poses an immediate problem when one wishes to apply a FRP sleeve onto it. In the wrinkled region, the diameter and geometric centre of the pipe change significantly over a very short length. This makes sleeve application very difficult. FRP sleeves are rectangular sheets wrapped around the pipe in a circular manner. To aid in FRP handling and placement in more conventional applications, the longitudinal fibres are often bound in the transverse direction by a small amount of fibre, by interweaving the fibres or by some type of backing mesh. In any event, this causes difficulty when the sheets are wrapped around the pipe. When wrapped, the sheets attempt to keep a constant diameter along their width (this corresponds to the longitudinal pipe direction). Because the pipe diameter changes in this region very rapidly, the sleeve cannot conform to the pipe and gaps between the pipe and the FRP form, causing variable bonding quality. The bonding problems were illustrated very clearly in Chapter 4. Without a sound bond between the sleeve and the pipe, the effectiveness of the sleeve is significantly reduced, along with the predictive capability of the model. Also stress

concentrations form in the debonded regions, which may lead to premature rupture of the sleeve.

Two methods were employed to eliminate this problem. The first attempt at a solution was to reduce the width of the sleeve strips, hoping that the narrower strips could conform easier to the wrinkle profile. In one test, for example, instead of using a single strip for a 100 mm wide sleeve section, four 25 mm wide strips were placed side by side. The 25 mm strips were unable to conform to the changing pipe diameter therefore smaller 12.5 mm strips were used in the vicinity of the wrinkle for the following test. The very narrow strips were also affected by the wrinkle geometry. In addition to gaps in the bond, the use of smaller strips made it difficult to control fibre placement between layers. A particular spot on the pipe near the wrinkle could have varying amounts of fibre placed above it, compared to an adjacent spot. This made the physical repair even more different from the assumed model, where the fibre thickness and amount of fibre was assumed to be constant.

The second method to insure proper bond that was attempted was to eliminate the changes in diameter caused by the wrinkle. A layer of epoxy putty was placed on the pipe around the wrinkle region in order to provide a constant diameter necessary for sleeve placement. The details of this method were outlined in Chapter 3. This technique solved two of the problems with sleeve installation that were encountered. First, the bond between the pipe and the sleeve (via the putty layer) was greatly improved. Second, the placement of fibres could now be done in wider strips. This insured equal placement of the fibres as well as significantly less installation time. The only drawback of this method was that the sleeve no longer matched the true profile of the pipe. However, since only in-plane effects have been considered, the out-of-plane angle difference between the sleeve and pipe wall was not anticipated to have a significant impact. The benefits gained by proper bond and sleeve placement and faster repair time far outweigh the slight error that may occur in modelling the sleeve with the same geometry of the pipe.

In this chapter, the key findings of this project, both through numerical analysis and laboratory testing, have been discussed. It has become apparent that FRP repair is a viable option for repair of wrinkled line pipe. Also, it has been shown that a FE model can be developed that reasonably predicts the behaviour of the pipe in the laboratory setting. Through laboratory examination, techniques that should be used when applying sleeves onto pipe have been identified.

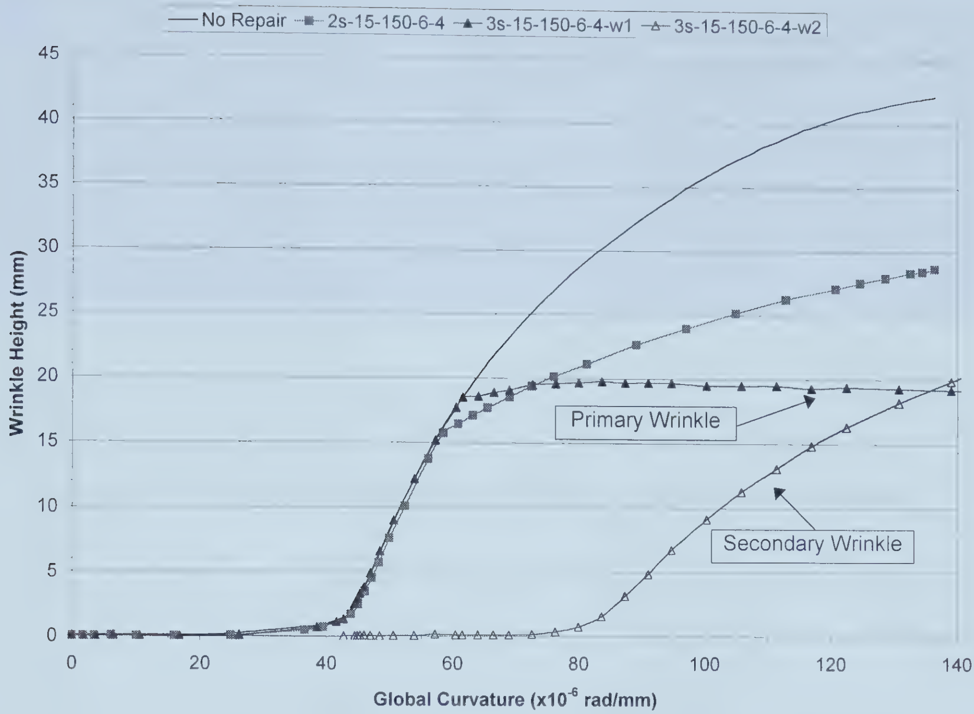

Figure 5.1 - Wrinkle Height vs. Global Curvature for Even and Odd FRP Repairs

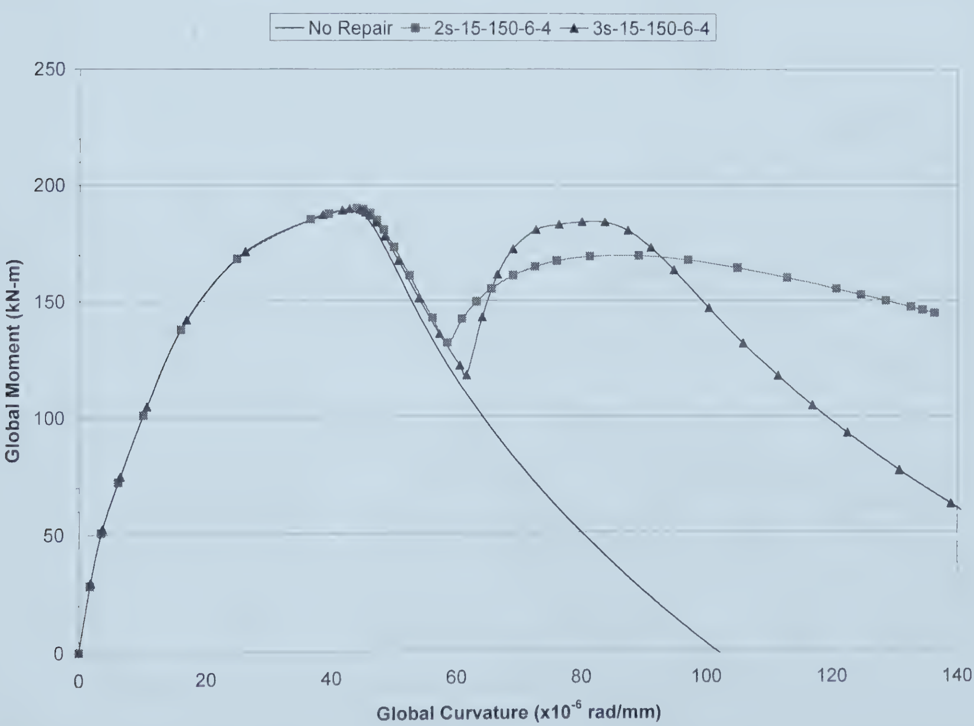

Figure 5.2 - Global Moment vs. Global Curvature for Even and Odd FRP Repairs

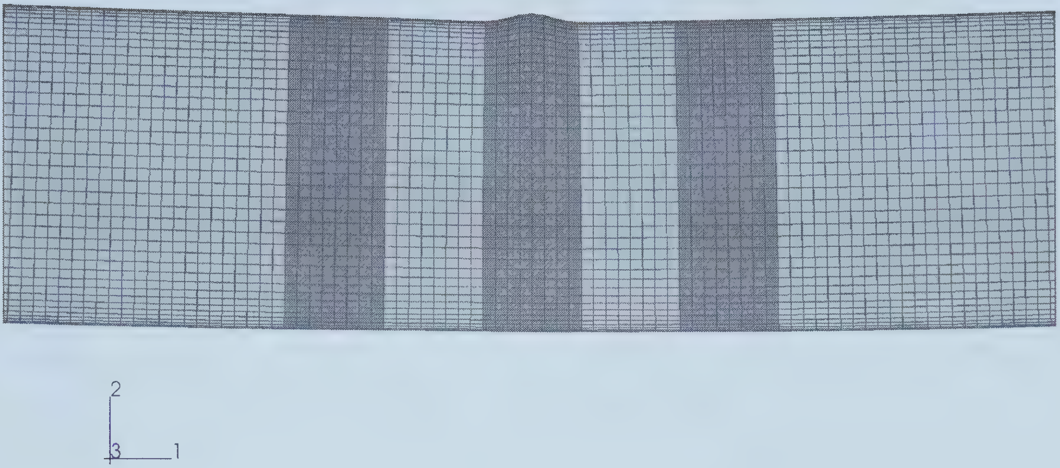

Figure 5.3 - Geometry of Odd Sleeve Used in Chapter 5 FE Modelling

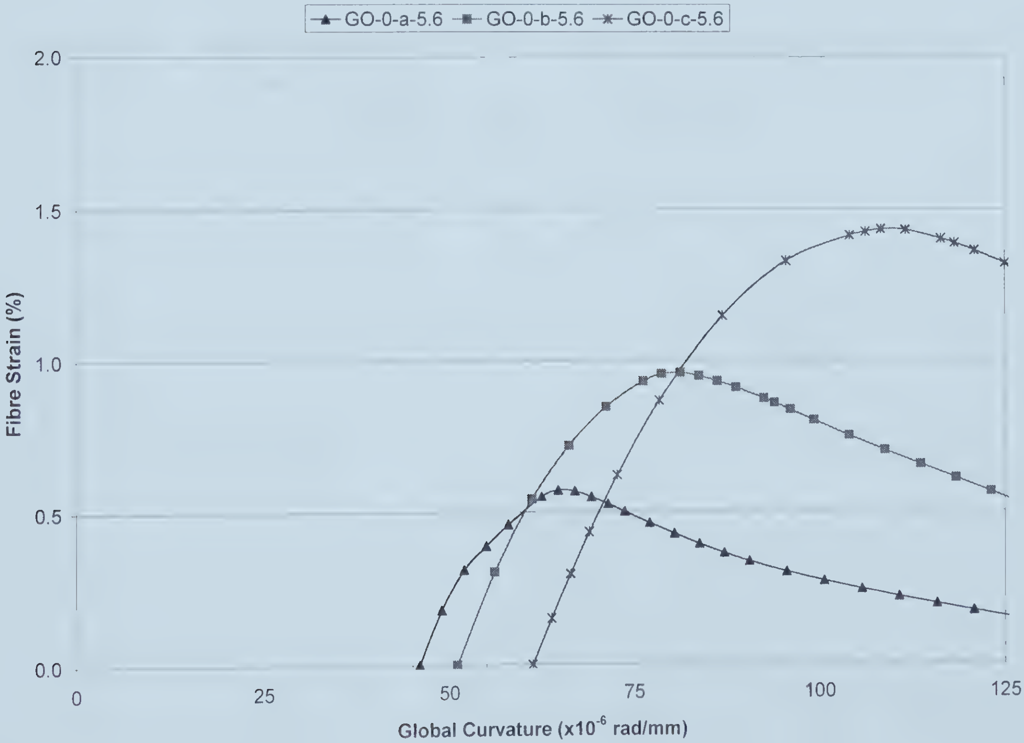

Figure 5.4 - Fibre Strain at Wrinkle Crest for GFRP Repairs (varying sleeve repair timing)

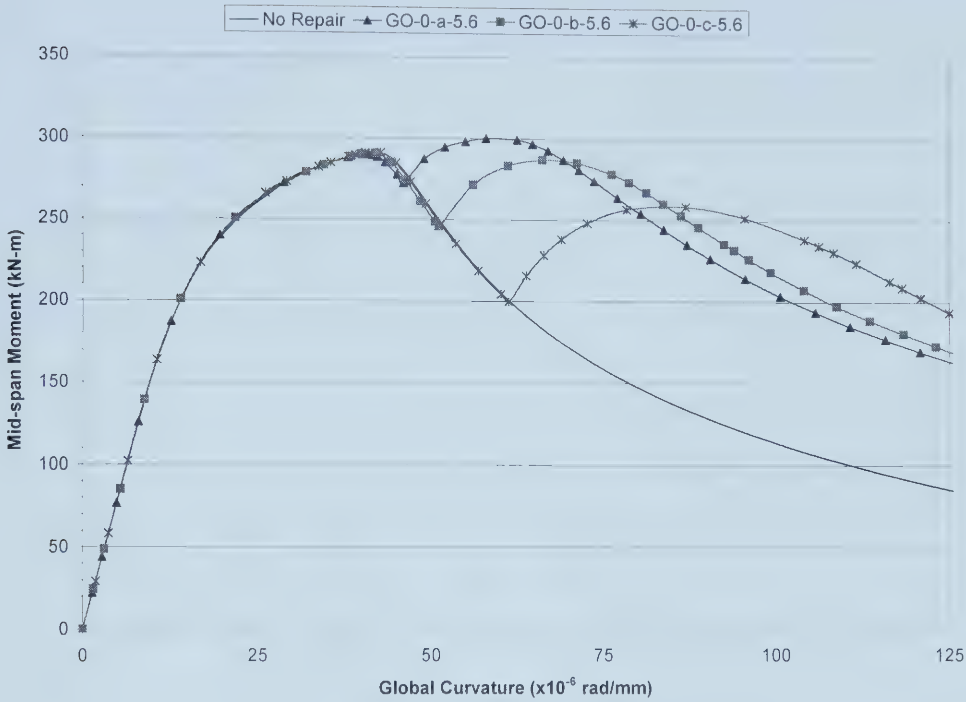

Figure 5.5 - Global Moment for GFRP Repairs (varying sleeve repair timing)

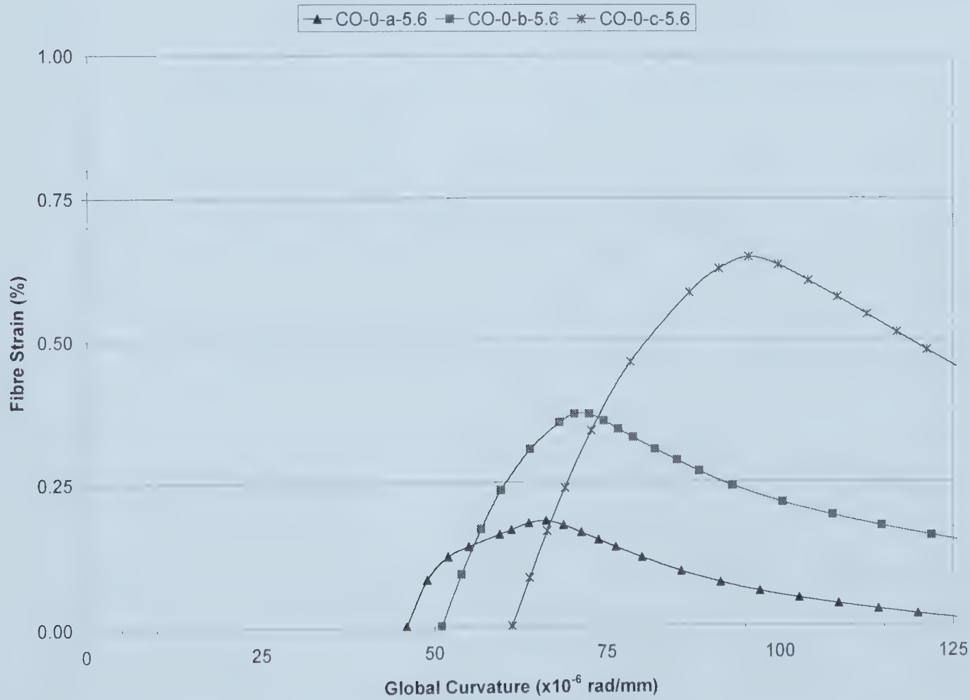

Figure 5.6 - Fibre Strain at Wrinkle Crest for CFRP Repairs (varying sleeve repair timing)

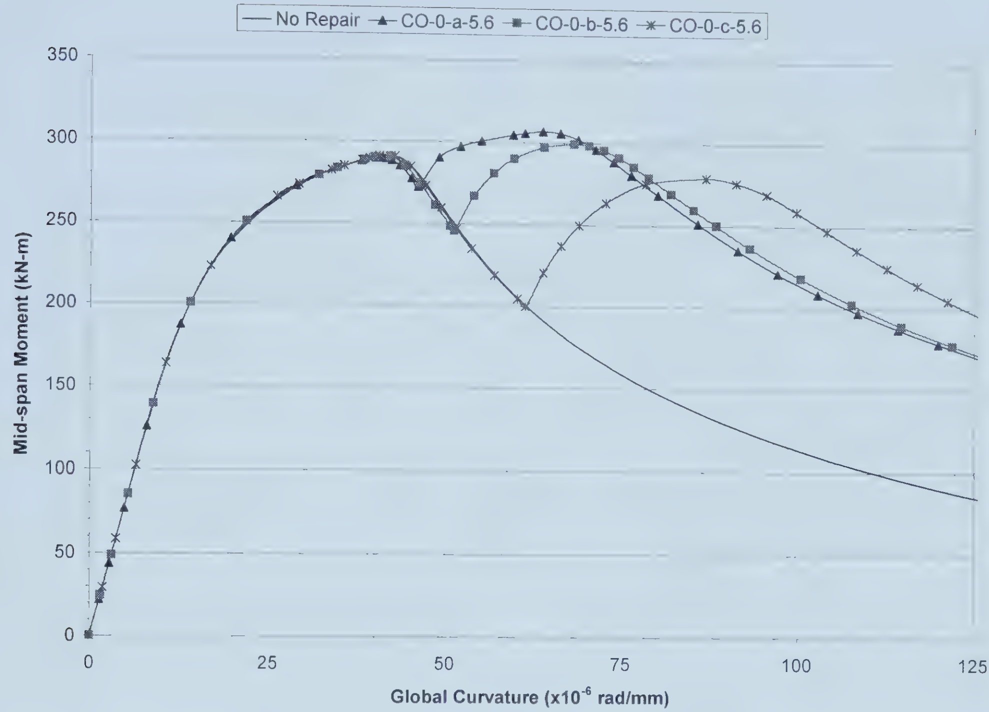

Figure 5.7 - Global Moment for CFRP Repairs (varying sleeve repair timing)

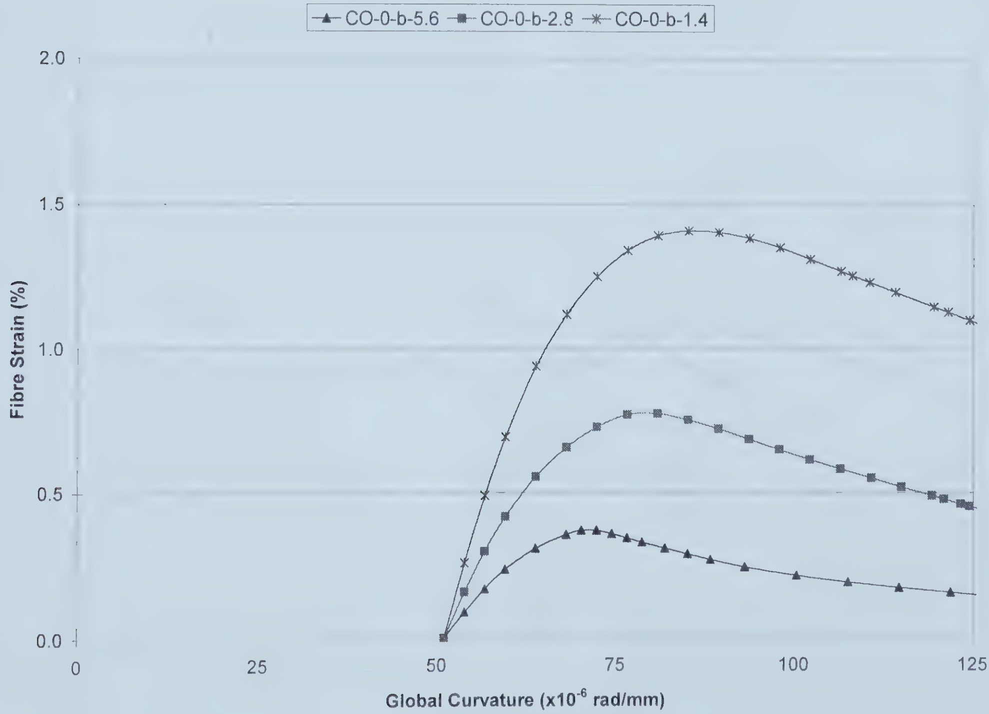

Figure 5.8 - Fibre Strain at Wrinkle Crest for CFRP Repairs (varying sleeve thickness)

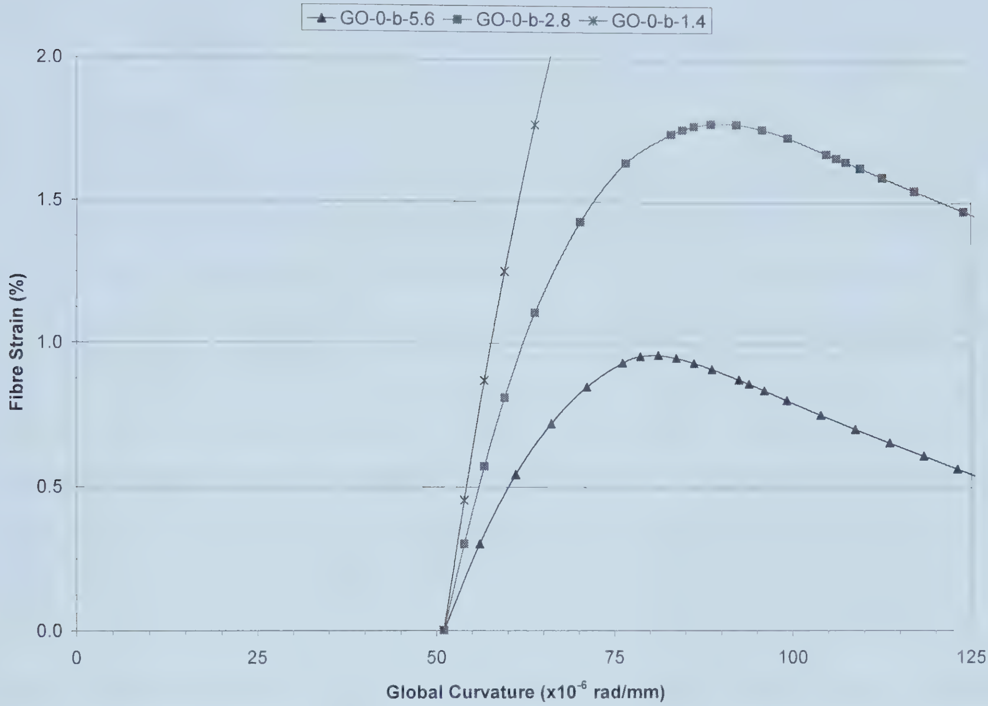

Figure 5.9 - Fibre Strain at Wrinkle Crest for GFRP Repairs (varying sleeve thickness)

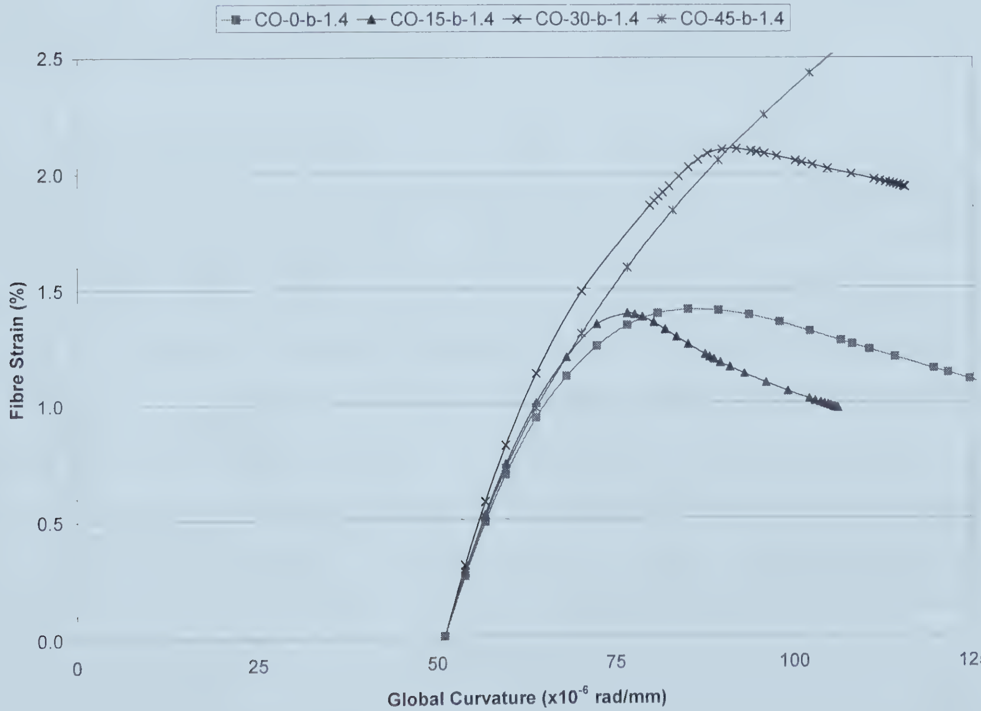

Figure 5.10 - Fibre Strain at Wrinkle Crest for CFRP Repairs (varying fibre angle)

6 SUMMARY, CONCLUSIONS AND RECCOMENDATIONS

6.1 SUMMARY

Inelastic local buckling of steel line pipe, also referred to as wrinkling, has been observed in laboratory experiments and in field settings. Geotechnical movements around buried pipe can create movements in the pipe large enough to create compressive strains exceeding local buckling limits. Specifically, settlements of discontinuous permafrost along the Norman Wells Pipeline have created instances of wrinkling. Research discussed in the literature review has shown that although wrinkles do not pose an immediate threat to pipeline integrity, they can lead to fracturing due to low-cycle fatigue. Current repair methods for wrinkled pipe are limited to costly cutout repairs. In limited cases, external steel sleeving has been used to repair wrinkles on the Norman Wells Pipeline. Finite element analysis of these repairs, conducted at the University of Alberta, has shown that although the steel sleeve repair stops wrinkle growth, secondary wrinkling adjacent to the sleeve is likely after very small amounts of additional pipe deflection. The use of alternate materials, specifically FRP composites, has been brought forward in this study as a potential improvement to steel sleeve repairs.

The first step in studying alternate sleeve repairs was to conduct a preliminary finite element study looking at different aspects of sleeve repairs not examined previously. The study focussed on the effects of different sleeve design parameters on the global flexural behaviour of a wrinkled pipe section similar to that on the Norman Wells pipeline. Three groups of parameters impacting moment – curvature behaviour of the pipe were identified. Sleeve geometry, specifically the number of sleeves, their spacing and their length, was seen to impact behaviour. Sleeve stiffness was found to have a profound impact on wrinkle growth and thus flexural behaviour of the pipe. The sleeve stiffness was found to be a product of both the material stiffness, quantified by the elastic modulus, and the sleeve thickness. Finally, the timing of the repair was observed to affect sleeve performance. From the FE analysis it was found that the behaviour of the pipe could be improved, over the steel sleeve repairs studied previously, by adjusting the three groups of parameters discussed.

An experimental program was conducted to verify observations made in the numerical study and to gain experience in FRP sleeve application techniques. Half-scale tests on NPS 6 pipe and full-scale tests on NPS 12 pipe were conducted. In all tests, the FRP sleeves did improve the behaviour of the wrinkled pipe. It was also discovered that FRP sleeves could be ruptured at the crest of the wrinkle if the sleeve was not designed to resist those strains. Improvements on sleeve application methods were made through the course of the laboratory tests.

The FE model used in the preliminary analysis was improved to better predict the results seen in the experimental program. Mesh refinement was instituted to capture the intricacies of the wrinkle geometry. This was especially necessary for sleeve repairs that were sensitive to sleeve placement relative to the wrinkle. The refined model was used to examine the effects of the sleeve design parameters on sleeve strain, in order to insure that when a sleeve is designed, fracture would be avoided.

6.2 CONCLUSIONS

Significant progress has been made in the study of repair methods for wrinkled pipes during this project. A number of important conclusions can be made based on the results of finite element and experimental work conducted with repair sleeves:

1. The growth rate of the wrinkle controls the behaviour of the pipe following local buckling. If wrinkle growth is slowed, the moment capacity of the pipe can be increased. However, if the wrinkle is slowed too much or stopped altogether, the accumulated energy in the pipe will create secondary wrinkling and a subsequent loss of moment capacity.
2. Multiple sleeve repairs provide for a much larger range of pipe behaviour compared to single sleeve repairs. By varying sleeve design parameters for multiple sleeves, the post-repair behaviour of the pipe can be significantly altered to suite the requirements of the pipeline operator. Single sleeve repairs impact the pipe in a relatively constant manner, regardless of the design parameters of the sleeve.

3. Sleeve stiffness has a significant impact on the behaviour of the wrinkled pipe for multiple sleeve repairs. By focussing the stiffness of the sleeve in the hoop direction of the pipe, large improvements in post-repair moment capacity and ductility can be gained. Uniaxial FRP sleeves wrapped around the pipe are ideal for this type of sleeve repair, since their stiffness is focussed in along the hoop direction of the pipe.
4. The even sleeve design allows for the greatest variability in pipe behaviour. By locating the sleeve stiffness on the periphery of the wrinkle, its growth rate can be controlled to the greatest extent. However, the even sleeve repair requires accurate knowledge of wrinkle geometry. If the sleeves are placed too close or too far apart, the effectiveness of the repair is dramatically reduced. The odd sleeve design, although somewhat less effective than the even sleeve design, is more robust. It can improve the behaviour of the pipe with less detailed knowledge of wrinkle geometry.
5. The timing of the repair impacts its behaviour. A repair on a smaller wrinkle, one discovered earlier in its life, leads to better results than a later repair.
6. Sleeve integrity must be considered during the design of the sleeve repair. It is very possible to fracture the sleeve, significantly reducing its effectiveness, if fibre strain limits are not set in the design. Strain can be limited in the sleeve by increasing its global stiffness. This can be accomplished by using a thicker sleeve or a higher modulus FRP, such as carbon fibre. In addition to modifying sleeve stiffness, applying the sleeve at an earlier time can significantly reduce peak strain in the fibre.
7. Special measures must be taken to insure proper bond between the FRP sleeve and the pipe, especially in the region of the wrinkle. The variable pipe diameter along the length of the wrinkle creates gaps in the bond between the pipe and the sleeve, which wants to remain at a constant diameter. Epoxy putty can be formed around the pipe in the wrinkle region to provide a constant diameter to which the sleeve can bond. This significantly reduces debonding between the pipe and the sleeve during wrinkle growth.

6.3 Recommendations

Work produced in this project has shown that with further study, FRP sleeves can be used to improve post-buckling behaviour of energy pipelines. Several aspects of FRP repair should be examined in order to gain confidence with this new repair technique:

1. Further full-scale laboratory testing is required to confirm the observations made in FE modelling following the experimental program conducted in this project. Repeated cases of repair without fibre fracture are required not only to gain confidence with the technology, but also to study pipe behaviour prior to and following secondary wrinkling.
2. The finite element model should be revised to incorporate the interaction between the pipe, the epoxy layer and the sleeve. Criteria for debonding of the sleeve should be placed in the model.
3. A more detailed finite element study should be conducted. Only one load case was examined in this project. The effects of internal pressure and axial load on the sleeve repair should be examined. In addition, the D/t ratio of the pipe should be varied to determine if FRP sleeves are viable for larger D/t ratio pipes, such as natural gas pipelines. Sleeve designs that optimize both flexural behaviour of the pipe and strain in the sleeve should be explored.
4. The effects of cyclic loading, both through FE modelling and laboratory experimentation, need to be examined. Cyclic loading has been shown to impact fracture development in the pipe wall and this aspect must be accounted for in repair design.
5. The feasibility of hybrid steel-FRP sleeve sleeves should be explored. These sleeves may be used for repairs on wrinkles that have grown too extensively for uniaxial FRP sleeve repair.
6. Finally, an application of FRP sleeve repair in a field setting should be sought out. It has been shown that even with sleeve fracture, the FRP sleeve improves the flexural behaviour of the pipe. A field test of the repair would provide valuable data for further refinement of the repair technology.

REFERENCES

American Petroleum Institute (1995). Specification for Line Pipe, API Specification 5L, 41st Edition, Washington, D.C.

American Society for Testing and Materials (ASTM) (2000a). "ASTM D3039/D3039M-00 Standard Test Method for Tensile Properties of Polymer Matrix Composite Materials," Annual Book of ASTM Standards, Vol. 15.03, pp. 106-118.

American Society for Testing and Materials (ASTM) (2000b). "ASTM A370-00 Standard Test Methods and Definition for Mechanical Testing of Steel Products," Annual Book of ASTM Standards, Vol. 03.01, pp. 4-60.

Bathe, K-J. (1996). Finite Element Procedures, Prentice Hall, Englewood Cliffs, New Jersey.

Bonfield, W. (1988). "Composites for medical applications," Engineering Applications of New Composites – International Symposium COMP '86, Patras, Greece, pp. 17-21.

Canadian Energy Pipeline Association (CEPA) (2000). Pipeline Safety – Industry Facts, Canadian Energy Pipeline Association, Calgary, Alberta.

Das, S., Cheng, J.J.R., Murray, D.W., Wilkie, S.A., Zhou, Z. (2000). "Laboratory Study of Local Buckling, Wrinkle Development, and Strains for NPS12 Linepipe," International Pipeline Conference – Volume 2, ASME, Calgary, Alberta, pp. 909-915.

DeGeer, D., and Cheng, J.J.R. (2000). "Predicting Pipeline Collapse Resistance," International Pipeline Conference – Volume 2, ASME, Calgary, Alberta, pp. 1083-1091.

DiBattista, J.D., Cheng, J.J.R., and Murray, D.W. (2000). "Behaviour of Sleeper-supported Line Pipe," Structural Engineering Report No. 230, Department of Civil Engineering, University of Alberta, Edmonton, Alberta.

Dorey, A.B., Cheng, J.J.R., and Murray, D.W. (2001). "Critical Buckling Strains for Energy Pipelines," Structural Engineering Report No. 237, Department of Civil Engineering, University of Alberta, Edmonton, Alberta.

Ellyin, F., Wolodko, J., Dorling, D., Glover, A., and Jack, T. (2000). "Fibre Reinforced Composites in Pipeline Applications: Design Issues and Current Research," International Pipeline Conference – Volume 1, ASME, Calgary, Alberta, pp. 491-500.

Ghali, A., and Neville, A.M. (1997). Structural Analysis: A unified classical and matrix approach, 4th Edition, E & FN Spon, London, England.

Hibbitt, Karlsson, & Sorenson, Inc. (HKS) (1999a). ABAQUS/Standard, Version 5.8-1 (computer software). Hibbitt, Karlsson, & Sorenson Inc., Pawtucket, Rhode Island.

Hibbitt, Karlsson, & Sorenson, Inc. (HKS) (1999b). ABAQUS/Standard User's Manual, Version 5.8. Hibbitt, Karlsson, & Sorenson Inc., Pawtucket, Rhode Island.

Kaw, A.K. (1997). Mechanics of Composite Materials, CRC Press, Boca Raton, Florida.

Kennedy, G.D., and Cheng, J.J.R. (1998). "Repair of Cracked Steel Elements using Composite Fibre Patching," Structural Engineering Report No. 221, Department of Civil Engineering, University of Alberta, Edmonton, Alberta.

Kuzik, M.D., Elwi, A.E., and Cheng, J.J.R. (1999). "Out-of-Plane Cyclic Behaviour of Masonry Walls Reinforced Externally with GFRP," Structural Engineering Report No. 228, Department of Civil Engineering, University of Alberta, Edmonton, Alberta.

Labossiere, P. (1993). Current and Future Applications of Advanced Composite Materials in Structural Engineering, Canadian Society for Civil Engineering, Montreal, Quebec.

Mirmiran, A., Shahawy, M., and Samaan, M. (1999). "Strength and Ductility of Hybrid FRP-Concrete Beam-Columns," Journal of Structural Engineering, October 1999, pp. 1085-1093.

Mohareb, M., Alexander, S.D.B., and Murray, D.W. (1993). "Laboratory Testing of Line Pipe to Determine Deformational Behaviour," Proceedings of the 12th International Conference on OMAE, Vol. V – Pipeline Technology, ASME, pp. 109-114.

Mohareb, M., Elwi, A.E., Kulak, G.L., and Murray, D.W. (1994). "Deformational Behaviour of Line Pipe," Structural Engineering Report No. 202, Department of Civil Engineering, University of Alberta, Edmonton, Alberta.

Murray, D.W. (1997). "Local Buckling, Strain Localization, Wrinkling, and Post-Buckling Response of Line Pipe," Engineering Structures, Vol. 19, No. 5, pp. 360-371.

Pantelides, C.P., Gergely, J., Reaveley, L.D., and Volnyy, V.A. (1999). "Retrofit of RC Bridge Pier with CFRP Advanced Composites," Journal of Structural Engineering, October 1999, pp. 1094-1099.

Souza, L.T., and Murray, D.W. (1994). "Prediction of Wrinkling Behaviour of Girth-Welded Line Pipe," Structural Engineering Report No. 197, Department of Civil Engineering, University of Alberta, Edmonton, Alberta.

Souza, L.T., and Murray, D.W. (1996). "Analysis for Wrinkling Behaviour of Girth-Welded Line Pipe," International Pipeline Conference – Volume 2, ASME, Calgary, Alberta, pp. 835-844.

True, W.R. (1995). "Composite wrap approved for U.S. gas-pipeline repairs," Oil & Gas Journal, October 9, 1995, pp. 67-71.

U.S. Steel Group (2001). Electrical Resistance Welding Manufacturing Process – McKeesport Facility, U.S. Steel Group, McKeesport, Pennsylvania.

Vinson, J.R., and Chou, T-W. (1975). Composite Materials and Their Use in Structures, Applied Science Publishers Ltd., Barking, England.

Wilkie, S.A., Doblanko, R.M., Fladager, S.J. (2000). "Case History of Local Wrinkling of a Pipeline," International Pipeline Conference – Volume 2, ASME, Calgary, Alberta, pp. 917-922.

Yao, J., and Murray, D.W. (2000). "Steel Sleeve Repairs for Buckled Pipelines," Draft Report Prepared for Enbridge Pipelines Inc., Department of Civil Engineering, University of Alberta, Edmonton, Alberta.

Yoosef-Ghodsi, N., Cheng, J.J.R., Murray, D.W., Doblanko, R.M., Wilkie, S.A. (2000). "Analytical Simulation and Field Measurements for a Wrinkle on the Norman Wells Pipeline," International Pipeline Conference – Volume 2, ASME, Calgary, Alberta, pp. 931-938.

Yoosef-Ghodsi, N., and Murray, D.W. (1999). "Numerical Study of the Buckle at KP 311+745 of Norman Wells – Zama Pipeline," Report Prepared for Enbridge Pipelines (NW) Inc., Department of Civil Engineering, University of Alberta, Edmonton, Alberta.

Zhou, Z.J., Boivin, R.P., Glover, A.G., and Kormann, P.J. (1996). "Pipeline Integrity Design for Differential Settlement in Discontinuous Permafrost Areas," International Pipeline Conference, ASME, Calgary, Alberta, pp. 603-612.

Zhou, Z.J., and Murray, D.W. (1995). "Analysis of Postbuckling Behaviour of Line Pipe Subjected to Combined Loads," International Journal of Solids and Structures, Vol. 32, No. 20, pp. 3015-3036.